

State space modeling of  
GROUNDWATER FLUCTUATIONS



# State space modeling of GROUNDWATER FLUCTUATIONS

Proefschrift

ter verkrijging van de graad van doctor  
aan de Technische Universiteit Delft,  
op gezag van de Rector Magnificus prof.dr.ir. J.T. Fokkema,  
voorzitter van het College voor Promoties,  
in het openbaar te verdedigen

op dinsdag 28 september 2004 om 15.30 uur

door

Wilbert Leonard BERENDRECHT

civil ingenieur  
geboren te Den Haag

Dit proefschrift is goedgekeurd door de promotor:  
Prof.dr.ir. A. W. Heemink

Samenstelling promotiecommissie:

Rector Magnificus, voorzitter  
Prof.dr.ir. A. W. Heemink, Technische Universiteit Delft, promotor  
Prof.dr.ir. C. van den Akker, Technische Universiteit Delft  
Prof.dr.ir. M. F. P. Bierkens, Universiteit Utrecht  
Prof.dr. G. J. Olsder, Technische Universiteit Delft  
Prof.dr.ir. P. A. Troch, Universiteit Wageningen  
Dr.ir. F. C. van Geer, Nederlands Instituut voor Toegepaste Geowetenschappen TNO, Utrecht  
Dr. J. C. Gehrels, Technische Universiteit Delft

Dr.ir. F. C. van Geer en dr. J. C. Gehrels hebben als begeleider in belangrijke mate aan de totstandkoming van het proefschrift bijgedragen.

**State space modeling of groundwater fluctuations**

Ph.D. thesis Delft University of Technology – with ref. – with summary in Dutch

ISBN 90-9018342-6

NUR 934, 919

Copyright © 2004 by Wilbert Berendrecht

All rights reserved

Cover design by Rosita Bouwsema

Printed in the Netherlands by PrintPartners Ipskamp B.V. Enschede

This project was carried out with financial support of the Netherlands Institute of Applied Geoscience TNO – National Geological Survey



# Voorwoord

**D**IT PROEFSCHRIFT is het resultaat van vier jaar onderzoek aan de Technische Universiteit Delft. Vier jaren die werkelijk zijn omgevlogen. Een periode waar ik met heel veel plezier op terugkijk, mede door alle mensen die om me heen stonden.

Allereerst wil mijn promotor Arnold Heemink heel hartelijk bedanken voor de mogelijkheid die hij mij heeft geboden om onder zijn hoede dit onderzoek uit te voeren. Ik denk dat ik me voor dit onderzoek geen betere promotor heb kunnen wensen. Als toegepast wiskundige, maar zeker ook als persoon. Arnold, bedankt voor alle tijd die je voor me nam en de inzet die je daarbij toonde!

Veel dank ben ik ook verschuldigd aan mijn begeleiders Frans van Geer en Hans Gehrels. Jullie expertise op het gebied van tijdreeksen gecombineerd met veel kennis van de hydrologische praktijk, was bijzonder waardevol. Frans, ik kon altijd met mijn vragen bij je binnenlopen. Meestal kwam ik met een hoop nieuwe vragen naar buiten. Je hebt me steeds weer verder aan het denken gezet en was daarmee een enorme stimulans voor mij. Hans, jouw enthousiasme werkte aanstekelijk. Daarnaast wil ik je in het bijzonder bedanken voor je kritische blik en gedegen commentaren op alle concepten, voorstellen en revisies. Ik heb een hoop van je geleerd.

Dank aan prof.dr.ir. C. van den Akker, prof.dr.ir. M.F.P. Bierkens, prof.dr. G.J. Olsder en prof.dr.ir. P.A. Troch, voor het zitting nemen in de promotiecommissie.

Van alle collega's aan de TU wil ik Judith Ormskerk bedanken voor het nodige papierwerk, en Mirjam Nieman voor de engelse correcties die de leesbaarheid van dit proefschrift aanmerkelijk hebben vergroot.

Het Nederlands Instituut voor Toegepaste Geowetenschappen TNO wil ik bedanken voor het medefinancieren van dit onderzoek en het beschikbaar stellen van alle benodigde faciliteiten. En meteen daarachteraan natuurlijk dank aan alle gezellige, leuke, gekke en enthousiaste collega's voor hun interesse en hulp. In het bijzonder wil ik Chris te Stroet bedanken voor de stimulans, inspiratie en het gegeven vertrouwen in de aanloop naar dit onderzoek. Bedankt ook voor je interesse en aanmoedigingen tijdens het onderzoek. Mijn (oud-) kamergenoten Ton Kremers en Aris Lourens – gekker kan niet! Ton, door jou weet ik nu (bijna) alles van zeilvliegen. Is het handboek nu eindelijk klaar, of heb ik je toch nog ingehaald? Aris... dan denk ik aan “hoera, het is weer maandag!”, aan een schijnbaar onuitputtelijk arsenaal aan liederen, samen lunchen, maar ook altijd bereid om mee te

denken en te helpen met bijvoorbeeld FORTRAN of met het bakken van een scriptje. En ook je secondenteller heeft tot op de laatste tel op mijn beeldscherm gestaan. Tot slot wil je ook nog mijn paranimf zijn. Dank je! Ook mijn andere paranimf en collega-promovendus, Peter Vermeulen, wil ik bedanken. Onze gezamenlijke congresbezoeken waren, naast leerzaam, ook erg gezellig. Maar ook je meeleven tijdens de beruchte laatste loodjes hebben me erg geholpen. Peter, bedankt voor je vriendschap.

Familie en vrienden wil ik bedanken voor de interesse in mijn onderzoek. Ik weet niet of het verhaal over tijdreeksen en grondwater altijd is overgekomen, maar dit is in ieder geval het resultaat. Rosita Bouwsema wil ik bedanken voor het ontwerpen van de omslag. Een speciaal woord van dank voor mijn moeder. Dank u voor wat u in de jaren voor mij persoonlijk betekend heeft.

Mijn lieve, lieve Marianne. Dank je dat ik deze vier jaar heb kunnen gebruiken om te promoveren. Dank je voor jouw geloof in mij. Dank je voor jouw grenzeloze steun. De laatste tijd leek het alleen maar om dit proefschrift te draaien. Maar je hebt mij altijd gestimuleerd, gesteund en ook nog eens een hoop andere werkzaamheden van me overgenomen. Je bent geweldig. I love you!

# Contents

<b>Voorwoord</b>	<b>5</b>
<b>Notation</b>	<b>11</b>
<b>1 General introduction</b>	<b>13</b>
1.1 Background . . . . .	15
1.2 Problem definition . . . . .	18
1.3 Research objectives . . . . .	19
1.4 Time series modeling in perspective . . . . .	19
1.5 Thesis outline . . . . .	20
<b>2 Theory of state space modeling</b>	<b>23</b>
2.1 Literature review . . . . .	24
2.1.1 Box-Jenkins models . . . . .	24
2.1.2 State space models . . . . .	25
2.2 Linear time series models . . . . .	26
2.3 Transfer function-noise models . . . . .	28
2.4 Linear state space models . . . . .	31
2.5 Linear Kalman filtering . . . . .	34
2.6 Nonlinear modeling and filtering . . . . .	37
2.7 Parameter estimation . . . . .	39
2.8 Smoothing . . . . .	42
<b>3 Decoupling of modeling and measuring interval</b>	<b>47</b>
3.1 Modeling framework . . . . .	48
3.2 Description of experiment . . . . .	51
3.2.1 Generation of groundwater time series . . . . .	51
3.2.2 Resampling of time series . . . . .	53
3.2.3 Evaluation criteria . . . . .	53
3.3 Comparison of model results for varying modeling and measuring interval . . . . .	54
3.3.1 Fit of deterministic component . . . . .	54
3.3.2 Parameter accuracy . . . . .	57
3.3.3 Adding high-frequency measurements . . . . .	58

3.4	Case study . . . . .	60
3.4.1	Description of the data set . . . . .	60
3.4.2	Modeling results . . . . .	60
3.5	Discussion and conclusions . . . . .	64
<b>4</b>	<b>Incorporation of a nonlinear root zone model</b>	<b>67</b>
4.1	A nonlinear reservoir model . . . . .	69
4.1.1	Root zone . . . . .	69
4.1.2	Percolation zone . . . . .	72
4.1.3	Saturated zone . . . . .	72
4.2	State space representation of the nonlinear reservoir model . . . . .	73
4.3	Example applications . . . . .	75
4.3.1	Description of the data sets . . . . .	75
4.3.2	Calibration and evaluation . . . . .	77
4.4	Summary and conclusions . . . . .	83
<b>5</b>	<b>State space modeling in switching regimes</b>	<b>85</b>
5.1	Water balance of a nonlinear phreatic groundwater system . . . . .	86
5.2	State space model of the phreatic system . . . . .	88
5.3	Application and evaluation of the nonlinear model . . . . .	91
5.3.1	Observation well 1 . . . . .	91
5.3.2	Observation well 2 . . . . .	93
5.3.3	Comparison with linear model . . . . .	96
5.4	Summary and conclusions . . . . .	99
<b>6</b>	<b>Multiple time series modeling</b>	<b>101</b>
6.1	Development of multiple-output state space model . . . . .	103
6.1.1	Deterministic component . . . . .	104
6.1.2	Stochastic component . . . . .	105
6.2	Evaluation of the reduced VTFN model: two case studies . . . . .	107
6.2.1	Description of data set and definition of the models . . . . .	107
6.2.2	Calibration and evaluation . . . . .	109
6.2.3	Decomposition of time series . . . . .	112
6.2.4	Interpretation of the common dynamic factor . . . . .	112
6.2.5	Analysis of the specific dynamic factors . . . . .	114
6.2.6	Cross validation of the VTFN-DF model . . . . .	114
6.3	Estimation of common trends . . . . .	116
6.4	Summary and conclusions . . . . .	119
<b>7</b>	<b>Summary and conclusions</b>	<b>121</b>
7.1	Decoupling of modeling and measuring interval . . . . .	122
7.2	Incorporation of a nonlinear root zone model . . . . .	124
7.3	State space modeling in switching regimes . . . . .	124



<b>Contents</b>	<b>9</b>
7.4 Multiple time series modeling . . . . .	125
7.5 Epilogue . . . . .	126
<b>Samenvatting en conclusies</b>	<b>129</b>
<b>Index</b>	<b>145</b>
<b>Curriculum vitae</b>	<b>151</b>



# Notation

In general, lowercase and uppercase *italic* type represent variables or functions. Lowercase **bold** type represents vectors. Uppercase **bold** type represents matrices.

## Lowercase roman symbols

$a_t$	zero-mean white-noise process
$c$	resistance of semi-impervious layer [T]
$f_c$	crop factor [-]
$f_i$	interception factor [-]
$f_t$	common dynamic factor
$h_t$	groundwater level [L]
$k$	number of common dynamic factors
$m$	dimension of the output vector, or empirical shape factor
$n$	dimension of the state vector, or empirical shape factor
$n_t$	stochastic noise process
$q$	dimension of the noise vector
$q_t$	flux [ $\text{LT}^{-1}$ ]
$r$	dimension of the input vector
$r_Q$	distance between extraction well and observation well [L]
$s_G$	standard deviation of the gain
$s_t$	specific dynamic factor, or drawdown [L]
$s_{obs}$	observed drawdown [L]
$s_r$	representative drawdown in an aquifer [L]
$t$	time [T]
$\mathbf{u}_t$	input vector
$\mathbf{v}_t$	measurement noise
$\mathbf{w}_t$	system noise
$\mathbf{x}_t$	state vector
$\mathbf{x}_{t t-1}$	projected state estimate
$\mathbf{x}_{t t}$	updated state estimate
$\mathbf{x}_{t T}$	smoothed state estimate

$\mathbf{y}_t$	output vector
$z^{-i}$	backward shift operator

## Uppercase roman symbols

$\mathbf{A}$	transition matrix
$\mathbf{B}$	system matrix
$\mathbf{C}$	system matrix
$D_e$	effective thickness of root zone [L]
$E_a$	actual evapotranspiration [ $\text{LT}^{-1}$ ]
$E_p$	potential evapotranspiration [ $\text{LT}^{-1}$ ]
$E_r$	Makkink reference evaporation [ $\text{LT}^{-1}$ ]
$\mathbf{F}_t$	innovation covariance matrix
$G$	steady-state gain
$\mathbf{G}$	system matrix
$\mathbf{I}$	identity matrix
$K$	unsaturated hydraulic conductivity [ $\text{LT}^{-1}$ ]
$K_s$	saturated hydraulic conductivity [ $\text{LT}^{-1}$ ]
$\mathbf{K}_t$	Kalman gain
$N$	number of groundwater level observations
$P_e$	net precipitation [ $\text{LT}^{-1}$ ]
$P_G$	gross precipitation [ $\text{LT}^{-1}$ ]
$\mathbf{P}_{t t-1}$	projected state covariance matrix
$\mathbf{P}_{t t}$	updated state covariance matrix
$\mathbf{P}_{t T}$	smoothed state covariance matrix
$Q$	groundwater withdrawal [ $\text{LT}^{-3}$ ]
$\mathbf{Q}$	system noise covariance matrix
$\mathbf{R}$	measurement noise covariance matrix
$R_C$	Cramer-Rao lower bound

$R_d$	drainage flux [ $\text{LT}^{-1}$ ]	$\theta$	moving-average parameter of stochastic component
$R_g$	flux from percolation zone to saturated zone [ $\text{LT}^{-1}$ ]	$\theta_r$	residual soil water content [-]
$R_p$	percolation flux [ $\text{LT}^{-1}$ ]	$\theta_s$	saturated soil water content [-]
$R_T^2$	coefficient of determination	$\lambda$	empirical shape factor, or eigenvalue
$S_e$	effective degree of water saturation [-]	$\nu_t$	innovation vector
$\tilde{S}_e$	transformed effective degree of water saturation [-]	$\xi_t$	residual component [L]
$S_r$	shape factor of the root water uptake function [-]	$\varphi$	storage coefficient [-]
$T$	transmissivity [ $\text{L}^2\text{T}^{-1}$ ] or number of time steps	$\phi$	autoregressive parameter of stochastic component
$\mathbf{U}$	eigenvectors	$\psi$	soil moisture pressure head [L]
		$\psi_o$	anaerobiosis point [L]
		$\psi_r$	reduction point [L]
		$\psi_w$	wilting point [L]
		$\omega$	moving-average parameter of deterministic component

### Lowercase greek symbols

$\alpha$	empirical shape factor
$\boldsymbol{\alpha}$	parameter vector
$\beta$	scaling factor
$\gamma$	drainage resistance [T]
$\delta$	autoregressive parameter of deterministic component
$\varepsilon$	specific yield [-]
$\varepsilon_t$	common-noise factor
$\eta_t$	specific-noise factor

### Uppercase greek symbols

$\boldsymbol{\Gamma}$	matrix of dynamic-factor loadings
$\boldsymbol{\Lambda}$	matrix of eigenvalues
$\boldsymbol{\Sigma}$	specific-noise covariance matrix
$\boldsymbol{\Phi}$	matrix of AR-parameters of specific factors
$\boldsymbol{\Psi}$	matrix of AR-parameters of common factors

# 1

## General introduction

AS GROUNDWATER RESOURCES are more intensively used, there is an increasing demand for monitoring of groundwater systems. To gain insight in the processes influencing the groundwater system, one needs knowledge of the essential variables and of how they fluctuate over time. One of the most important hydrological variables is groundwater head, which is therefore monitored frequently at many locations throughout the world. Groundwater head is easy to measure. The data contain relatively small measurement errors and are practically independent of the method of determination. In the Netherlands, groundwater head has been monitored countrywide since 1948. At present, over 30,000 time series are available, each containing valuable information on characteristics of the hydrological system and processes influencing the system. A useful and effective technique for extracting this information from the data is referred to as time series modeling.

Time series modeling refers to a statistical approach to analyze and describe one or more time series. Time series models are stochastic models, which means that they describe the probability structure of an observed phenomenon. They are also data-based, empirical models (also referred to as “black-box” models), which means that their structure is based on data; not on a physical description of the system.

Time series modeling has been applied in groundwater studies since the 1980s. However, the framework applied for modeling groundwater time series involves several practical problems influencing the results of these models; some problems even limit the applicability of these models to the field of groundwater hydrology altogether. The main objective of the research presented in this thesis is therefore to develop a more generic and flexible framework for modeling groundwater time series, in order to obtain a more accurate description of groundwater fluctuations. This framework is known as state space modeling and was originally developed in system theory. Basically, the state space approach described in this thesis, comprises the formulation of time series models in state space (with a model structure that may be deduced from physical concepts), filtering of the model, and estimation of the model parameters. Merits of the state space approach will be discussed in the course of this thesis.

This chapter gives an introduction to typical problems in groundwater hydrol-

ogy for which time series models are often applied. This is followed by a definition of technical problems encountered when applying time series models. A description of the research objectives is given, followed by a section that positions time series modeling within the field of groundwater modeling. The chapter concludes with an outline of the thesis.

## 1.1 Background

In densely populated areas, land use and planning are closely related to demands on water management of, for example, natural, agricultural and recreational areas. It is therefore important to base management of groundwater systems on these demands. This requires a thorough analysis and characterization of the groundwater regime. For this purpose, monitoring systems are needed to describe causes and effects – structural or otherwise – of groundwater fluctuations.

In the early 1990s, awareness grew that groundwater levels had significantly declined in large parts of the Netherlands [Ministry of VROM, 1989; Rolf, 1989; Gehrels, 1999]. Several studies were carried out to answer the following question: can the observed decline be accounted for by meteorological causes or by other influences? Among others, time series models were applied to separate the “natural” part of the groundwater fluctuations from the “non-natural” part [e.g. Van Geer and Defize, 1987; Van Geer, 1989]. The general conclusion from these studies was that the lowering of groundwater levels cannot be explained by meteorological factors alone. The groundwater level has lowered due to causes such as an increase in groundwater withdrawal, intensified artificial drainage of agricultural land, and urbanization. In reaction to these findings, in several parts of the Netherlands a “standstill policy” has been pursued with respect to interventions in the groundwater system that



**Figure 1.1:** A groundwater observation well; the inset shows four piezometers inside the well, each representing groundwater head at another depth. The groundwater head is measured manually with a tape measure.

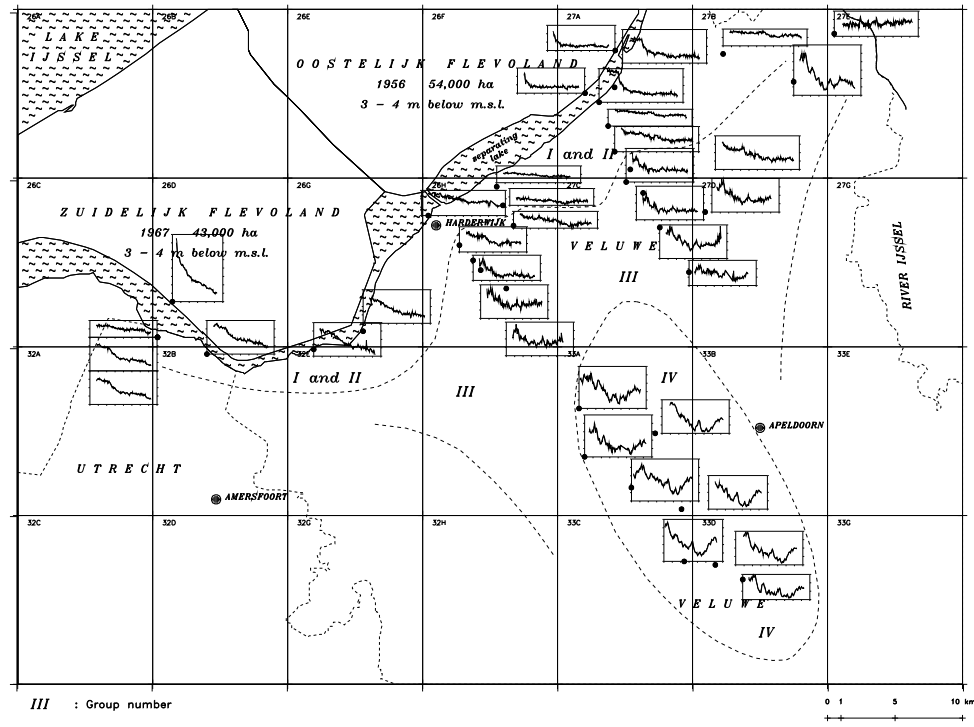


**Figure 1.2:** Clusters of residual time series representing part of the groundwater fluctuations that cannot be accounted for by meteorological causes; the map represents the Veluwe area in the middle of the Netherlands [from Gehrels, 1999]

may cause further lowering of groundwater levels. At this moment, policy makers want to know whether this policy has resulted in a rise of the groundwater level or at least has stopped the decline. If a structural change will be observed, it is important to determine whether measures taken within this policy, such as reduction of groundwater withdrawal, have indeed contributed to this structural change.

A common problem in the detection of structural changes in groundwater levels is that the estimated structural change has a high level of uncertainty, in particular when this change has to be estimated from short time series. In many practical applications, time series are short, since trends – both as a result from changes in natural conditions and through anthropogenic activity – need to be assessed as soon as possible. For instance, in the Netherlands, there have been several cases in which farming communities accused drinking water companies of crop damage caused by groundwater withdrawal (or stopping of withdrawal). However, part of the groundwater lowering (or rise) may have been caused by meteorological factors. As damage claims are high, it is of great importance that techniques are available which can estimate the influence of groundwater withdrawal with a high level of certainty.





*Figure 1.3: In dry periods, groundwater is extracted for sprinkler irrigation*

Generally, structural changes detected in the groundwater level are not constrained to one point in space. Fluctuations in large-scale groundwater withdrawal has a regional effect, resulting in a spatial pattern of temporal trends. During the 1990s, *Gehrels* [1999] carried out a study in the Veluwe area, the Netherlands, to detect structural changes in the groundwater level using time series modeling. Figure 1.2 gives a regional overview of results from the time series modeling. The charts denote residual series representing non-natural structural changes. The map features the spatial distribution of the trends present in the residuals. On the basis of similarity of trends, several clusters can be identified. This clearly demonstrates the spatial coherence of time series, and suggests that results of time series modeling can be improved by modeling groundwater time series simultaneously.

In many agricultural areas, groundwater is temporarily extracted for irrigation purposes. The effects of these groundwater withdrawals on the geohydrological system may be significant. A striking example is found in the southern part of the Netherlands. In this area, groundwater is extracted from a semi-confined aquifer at a depth of approximately 50 to 200 m. Although the irrigation has a positive effect on the phreatic water level, it lowers the groundwater head in the semi-confined aquifer throughout the region. As a lowering of groundwater head is a threat to groundwater-dependent valuable vegetation types in exfiltration areas, regional effects of groundwater withdrawals should be quantified.

The construction of civil engineering works such as roads and tunnels generally has a significant impact on the groundwater level at local scale. Within the construction period, dewatering systems are installed, causing a drawdown in the vicinity of the site. As this may lead to subsidence of the soil and adjacent build-

ings, it is often necessary to set up a monitoring programme. The major challenge is to detect and accurately quantify the effect of dewatering as soon as possible. This requires real-time techniques for processing and modeling of data.

Finally, time series models can be used to extrapolate observed groundwater time series. Often, monitoring periods are too short for the information on groundwater dynamics to reflect the prevailing climatic conditions. In that case, time series models can be applied to extrapolate observed groundwater time series to series of sufficient length, from which the required geohydrological characteristics can be calculated.

## 1.2 Problem definition

The previous section demonstrates the need for models that can accurately model and decompose time series of groundwater head. Until now, most time series of groundwater head have been modeled following the “Box-Jenkins approach” (named after the authors of the seminal textbook *Time series analysis: forecasting and control* published in 1970). However, Box-Jenkins models give rise to some practical difficulties, because they are designed for use with time series that are measured at equally spaced time intervals. In the Netherlands, equally spaced time series are the exception rather than the rule since at most locations groundwater head is measured on the 14th and 28th of each month. Moreover, the observation interval of input and output data need to be equal, which implies that generally available, high-frequency measurements of precipitation and evaporation cannot be used in the case that groundwater measurements are only available bimonthly. This is obviously a waste of valuable information. Finally, there is a growing use of automatic data loggers which easily allow for high-frequency measurements. This will result in a large number of time series with a shift in measurement frequency from bimonthly to, for instance, daily. Little is known about the influence of these high-frequency groundwater measurements on the performance of time series models.

A major challenge in time series modeling of groundwater fluctuations is to accurately estimate structural changes in groundwater regimes. However, the previous section already mentioned that estimated trends often have a high level of uncertainty. One reason is that the time series model may give an incorrect description of the system. Conventional time series models generally assume a linear relation between precipitation excess and groundwater head. As in many groundwater systems the response of groundwater head to precipitation excess is nonlinear, a linear model declares part of the natural component as “non-natural”. Consequently, the non-natural component becomes noisy, increasing the uncertainty of an estimated trend. This is particularly observed in systems with deep groundwater levels. Although it is often suggested that nonlinear models may give more accurate results [e.g. *Gehrels*, 1999], little is actually known about the influence of introducing nonlinearities on the accuracy of groundwater time series models.

Another reason for high uncertainty of estimated trends is lack of data. If the

length of a time series is limited, it is difficult to accurately decompose a time series. A solution for this may be to use spatial coherence between groundwater time series at several other locations to improve model performance at the location where data is limited. However, a practical problem with such multiple time series modeling is that the number of time series that can be modeled simultaneously, is limited. This is because the number of model parameters to be estimated, increases dramatically with the number of time series.

### 1.3 Research objectives

The main objective of the research presented in this thesis was to develop a generic and flexible framework for modeling groundwater time series based on the state space approach, in order to describe groundwater fluctuations more accurately. More specifically, the following objectives were defined:

- to quantify the effect of reducing the modeling interval – i.e., using high-frequency input data – on the performance of groundwater time series models. Of particular interest is the influence of high-frequency measurements of groundwater head;
- to develop methods for modeling groundwater fluctuations in nonlinear systems in order to characterize the groundwater regime, to obtain reliable predictions of groundwater head, and to obtain accurate estimates of structural changes in groundwater regimes;
- to develop a computationally efficient multiple time series model of groundwater fluctuations, in order to utilize spatial coherence between time series.

### 1.4 Time series modeling in perspective

Time series modeling is just one class of techniques within a whole range of groundwater modeling approaches. At the moment, the most commonly applied type of model in geohydrological practice is obviously the physical-mechanistic numerical groundwater model. This section therefore aims to position time series modeling in the field of groundwater modeling by showing the strengths and weaknesses of time series modeling with respect to numerical modeling of groundwater flow.

Time series models only represent the groundwater fluctuations at the location of the observation well. In this sense, they can be well compared with one-dimensional (1D) numerical model codes such as HYDRUS-1D [Šimunek *et al.*, 1998] and SWAP [Van Dam, 2000]. The main distinction between time series models and 1D numerical models is that the first describe groundwater fluctuations, while the latter describe unsaturated groundwater flow. Besides, both model types fundamentally differ in the way their structure is defined. In physical-mechanistic modeling, the model structure is based on the assumption that the physical system can be described well by deterministic mathematical equations. The model structure is thus based on (and often limited by) the modeler's knowledge of the physical system. In

time series modeling, however, the model structure is primarily based on observation data. As a result, the model characterizes the behavior of the hydrological processes without the restriction of physical preconceptions. In addition, time series models only need data on input and output, whereas physical-mechanistic models generally need a huge amount of additional information (e.g. soil physical properties), which is often limited available. As a consequence, it requires a lot of effort to apply physical-mechanistic models to many locations. A disadvantage of empirical time series models is their limited applicability for predicting the effect of future structural changes in the hydrological system (scenario analysis). Although physical knowledge may be incorporated in the time series model, physical-mechanistic models are generally more suitable for scenario analysis. Moreover, 1D physical-mechanistic models have the advantage that they give an estimate of important physical variables and the soil water profile.

A widely applied groundwater model is the three-dimensional (3D) numerical model. A well-known computer code is MODFLOW [McDonald and Harbaugh, 1988] which is based on a finite-difference approximation of groundwater flow. The most distinct difference between a 3D model and a time series model is that the 3D model is mainly designed for spatial modeling of groundwater flow, whereas the time series model is designed for temporal modeling of groundwater fluctuations. Hence, the 3D model is very well suited for spatial interpolation of groundwater head. This generally requires an enormous amount of data and modeling detail. If physical data is scarce, construction of 3D models becomes problematic or even practically impossible. In that case, regionalized time series models may be more appropriate [Bierkens *et al.*, 2001; Knotters, 2001]. Computational costs of 3D groundwater models are generally high. Although recent advances in model reduction give promising results [Vermeulen *et al.*, 2004], computational costs of time series models are lower.

An application for which time series models are superior is real-time modeling of groundwater head. For instance, time series models can be used for real-time forecasting and control of groundwater levels, and real-time detection of effects of interventions.

Summarizing, the primary criterion for selecting between time series models and numerical models is the objective of the study. The availability of physical data, financial and computational resources, and the time available to build a numerical model are important constraints.

## 1.5 Thesis outline

Chapter 2 gives an introduction to the theory of time series analysis. It discusses the main statistical concepts as well as some basics in time series modeling. The chapter also presents the most important theory on state space modeling, Kalman filtering and parameter estimation.

Chapter 3 analyzes the effect of using high-frequency meteorological observa-

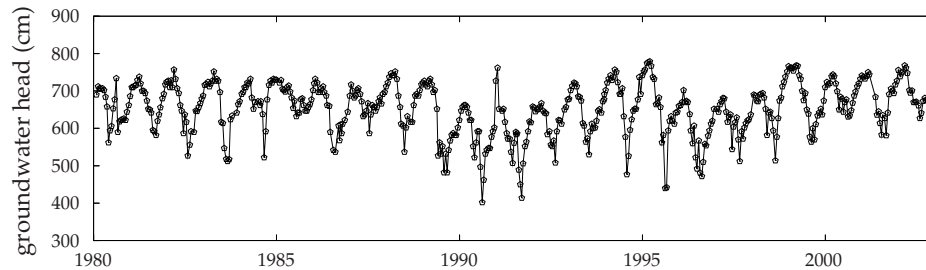


*Figure 1.4: Example of a time series of groundwater head observed bimonthly*

tions (e.g. daily) as input for modeling groundwater head data containing low-frequency observations. This means that the modeling interval – which is equal to the observation interval of meteorological data – is decoupled from the measuring interval of groundwater head. Groundwater time series are generated using pre-defined transfer functions to test model performance. Two measures of the model performance are defined and evaluated for several combinations of modeling and measuring intervals. A case study illustrates the effect of reducing the modeling interval as well as that of adding high-frequency measurements to the time series.

In Chapter 4, a nonlinear state space model is developed for modeling fluctuations of deep groundwater levels. Nonlinearity is introduced by modeling the (unobserved) degree of water saturation of the root zone. The nonlinear relations are based on physical concepts describing the dependence of both the actual evapotranspiration and the percolation rate on the degree of saturation of the root zone. Two test cases compare the results of the nonlinear model with those of a linear model.

Chapter 5 develops a nonlinear state space model for describing groundwater fluctuations in switching groundwater regimes such as drained fields. The drainage flux is modeled as a nonlinear function of the groundwater level in the sense that it switches from no flux if the water table is below drainage level to a flux that is linearly related to the groundwater level if the water table is above drainage level. Applications illustrate the applicability of the nonlinear state space model for estimating the effect of interventions, characterization of groundwater regimes, simulation, and prediction.

Chapter 6 provides an approach for modeling multiple time series of groundwater head. The model is based on the vector transfer-function noise (VTFN) model. Correlation among time series is described by a factor model. Results show that the model produces a description of the system that is similar to that of less parsimonious, conventional VTFN models. Consequently, larger systems, which cannot be described with a conventional VTFN model, can be efficiently described with the model developed in this chapter. In addition, the model can be used to describe regional patterns in groundwater fluctuations.

Chapter 7 concludes the thesis with a summary of the main results, conclusions, recommendations, and topics for further research.



# 2

## Theory of state space modeling

TO FOLLOW THE CONTENT of the next chapters, one needs knowledge of statistical concepts of and basic theory on time series modeling and Kalman filtering. Therefore, this chapter outlines the most important theoretical issues concerning state space modeling of time series. First of all, a review of relevant literature indicates the most important developments in time series analysis, particularly with application to hydrological problems. Those who are interested in a comprehensive theoretical discussion are referred to standard textbooks on time series analysis [Box and Jenkins, 1970; Hipel and McLeod, 1994], state space modeling [Harvey, 1989; Aoki, 1990; Koopman and Durbin, 2001], filtering theory [Jazwinsky, 1970; Schweppe, 1973; Anderson and Moore, 1979; Maybeck, 1979], and parameter optimization [Bryson and Ho, 1975; Gill et al., 1981; Tarantola, 1987].

## 2.1 Literature review

There are several ways to classify time series models. One of the most fundamental ways is classifying them as time-domain models or frequency-domain models. A disadvantage of frequency-domain models is that they are only suitable for stationary processes. Besides, they cannot be used for forecasting. For groundwater studies, it is therefore usually most convenient to carry out time series analysis in the time domain.

### 2.1.1 Box-Jenkins models

Although methods for analyzing time series have existed for decades [Wiener, 1949; Winters, 1960; Hannan, 1970], time series models only became widely accepted for practical applications after the publication of the textbook of Box and Jenkins called *Time series analysis: forecasting and control* in 1970. This book gives a comprehensive description of a variety of useful time series models. Moreover, it discusses the three stages of model construction: identification (i.e., selection of appropriate models to fit the data), estimation of model parameters, and diagnostic checking to ensure that the key modeling assumptions are satisfied. Examples of model construction can be found in, e.g., Granger and Newbold [1977], Salas and Obeysekera [1982], and in Pandit and Wu [1983].

Time series analysis also became an important tool for modeling hydrological systems. A special class of time series models called transfer function-noise (TFN)



models became very popular for describing dynamic causal relationships between time series. Hydrological applications of TFN models include rainfall-runoff modeling [Young *et al.*, 1997], streamflow modeling and forecasting [Anselmo and Ubertini, 1979; Chow *et al.*, 1983; Alley, 1985], urban water-use modeling [Maidment *et al.*, 1985], and reservoir modeling [Hipel *et al.*, 1977]. In the 1980s, time series analysis was introduced in groundwater modeling. Adamowski and Hamory [1983] analyzed groundwater level fluctuations predominantly affected by streamflow. Van Geer and Defize [1987] and Gehrels *et al.* [1994] included precipitation excess and an artificial trend in a TFN model for detection of natural and artificial causes of groundwater fluctuations. Bidwell *et al.* [1985] used a TFN model relating recharge to groundwater level. Tankersley *et al.* [1993] compared forecast accuracies for groundwater fluctuations of univariate and TFN models. Tankersley and Graham [1994] applied a TFN model to generate a control strategy for the purpose of managing groundwater fluctuations at ecologically vulnerable locations.

An often-heard criticism of black-box models is that they emphasize the statistical explanation of the data instead of giving a physical explanation. In order to counteract such criticism, in several publications conceptual or physically based models are used as a basis for model construction. Young [2001] discerns two main approaches for doing this: the ‘hypothetico-deductive’ approach and the ‘inductive’ approach. In the first approach, the model structure is a priori based on a conceptual or physical model. Examples are found in Moss and Bryson [1974], Spolia and Chander [1974], and Salas and Smith [1981], who applied physically based Markovian models for runoff. Parlange *et al.* [1992] formulated a Markovian model of soil water content on the basis of the hydrologic budget and a soil water transport equation. Knotters and Bierkens [2000] used a physically based time series model to predict the effect of interventions on water table dynamics. In contrast, the second (inductive) approach avoids preconceptions on the model structure. The model structure is not prespecified, but it is inferred from the data. However, the estimated model is only accepted as a credible representation of the system if, in addition to explaining the data well, it also provides a description that has direct relevance to the physical reality of the system. This approach is also referred to as data-based mechanistic (DBM) modeling and has been applied in many areas, including rainfall-flow modeling [Young and Beven, 1994; Young *et al.*, 1997] and solute transport modeling [Young and Wallis, 1994].

### 2.1.2 State space models

Although the Box-Jenkins approach to time series modeling dominated the statistical literature in the 1970s and 1980s, in control engineering, the state space approach was prevalent. This was partly because of the engineers’ familiarity with the Kalman filter, which has been a fundamental algorithm in control engineering since its appearance in Kalman [1960] and Kalman and Bucy [1961]. State space models have been used extensively in many areas, including control theory [Bucy and Joseph, 1968; Gelb, 1974], economics [Harvey, 1989; Koopman and Durbin, 2001], and

communication theory [Snyder, 1969].

State space models may be regarded as generalizations of Box-Jenkins models. The main distinction between both model types is the way they represent time series. Time series analysis following the Box-Jenkins approach is primarily directed towards scalar-valued data, and usually represents time series or their differenced version by (scalar) autoregressive models, moving-average models, or autoregressive moving-average models. State space models treat several variables simultaneously as vector-valued or state variables, the values of which are sufficient to describe the system behavior completely. Although these two ways of representing dynamic phenomena are theoretically equivalent, their numerical and statistical properties are different.

State space models have several advantages as compared with Box-Jenkins models that make them attractive for application in hydrology. For instance, Szollosi-Nagy *et al.* [1977] and Todini and Wallis [1978] combined the state space model with a Kalman filter for real-time forecasting of streamflow from rainfall, real-time flow routing, and real-time decision-making and control in water resource systems. Van Geer and Zuur [1997] applied a state space representation of the TFN model for spatial interpolation of groundwater head. They also recognized that the Kalman filter provides a framework that allows for flexible measurement schemes and varying measurement frequency. This has been described in more detail by Bierkens *et al.* [1999], who showed that the state space representation and Kalman filter are perfectly designed for modeling time series consisting of sparsely and irregularly observations. Finally, Bierkens *et al.* [2001] and Knotters [2001] combined a regionalized time series model with a Kalman filter for space-time interpolation of water table depth.

The state space representation is also very suitable for incorporation of a priori physical knowledge into the model. Aboitiz *et al.* [1986], for example, used the water balance equation and reference evapotranspiration for an irrigated field to develop a state space model capable of estimating and forecasting soil water depletion and crop evapotranspiration. Skaggs and Mohanty [1998] developed a state space model for water table depths midway drains, using a deterministic physically based drainage model. Bierkens [1998] modeled a combined system of soil water and shallow groundwater with mass balance equations assuming equilibrium soil moisture conditions. Wu *et al.* [2001] developed a state space model that describes soil water and salinity dynamics based on mass balance principles and empirical flux laws.

The next sections give an overview of the theory on state space modeling of time series used in this thesis. In addition, some basic statistical concepts are discussed.

## 2.2 Linear time series models

A simple but extremely useful stochastic model is the autoregressive (AR) model. In this model, the current value of the process  $n_t$  is linearly related to previous values

### Definitions

A **time series** is a set of observations that are arranged chronologically. A mathematical expression which describes the probability structure of the time series is referred to as a **stochastic process**. When the joint distribution of any possible set of random variables from the process is time independent, then the process is said to possess **strict stationarity**. When only the statistical moments up to order  $f$  are time independent, the process is said to possess **weak stationarity** of order  $f$ . The term **white noise** refers to a sequence of uncorrelated random variables having a fixed distribution with mean zero. When the current value of a process only depends upon the previous value plus a random shock, the process is called a **Markov process**.

The general purpose of **forecasting** or **prediction** is to provide the best estimate of what will happen at specific points in time in the future. The objective of **simulation** is to use a fitted model to generate possible future values of a time series.

of the process and a random shock at time  $t$ ,  $a_t$ :

$$n_t = \phi_1 n_{t-1} + \phi_2 n_{t-2} + \dots + \phi_p n_{t-p} + a_t, \quad (2.1)$$

where  $\phi_i$  is the  $i$ th AR parameter and  $p$  is the order of the AR( $p$ ) process. The  $a_t$  sequence is commonly referred to as white-noise terms. This means that  $a_t$  is identically independently distributed (IID) with a mean of 0 and variance of  $\sigma_a^2$ :  $\text{IID}(0, \sigma_a^2)$ . Often it is assumed that the white-noise terms have a Gaussian distribution.

By introducing the backward shift operator  $z^{-i}$ , which is defined by  $z^{-i}n_t = n_{t-i}$ , Equation 2.1 can be written in the following operator form:

$$\phi(z^{-1})n_t = a_t, \quad (2.2)$$

where the AR( $p$ ) operator is defined as

$$\phi(z^{-1}) = 1 - \phi_1 z^{-1} - \phi_2 z^{-2} - \dots - \phi_p z^{-p}.$$

A necessary and sufficient condition for the process  $n_t$  to have stationarity is that the roots of the characteristic equation  $\phi(z^{-1}) = 0$  must fall outside the unit circle [Box and Jenkins, 1970]. For an AR(1) process, this means that  $|\phi_1| < 1$ .

Another type of stochastic model is the moving average (MA) model:

$$n_t = a_t - \theta_1 a_{t-1} - \theta_2 a_{t-2} - \dots - \theta_q a_{t-q}. \quad (2.3)$$

Similar to Equation 2.2, the MA model may be written as

$$n_t = \theta(z^{-1})a_t, \quad (2.4)$$

where the MA( $q$ ) operator is defined as

$$\theta(z^{-1}) = 1 - \theta_1 z^{-1} - \theta_2 z^{-2} - \dots - \theta_q z^{-q}.$$

On the basis of Equations 2.2 and 2.4, one can construct many different model forms. The most straightforward extension is the autoregressive moving-average (ARMA) model for linear stationary processes:

$$\phi(z^{-1})n_t = \theta(z^{-1})a_t,$$

or

$$n_t = \frac{\theta(z^{-1})}{\phi(z^{-1})}a_t = \psi(z^{-1})a_t. \quad (2.5)$$

Other well-known model forms are the autoregressive integrated moving-average (ARIMA) model for linear nonstationary processes and the seasonal autoregressive integrated moving-average (SARIMA) model for linear nonstationary seasonal processes. *Box and Jenkins* [1970] and *Hipel and McLeod* [1994] describe these model forms in detail.

### 2.3 Transfer function-noise models

Hydrological studies often require a model that describes dynamic relationships between input and output series. A well-known stochastic type of model that relates one (physical) phenomenon to another is the transfer function-noise (TFN) model [Box and Jenkins, 1970]. Basically, a TFN model consists of two components: a dynamic or deterministic component, and a noise or stochastic component (see Figure 2.1).

**The deterministic component** describes the dynamic relationship between the input variable  $u$  and the output variable  $y$  as

$$\begin{aligned} y_t &= v_0 u_t + v_1 u_{t-1} + v_2 u_{t-2} + \dots \\ &= v(z^{-1})u_t, \end{aligned} \quad (2.6)$$

where  $v(z^{-1}) = v_0 + v_1 z^{-1} + v_2 z^{-2} + \dots$  is referred to as the transfer function and the coefficients  $v_0, v_1, v_2, \dots$  are called the impulse response function or impulse response weights. Similar to the ARMA model in Equation 2.5, the transfer function  $v(z^{-1})$  can be written as

$$v(z^{-1}) = \frac{\omega(z^{-1})}{\delta(z^{-1})} = \frac{\omega_0 - \omega_1 z^{-1} - \omega_2 z^{-2} - \dots - \omega_m z^{-m}}{1 - \delta_1 z^{-1} - \delta_2 z^{-2} - \dots - \delta_n z^{-n}}, \quad (2.7)$$

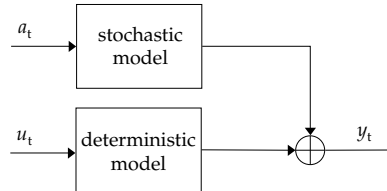


Figure 2.1: Components of the transfer function-noise model

where  $\omega(z^{-1})$  is the moving-average operator of order  $m$ ,  $\omega_0, \omega_1, \dots, \omega_m$  are the moving-average parameters,  $\delta(z^{-1})$  is the autoregressive operator of order  $n$ , and  $\delta_1, \delta_2, \dots, \delta_n$  are the autoregressive parameters. The denominator of  $v(z^{-1})$  reveals that this is an  $n$ th-order system model. The dynamic behavior of the system can be described by the poles of  $v(z^{-1})$ , i.e. by the roots of this denominator. Stability requires that the poles lie outside the unit circle [Box and Jenkins, 1970]. For a stable system, the steady-state gain  $G$  is defined as

$$G = \sum_{i=0}^{\infty} v_i = \frac{\omega_0 - \omega_1 - \omega_2 - \dots - \omega_m}{1 - \delta_1 - \delta_2 - \dots - \delta_n}, \quad (2.8)$$

and represents the steady-state level of the output obtained when the input is held at unit value.

For situations where  $y_t$  and  $u_t$  have nonzero means  $\mu_y$  and  $\mu_u$ , and where there is a delay time  $d$  before  $u$  affects  $y$ , Equation 2.6 can be written as

$$y_t - \mu_y = v(z^{-1})z^{-d}(u_t - \mu_u). \quad (2.9)$$

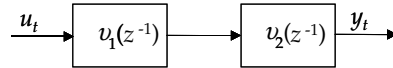
Two specific classes of transfer functions are particularly useful in hydrological applications, because they allow for a meaningful physical interpretation. The first class of transfer functions is written as

$$v(z^{-1}) = \frac{\omega_0}{1 - \delta_1 z^{-1} - \delta_2 z^{-2} - \dots - \delta_n z^{-n}}. \quad (2.10)$$

This transfer function can also be expressed as

$$\begin{aligned} v(z^{-1}) &= \omega_0 \prod_{i=1}^n \frac{1}{1 - \lambda_i z^{-1}} \\ &= G \prod_{i=1}^n \frac{1 - \lambda_i}{1 - \lambda_i z^{-1}} = \prod_{i=1}^n v_i(z^{-1}), \end{aligned} \quad (2.11)$$

with  $|\lambda_i| < 1$  and  $G$  the steady-state gain. Equation 2.11 represents a serial connection of  $n$  first-order processes in series, each with unity gain. For  $n = 2$ , this system may be visualized as



This model form – also referred to as the linear reservoir model – is often applied in hydrology to describe, for example, advective-dispersive flow.

The second class of transfer function models is written as

$$v(z^{-1}) = \frac{\omega_0 - \omega_1 z^{-1} - \omega_2 z^{-2} - \dots - \omega_{n-1} z^{-n+1}}{1 - \delta_1 z^{-1} - \delta_2 z^{-2} - \dots - \delta_n z^{-n}}. \quad (2.12)$$

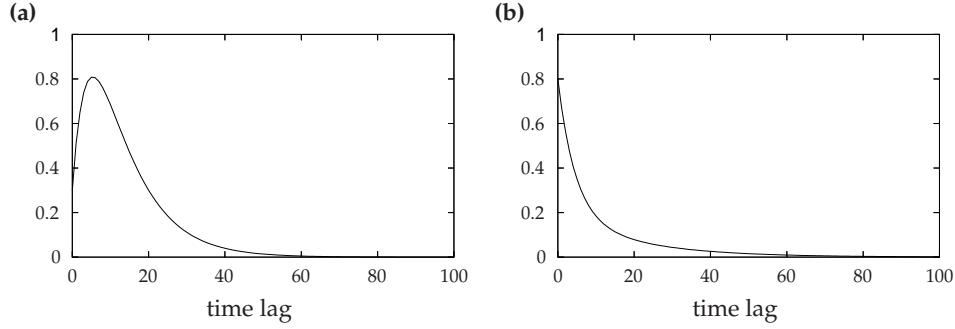
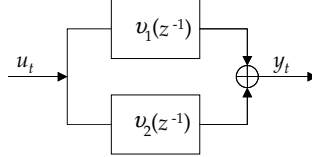


**Figure 2.2:** Example of impulse response functions for (a) serial connection ( $n = 2$ ) and (b) parallel connection ( $n = 2$ )

This function can be expressed as

$$v(z^{-1}) = \sum_{i=1}^n \frac{g_i}{1 - \lambda_i z^{-1}} = \sum_{i=1}^n v_i(z^{-1}), \quad (2.13)$$

representing  $n$  reservoirs in a parallel connection. For instance, if  $n = 2$ , this can be visualized as



where  $\oplus$  denotes addition. Parallel connection may represent preferential or lateral flow. By way of illustration, Figure 2.2 shows two impulse response functions for a serial and parallel connection, respectively. Hydrological applications of these model forms are found in, e.g. *Young and Minchin* [1991] and *Young* [2001], who decomposed a rainfall-flow transfer-function model into two parallel components representing surface flow and base flow.

**The stochastic component** describes the variation in the output that cannot be described by the deterministic component. Because the stochastic component is generally autocorrelated and not white, it can be conveniently modeled using the ARMA model in Equation 2.5. The complete TFN model is then formed by combining Equations 2.5 and 2.9:

$$y_t - \mu_y = \frac{\omega(z^{-1})}{\delta(z^{-1})} z^{-d} (u_t - \mu_u) + \frac{\theta(z^{-1})}{\phi(z^{-1})} a_t. \quad (2.14)$$

A special case of the TFN model is the autoregressive moving-average exogenous variables (ARMAX) model [Hannan, 1970]:

$$y_t - \mu_y = \frac{\omega(z^{-1})}{\phi(z^{-1})} z^{-d} (u_t - \mu_u) + \frac{\theta(z^{-1})}{\phi(z^{-1})} a_t. \quad (2.15)$$

A feature of the ARMAX model is that the response variable is written directly as an autoregression. However, the TFN model has several theoretical and practical advantages over the ARMAX model. First, the TFN model is a more general representation of a stochastic dynamic system than the ARMAX model. As a result, it is more flexible in describing the system. Second, the TFN model clearly separates out the deterministic component from the stochastic component. This is particularly advantageous in geohydrological applications.

## 2.4 Linear state space models

The deterministic model given in Equation 2.6 can be generalized to a time-varying first-order vector difference equation with associated output relation as [Maybeck, 1979]

$$\mathbf{x}_t = \mathbf{A}_t \mathbf{x}_{t-1} + \mathbf{B}_t \mathbf{u}_t, \quad (2.16a)$$

$$\mathbf{y}_t = \mathbf{C}_t \mathbf{x}_t, \quad (2.16b)$$

where  $\mathbf{x}_t$  is an unobserved,  $n$ -dimensional state vector (the  $n$  dimensions correspond to the fact that the system is described by  $n$ th-order dynamics),  $\mathbf{y}_t$  is a  $1 \times m$  multiple-output vector,  $\mathbf{u}_t$  is a  $1 \times r$  multiple-input vector,  $\mathbf{A}_t$  is an  $n \times n$  transition matrix,  $\mathbf{B}_t$  is an  $n \times r$  matrix relating the input vector to the state vector, and  $\mathbf{C}_t$  is an  $m \times n$  matrix relating the state vector to the output vector. Time subscripts on the system matrices  $\mathbf{A}$ ,  $\mathbf{B}$  and  $\mathbf{C}$  indicate the possibility that they may change over time. Unless mentioned explicitly, these matrices are taken to be constant. Equation 2.16 is the state space representation of a linear dynamic system. Equation 2.16a and 2.16b are referred to as the state equation and the measurement equation, respectively.

It can be shown that the transfer function model of Equation 2.6 can be written in terms of Equation 2.16, as

$$y_t = \mathbf{c} [z\mathbf{I} - \mathbf{A}]^{-1} \mathbf{b} u_t, \quad (2.17)$$

with  $z$  defined as  $zx_t = x_{t+1}$  and  $\mathbf{I}$  is the identity matrix. Notice that for a single-input single-output model the matrices  $\mathbf{B}$  and  $\mathbf{C}$  reduce to an  $n$ -dimensional column vector  $\mathbf{b}$  and row vector  $\mathbf{c}$ , respectively. Given an  $n$ th-order transfer function model, it is possible to generate an  $n$ -dimensional state space representation that has input-output characteristics that are equivalent to those of the transfer function model. For this purpose, the transfer function model of Equation 2.6 is written as

$$y_t = \delta_1 y_{t-1} + \dots + \delta_n y_{t-n} + \omega_0 u_t - \omega_1 u_{t-1} - \dots - \omega_{n-1} u_{t-n+1}. \quad (2.18)$$

### Definition of state

The **state vector** is defined as a minimal collection of information which, along with future input to the system, is sufficient to determine the future evolution of the dynamic system. *Bryson and Ho* [1975] define the state property as follows: “At any time  $t$  there exists a finite-dimensional vector  $\mathbf{x}$ , which, when specified, makes the future of the process independent of the past and vice versa.” The dependence of the future on the present is expressed by a difference equation that governs the transition from one instant to another.

Although here, the order of the MA part is  $m = n - 1$ , there is no loss of generality since terms can always be added with values of zero. An  $n$ -dimensional state vector  $\mathbf{x}_t$  is defined through the following relations:

$$\begin{aligned} x_{1,t} &= \delta_1 x_{1,t-1} + x_{2,t-1} + \omega_0 u_t, \\ x_{2,t} &= \delta_2 x_{1,t-1} + x_{3,t-1} - \omega_1 u_t, \\ &\vdots \\ x_{n-1,t} &= \delta_{n-1} x_{1,t-1} + x_{n,t-1} - \omega_{n-2} u_t, \\ x_{n,t} &= \delta_n x_{1,t-1} - \omega_{n-1} u_t, \end{aligned}$$

with

$$y_t = x_{1,t}.$$

In the form of a system equation, with given initial condition  $\mathbf{x}_0$ , this becomes

$$\mathbf{x}_t = \mathbf{A}_d \mathbf{x}_{t-1} + \mathbf{b}_d u_t, \quad (2.19a)$$

$$y_t = \mathbf{c}_d^T \mathbf{x}_t, \quad (2.19b)$$

with

$$\mathbf{A}_d = \begin{bmatrix} \delta_1 & 1 & 0 & \cdots & 0 \\ \delta_2 & 0 & \ddots & \ddots & \vdots \\ \vdots & \vdots & \ddots & \ddots & 0 \\ \delta_{n-1} & \vdots & & \ddots & 1 \\ \delta_n & 0 & \cdots & \cdots & 0 \end{bmatrix}, \quad \mathbf{b}_d = \begin{bmatrix} \omega_0 \\ -\omega_1 \\ \vdots \\ -\omega_{n-2} \\ -\omega_{n-1} \end{bmatrix}, \quad \mathbf{c}_d^T = \begin{bmatrix} 1 \\ 0 \\ \vdots \\ 0 \end{bmatrix}. \quad (2.20)$$

Equation 2.19 gives a state space representation of the transfer function model and is known as the observer canonical form [*Olsder*, 1994]. The state space representation is not unique. In fact, there is an infinite number of representations. *May-beck* [1979] shows that various equivalent state space representations can be related through similarity transformations.



The state space model of a stochastic dynamic system is easily obtained by extending Equation 2.16 with noise terms:

$$\mathbf{x}_t = \mathbf{A}\mathbf{x}_{t-1} + \mathbf{B}\mathbf{u}_t + \mathbf{G}\mathbf{w}_t, \quad (2.21a)$$

$$\mathbf{y}_t = \mathbf{C}\mathbf{x}_t + \mathbf{v}_t. \quad (2.21b)$$

Here, the system noise  $\mathbf{w}_t$  is a  $q$ -dimensional column vector,  $\mathbf{G}$  is an  $n \times q$  matrix, and  $\mathbf{v}_t$  is an  $m$ -dimensional column vector representing measurement noise. The disturbances  $\mathbf{w}_t$  and  $\mathbf{v}_t$  are serially and mutually uncorrelated with mean zero and covariance matrix  $\mathbf{Q}$  and  $\mathbf{R}$ , respectively:

$$\mathbb{E}(\mathbf{w}_t) = \mathbf{0}, \quad \mathbb{E}(\mathbf{v}_t) = \mathbf{0}, \quad (2.22)$$

and

$$\mathbb{E}(\mathbf{w}_t \mathbf{w}_k^T) = \mathbf{Q} \delta_{t,k}, \quad \mathbb{E}(\mathbf{v}_t \mathbf{v}_k^T) = \mathbf{R} \delta_{t,k}, \quad \mathbb{E}(\mathbf{w}_t \mathbf{v}_k^T) = \mathbf{0}, \quad (2.23)$$

where  $\delta_{t,k}$  is the Kronecker delta defined as

$$\delta_{t,k} = \begin{cases} 1 & t = k, \\ 0 & t \neq k. \end{cases}$$

It is further assumed that the initial state vector,  $\mathbf{x}_0$ , has a mean of  $\chi_0$  and a covariance matrix  $\mathbf{P}_0$ :

$$\mathbb{E}(\mathbf{x}_0) = \chi_0 \quad \text{var}(\mathbf{x}_0) = \mathbf{P}_0. \quad (2.24)$$

Besides, the disturbances  $\mathbf{w}_t$  and  $\mathbf{v}_t$  are assumed to be uncorrelated with the initial state:

$$\mathbb{E}(\mathbf{w}_t \mathbf{x}_0^T) = \mathbf{0}, \quad \mathbb{E}(\mathbf{v}_t \mathbf{x}_0^T) = \mathbf{0} \quad \text{for all } t = 1, \dots, T. \quad (2.25)$$

The TFN model defined in Equation 2.14 can be written in the state space form of Equation 2.21 as a decoupled system describing a deterministic component and a stochastic component. The deterministic component was already given in Equations 2.19 and 2.20. Similarly, the stochastic component can be written as the following state space representation of an ARMA model:

$$\mathbf{x}_t = \mathbf{A}_s \mathbf{x}_{t-1} + \mathbf{g}_s w_t, \quad (2.26a)$$

$$y_t = \mathbf{c}_s^T \mathbf{x}_t, \quad (2.26b)$$

with

$$\mathbf{A}_s = \begin{bmatrix} \phi_1 & 1 & 0 & \cdots & 0 \\ \phi_2 & 0 & \ddots & \ddots & \vdots \\ \vdots & \vdots & \ddots & \ddots & 0 \\ \phi_{p-1} & \vdots & & \ddots & 1 \\ \phi_p & 0 & \cdots & \cdots & 0 \end{bmatrix}, \quad \mathbf{g}_s = \begin{bmatrix} 1 \\ -\theta_1 \\ \vdots \\ -\theta_{p-2} \\ -\theta_{p-1} \end{bmatrix}, \quad \mathbf{c}_s^T = \begin{bmatrix} 1 \\ 0 \\ \vdots \\ 0 \end{bmatrix}. \quad (2.27)$$

Combining the deterministic and stochastic component yields the state space representation of the TFN model:

$$\begin{bmatrix} \mathbf{x}_{d,t} \\ \mathbf{x}_{s,t} \end{bmatrix} = \begin{bmatrix} \mathbf{A}_d & 0 \\ 0 & \mathbf{A}_s \end{bmatrix} \begin{bmatrix} \mathbf{x}_{d,t-1} \\ \mathbf{x}_{s,t-1} \end{bmatrix} + \begin{bmatrix} \mathbf{b}_d \\ 0 \end{bmatrix} u_t + \begin{bmatrix} 0 \\ \mathbf{g}_s \end{bmatrix} w_t, \quad (2.28a)$$

$$y_t = \begin{bmatrix} \mathbf{c}_d & \mathbf{c}_s \end{bmatrix} \begin{bmatrix} \mathbf{x}_{d,t} \\ \mathbf{x}_{s,t} \end{bmatrix} + y_r + v_t, \quad (2.28b)$$

with  $\mathbf{x}_d$  and  $\mathbf{x}_s$  representing the deterministic and stochastic component, respectively,  $\mathbf{A}_d$ ,  $\mathbf{b}_d$ , and  $\mathbf{c}_d$  are defined as in Equation 2.20,  $\mathbf{A}_s$ ,  $\mathbf{g}_s$ , and  $\mathbf{c}_s$  are defined as in Equation 2.27,  $y_r$  denotes the reference level of  $y_t$ , and  $v_t$  is the measurement noise.

**Missing observations** Usually, groundwater head observations are spaced irregularly. For multiple-output systems this implies that the number of observations may vary over time. As a result, the dimension of the observation vector,  $m$ , becomes time variant:  $m_t$ . The observation matrix  $\mathbf{C}$  in Equation 2.21 then becomes a time-varying  $m_t \times n$  matrix, for  $m_t \geq 1$  [Harvey, 1989]:

$$\mathbf{C}_t = \mathbf{W}_t \mathbf{C}, \quad (2.29)$$

where  $\mathbf{W}_t$  is a  $m_t \times m$  matrix of fixed weights. For example, if there are  $m = 5$  time series and at time  $t$  only observations of the first and fourth series are available ( $m_t = 2$ ), then

$$\mathbf{W}_t = \begin{bmatrix} 1 & 0 & 0 & 0 & 0 \\ 0 & 0 & 0 & 1 & 0 \end{bmatrix}. \quad (2.30)$$

Similarly, the time-variant  $m_t \times m_t$  covariance matrix of measurement errors  $\mathbf{R}_t$  is written as

$$\mathbf{R}_t = \mathbf{W}_t \mathbf{R} \mathbf{W}_t^T. \quad (2.31)$$

## 2.5 Linear Kalman filtering

In general, the elements of the state vector  $\mathbf{x}_t$  are not observed directly. Consequently, the state vector needs to be estimated. On the assumption that the system matrices together with the initial conditions  $\mathbf{x}_0$  and  $\mathbf{P}_0$  are known, and given all measurements up to the present time, the most likely values of the state variables can be determined. The process of determining these most likely values is called smoothing, filtering, or prediction, depending on whether past, present, or future values of the state variables are found. In terms of conditional expectation, the estimation problem consists of computing and estimate of  $\mathbf{x}_t$  based on  $\mathbf{Y}_T = \{\mathbf{y}_1, \dots, \mathbf{y}_T\}$ , that is  $\hat{\mathbf{x}}_{t|T} = E(\mathbf{x}_t | \mathbf{Y}_T)$ . If  $t < T$ , the problem is called a

smoothing problem; if  $t = T$ , it is called a filtering problem; and if  $t > T$ , it is called a prediction problem. In this section, the filtering and prediction problems are treated. The smoothing problem is dealt with in Section 2.8.

A well-known and widely applied filtering algorithm is the Kalman filter, which was originally developed by *Kalman* [1960] and *Kalman and Bucy* [1961]. Roughly speaking, the Kalman filter combines the measurement data taken from the actual system with the information provided by the system model and the statistical description of uncertainties, in order to obtain an “optimal” estimate of the system state. Generally, the “optimality” of the estimate depends upon what performance criterion is chosen. A comprehensive discussion on optimality of the Kalman filter is found in e.g. *Jazwinsky* [1970, Ch. 7].

For an intuitive derivation of the Kalman filter, consider the linear time-invariant multiple-input multiple-output (MIMO) system model of Equation 2.21:

$$\begin{aligned}\mathbf{x}_t &= \mathbf{A}\mathbf{x}_{t-1} + \mathbf{B}\mathbf{u}_t + \mathbf{G}\mathbf{w}_t, \\ \mathbf{y}_t &= \mathbf{C}\mathbf{x}_t + \mathbf{v}_t,\end{aligned}$$

with initial conditions  $\mathbf{x}_0$  and  $\mathbf{P}_0$ , and where  $\mathbf{w}_t$  and  $\mathbf{v}_t$  are assumed to be mutually independent Gaussian random vector variables with properties as those defined in Equations 2.22 and 2.23. Since the expected value of  $\mathbf{w}_t$  is zero, the best estimate of  $\mathbf{x}_t$  is given by

$$\hat{\mathbf{x}}_{t|t-1} = \mathbf{A}\hat{\mathbf{x}}_{t-1|t-1} + \mathbf{B}\mathbf{u}_t. \quad (2.32)$$

Here,  $\hat{\mathbf{x}}_{t-1|t-1}$  denotes the estimate of  $\mathbf{x}$  at time  $t-1$ , based on the information available at time  $t-1$ . The estimation error  $\tilde{\mathbf{x}}_{t|t-1}$  is

$$\tilde{\mathbf{x}}_{t|t-1} = \mathbf{A}\tilde{\mathbf{x}}_{t-1|t-1} + \mathbf{G}\mathbf{w}_t. \quad (2.33)$$

The accuracy of  $\hat{\mathbf{x}}_{t|t-1}$  is given by the covariance matrix of the estimation error:

$$\begin{aligned}\mathbf{P}_{t|t-1} &= \mathbf{E}(\tilde{\mathbf{x}}_{t|t-1}\tilde{\mathbf{x}}_{t|t-1}^T) \\ &= \mathbf{E}\left(\mathbf{A}\tilde{\mathbf{x}}_{t-1|t-1}\tilde{\mathbf{x}}_{t-1|t-1}^T\mathbf{A}^T + \mathbf{G}\mathbf{w}_t\mathbf{w}_t^T\mathbf{G}^T\right) \\ &= \mathbf{A}\mathbf{P}_{t-1|t-1}\mathbf{A}^T + \mathbf{G}\mathbf{Q}\mathbf{G}^T.\end{aligned} \quad (2.34)$$

A measurement  $\mathbf{y}_t$  has now been obtained. At this moment, two estimates of  $\mathbf{x}_t$  are available:  $\hat{\mathbf{x}}_{t|t-1}$ , which is the best what could be obtained before carrying out the measurement, and  $\mathbf{y}_t$ , which is the best what can be achieved when considering only the measurement. A reasonable estimate would combine these two estimates as follows:

$$\hat{\mathbf{x}}_{t|t} = [\mathbf{I} - \mathbf{K}_t\mathbf{C}]\hat{\mathbf{x}}_{t|t-1} + \mathbf{K}_t\mathbf{y}_t, \quad (2.35)$$

where  $\mathbf{K}_t$  is a weighting matrix referred to as the filter gain or Kalman gain. Similar to Equation 2.34, the error covariance matrix of  $\hat{\mathbf{x}}_{t|t}$  is written as

$$\mathbf{P}_{t|t} = [\mathbf{I} - \mathbf{K}_t\mathbf{C}]\mathbf{P}_{t|t-1}[\mathbf{I} - \mathbf{K}_t\mathbf{C}]^T + \mathbf{K}_t\mathbf{R}\mathbf{K}_t^T. \quad (2.36)$$

When choosing  $\mathbf{K}_t$ , it is necessary to consider how much weight is given to  $\mathbf{y}_t$  and how much to  $\hat{\mathbf{x}}_{t|t-1}$ . It makes sense to attribute more weight to the more accurate of these two estimates. This is what guides the optimal choice of the matrix  $\mathbf{K}_t$  provided by the Kalman filter. It can be proven that the optimal choice of  $\mathbf{K}_t$ , which ensures that the filter is of minimum variance, is given by [Jazwinsky, 1970]

$$\mathbf{K}_t = \mathbf{P}_{t|t-1} \mathbf{C}^T [\mathbf{C} \mathbf{P}_{t|t-1} \mathbf{C}^T + \mathbf{R}]^{-1}. \quad (2.37)$$

Substituting for  $\mathbf{K}_t$  in Equation 2.36 results in

$$\mathbf{P}_{t|t} = [\mathbf{I} - \mathbf{K}_t \mathbf{C}] \mathbf{P}_{t|t-1}. \quad (2.38)$$

which is the covariance matrix of filtering errors obtained by using the value of  $\mathbf{K}_t$  given by Equation 2.37.

Equation 2.35 can also be written as

$$\begin{aligned} \hat{\mathbf{x}}_{t|t} &= \hat{\mathbf{x}}_{t|t-1} + \mathbf{K}_t [\mathbf{y}_t - \mathbf{C} \hat{\mathbf{x}}_{t|t-1}], \\ &= \hat{\mathbf{x}}_{t|t-1} + \mathbf{K}_t \boldsymbol{\nu}_t, \end{aligned} \quad (2.39)$$

where

$$\boldsymbol{\nu}_t = \mathbf{y}_t - \mathbf{C} \hat{\mathbf{x}}_{t|t-1} \quad (2.40)$$

is known as the vector of innovations, since the elements of  $\boldsymbol{\nu}_t$  represent the new information contained in  $\mathbf{y}_t$ . The covariance matrix of innovations is written as follows:

$$\mathbf{F}_t = \mathbf{C} \mathbf{P}_{t|t-1} \mathbf{C}^T + \mathbf{R}. \quad (2.41)$$

Using Equation 2.41, the Kalman gain in Equation 2.37 can be conveniently written as

$$\mathbf{K}_t = \mathbf{P}_{t|t-1} \mathbf{C}^T \mathbf{F}_t^{-1}. \quad (2.42)$$

Given the initial conditions, the Kalman filter delivers the optimal estimator of the state vector as each new measurement becomes available. When all measurements have been processed, the filter yields the optimal estimator of the current state vector and contains all the information needed to make optimal predictions of future values of both the state and the observations. The Kalman filter recursions are summarized in Equation 2.43. Figure 2.3 illustrates graphically the evolution of the density function for the update step of the Kalman filter. Finally, note that if the Gaussian assumptions are dropped, the recursions given in Equation 2.43 are still optimal in the sense that they provide a linear unbiased minimum variance estimate.

### The linear Kalman filter

The optimal state estimate is **propagated** from measurement time  $t - 1$  to measurement time  $t$  by the relations

$$\hat{\mathbf{x}}_{t|t-1} = \mathbf{A}\hat{\mathbf{x}}_{t-1|t-1} + \mathbf{B}\mathbf{u}_t, \quad (2.43a)$$

$$\mathbf{P}_{t|t-1} = \mathbf{A}\mathbf{P}_{t-1|t-1}\mathbf{A}^T + \mathbf{G}\mathbf{Q}\mathbf{G}^T. \quad (2.43b)$$

At time  $t$ , the measurement  $\mathbf{y}_t$  becomes available. The estimate is **updated** by defining the Kalman filter gain and employing it in both mean and covariance relations:

$$\boldsymbol{\nu}_t = \mathbf{y}_t - \mathbf{C}\hat{\mathbf{x}}_{t|t-1}, \quad (2.43c)$$

$$\mathbf{F}_t = \mathbf{C}\mathbf{P}_{t|t-1}\mathbf{C}^T + \mathbf{R}, \quad (2.43d)$$

$$\mathbf{K}_t = \mathbf{P}_{t|t-1}\mathbf{C}^T\mathbf{F}_t^{-1}, \quad (2.43e)$$

$$\hat{\mathbf{x}}_{t|t} = \hat{\mathbf{x}}_{t|t-1} + \mathbf{K}_t\mathbf{n}_t, \quad (2.43f)$$

$$\mathbf{P}_{t|t} = [\mathbf{I} - \mathbf{K}_t\mathbf{C}]\mathbf{P}_{t|t-1}. \quad (2.43g)$$

If at time  $t$  no measurement is available, the Kalman filter updating equations are skipped:

$$\hat{\mathbf{x}}_{t|t} = \hat{\mathbf{x}}_{t|t-1} \quad \text{and} \quad \mathbf{P}_{t|t} = \mathbf{P}_{t|t-1}.$$

The initial conditions for the recursion are given by  $\hat{\mathbf{x}}_{0|0} = \boldsymbol{\chi}_0$  and  $\mathbf{P}_{0|0} = \mathbf{P}_0$ .

## 2.6 Nonlinear modeling and filtering

This section discusses the estimation problem involving systems for which a linear model does not provide a valid description. In other words, nonlinearities in the system dynamics are not negligible anymore. For this reason, the dynamics will be described by the following nonlinear stochastic difference equation:

$$\mathbf{x}_t = \mathcal{F}[\mathbf{x}_{t-1}, \mathbf{u}_t, t] + \mathbf{G}_t\mathbf{w}_t, \quad (2.44a)$$

$$\mathbf{y}_t = \mathbf{C}\mathbf{x}_t + \mathbf{v}_t, \quad (2.44b)$$

where  $\mathcal{F}[\cdot, \cdot, \cdot]$  is a known  $n$ -dimensional vector of functions of state, input and time,  $\mathbf{u}_t$  is an  $r$ -dimensional input vector, and  $\mathbf{w}_t$  is a zero-mean white Gaussian noise process. Equation 2.44 can be viewed as a generalization of the linear model of Equation 2.21, replacing  $[\mathbf{A}\mathbf{x}_t + \mathbf{B}\mathbf{u}_t]$  by  $\mathcal{F}[\mathbf{x}_{t-1}, \mathbf{u}_t, t]$ . From now on, the time argument  $t$  is omitted for convenience of notation.

The theory of nonlinear filtering is much more complex than that of linear filtering. As *Maybeck* [1982] points out, propagating and updating an entire density function for the state conditioned on observed measurements is not implementable. To obtain practically feasible algorithms, one needs expansions truncated to some low order. This section only presents two first-order filters: the extended Kalman filter and the truncated first-order filter. Both filters will be given without any fur-

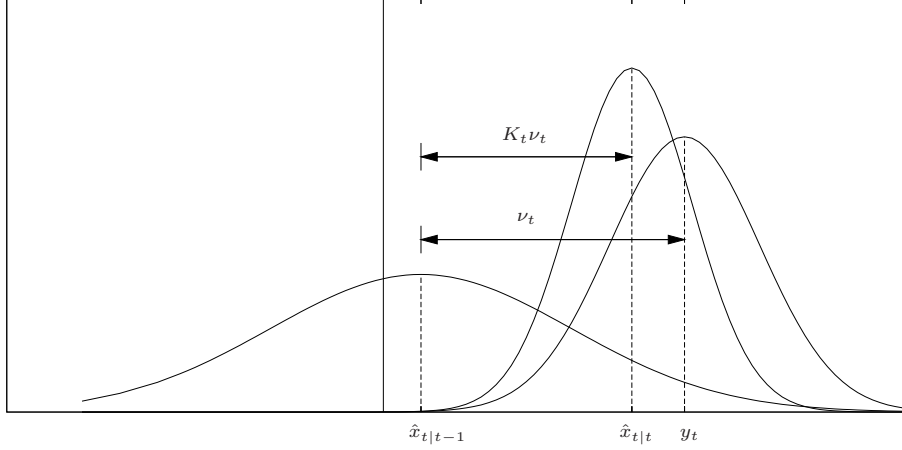


**Figure 2.3:** Density functions of propagated state estimate  $\hat{x}_{t|t-1}$  with variance  $P_{t|t-1}$ , measurement  $y_t$  with variance  $R$ , and updated state estimate  $\hat{x}_{t|t} = \hat{x}_{t|t-1} + K_t \nu_t$  with variance  $P_{t|t}$

ther proof. The reader is referred to Jazwinsky [1970] and Maybeck [1982] for a comprehensive discussion on nonlinear filtering.

**Extended Kalman filter** If the nonlinear function  $\mathcal{F}[\mathbf{x}_{t-1}, \mathbf{u}_t]$  of Equation 2.44 is sufficiently smooth, it can be expanded in Taylor series about the conditional mean, i.e.,  $\hat{\mathbf{x}}_{t-1|t-1}$ :

$$\mathcal{F}[\mathbf{x}_{t-1}, \mathbf{u}_t] = \mathcal{F}[\hat{\mathbf{x}}_{t-1|t-1}, \mathbf{u}_t] + \frac{\partial \mathcal{F}[\mathbf{x}, \mathbf{u}_t]}{\partial \mathbf{x}} (\mathbf{x}_{t-1} - \hat{\mathbf{x}}_{t-1|t-1}) + \dots \quad (2.45)$$

with the derivative evaluated at  $\mathbf{x} = \hat{\mathbf{x}}_{t-1|t-1}$ . Equation 2.45 is a reasonable approximation as long as the deviations from  $\hat{\mathbf{x}}_{t-1|t-1}$  are small enough for the higher-order terms to be negligible. The well-known extended Kalman filter is based on this first-order approximation. Maybeck [1982, Ch. 9] describes this nonlinear filter in detail, showing that it differs from the linear Kalman filter only in the time propagation:

$$\hat{\mathbf{x}}_{t|t-1} = \mathcal{F}[\hat{\mathbf{x}}_{t-1|t-1}, \mathbf{u}_t], \quad (2.46a)$$

$$\mathbf{P}_{t|t-1} = \frac{\partial \mathcal{F}[\mathbf{x}, \mathbf{u}_t]}{\partial \mathbf{x}} \mathbf{P}_{t-1|t-1} \frac{\partial \mathcal{F}^T[\mathbf{x}, \mathbf{u}_t]}{\partial \mathbf{x}} + \mathbf{G} \mathbf{Q} \mathbf{G}^T, \quad (2.46b)$$

with the derivative evaluated at  $\mathbf{x} = \hat{\mathbf{x}}_{t-1|t-1}$ . The update equations are identical to those of the linear filter (Equations 2.43c – 2.43g).

**Truncated first-order filter** If  $\mathbf{G}_t$  is allowed to be a function of state as well, then Equation 2.44a may be written as

$$\mathbf{x}_t = \mathcal{F}[\mathbf{x}_{t-1}, \mathbf{u}_t] + \mathcal{G}[\mathbf{x}_t] \mathbf{w}_t, \quad (2.47)$$

with  $\mathcal{G}[\cdot]$  a function of state. For this model, the time propagation is given by the truncated first-order filter [Maybeck, 1982, Ch. 12], introducing an additional term beyond the computations of the extended Kalman filter (Equation 2.46b):

$$\hat{\mathbf{x}}_{t|t-1} = \mathcal{F}[\hat{\mathbf{x}}_{t-1|t-1}, \mathbf{u}_t], \quad (2.48a)$$

$$\begin{aligned} \mathbf{P}_{t|t-1} = & \frac{\partial \mathcal{F}[\mathbf{x}, \mathbf{u}_t]}{\partial \mathbf{x}} \mathbf{P}_{t-1|t-1} \frac{\partial \mathcal{F}^T[\mathbf{x}, \mathbf{u}_t]}{\partial \mathbf{x}} + \mathcal{G}[\hat{\mathbf{x}}_{t-1|t-1}] \mathbf{Q} \mathcal{G}^T[\hat{\mathbf{x}}_{t-1|t-1}] \\ & + \text{tr} \left\{ \frac{\partial \mathcal{G}[\mathbf{x}]}{\partial \mathbf{x}} \mathbf{Q} \frac{\partial \mathcal{G}^T[\mathbf{x}]}{\partial \mathbf{x}} \mathbf{P}_{t-1|t-1} \right\}. \end{aligned} \quad (2.48b)$$

**Evaluation of filter performance** First-order linearization of the nonlinear model is only useful for weakly nonlinear models. When nonlinearities are strong, a truncated second-order filter outperforms a first-order filter. This is primarily due to the fact that the second-order filter introduces a “bias correction term” in the time propagation of the state estimate:

$$\hat{\mathbf{x}}_{t|t-1} = \mathcal{F}[\hat{\mathbf{x}}_{t-1|t-1}, \mathbf{u}_t] + \frac{1}{2} \frac{\partial^2 \mathcal{F}}{\partial \mathbf{x}^2} \mathbf{P}_{t|t}. \quad (2.49)$$

Ignoring this term generally results in a more biased estimate.

In order to quantify the relative importance of the bias, Verlaan and Heemink [2001] propose the following nondimensional number:

$$V \equiv \sqrt{N^{-1} \mathbf{b}^T \mathbf{P}^{-1} \mathbf{b}}, \quad (2.50)$$

where  $N$  is the number of observations and  $\mathbf{b}$  is the bias of the first-order filter. The time propagation and measurement update for the bias are given by

$$\hat{\mathbf{b}}_{t|t-1} = \frac{\partial \mathcal{F}}{\partial \mathbf{x}} \hat{\mathbf{b}}_{t|t} + \frac{\partial^2 \mathcal{F}}{\partial \mathbf{x}^2} \mathbf{P}_{t|t}, \quad (2.51)$$

$$\hat{\mathbf{b}}_{t|t} = [\mathbf{I} - \mathbf{K}_t \mathbf{C}] \hat{\mathbf{b}}_{t|t-1}, \quad (2.52)$$

with initial condition  $\hat{\mathbf{b}}_{0|0} = 0$ . It is likely that the bias is insignificant if  $V \ll 1$ . In that case, the second-order filter will produce similar results as the first-order filter, and one may expect the first-order filter to perform well.

## 2.7 Parameter estimation

In order to fit a state space model to a given time series, one needs to estimate the unknown parameters in the system matrices. The vector of these parameters will be denoted by the  $N_\alpha$ -dimensional vector  $\alpha$  and can be estimated by maximum likelihood. The output of the Kalman filter makes it possible to evaluate the log likelihood function via the prediction error decomposition for given  $\alpha$ .

The Gaussian log likelihood function for a linear state space model (Equation 2.21) is given by [Schweppe, 1973]

$$\log \mathcal{L} = -\frac{N}{2} \log 2\pi - \frac{1}{2} \sum_{t=1}^T \log |\mathbf{F}_t| - \frac{1}{2} \sum_{t=1}^T \boldsymbol{\nu}_t^T \mathbf{F}_t^{-1} \boldsymbol{\nu}_t, \quad (2.53)$$

where  $N$  is the total number of observations, and  $\boldsymbol{\nu}_t$  and  $\mathbf{F}_t$  are defined in Equation 2.43c and 2.43d, respectively. Note that the likelihood function is only evaluated for time instants  $t = 1, \dots, T$ , where measurements are actually available. Although the likelihood function only provides a maximum likelihood estimate of the parameters if the state equation is linear, Equation 2.53 can still be used to obtain approximate maximum likelihood estimates when the state equation is nonlinear [Bierkens, 1998].

A basic assumption in the derivation of the Kalman filter is that the initial state vector and associated error covariance matrix are known. However, this is generally not the case. There are several ways to define the initial conditions [e.g. Gardner *et al.*, 1980; De Jong, 1988; Koopman and Durbin, 2000]. A simple but effective initialization is to let  $\mathbf{P}_0$  be a diagonal matrix of relatively large values (relative to  $\mathbf{x}_0$ ), representing a high level of uncertainty in the initial estimate. In this way, the first few measurements are used to “update” the initial state vector. Janacek and Swift [1993] show that the first  $n$  measurements are needed for this “update”, with  $n$  the dimension of the state vector. Hence, the first  $n$  innovations and their associated covariance matrices must not be included in the likelihood function.

Generally, the dimension of the parameter space can be reduced by exploiting any linearities in the likelihood function. For instance, Harvey [1989] shows how a univariate model can be reparameterized so that the number of unknown parameters reduces with one.

Maximization of Equation 2.53 (or minimization of  $-2 \log \mathcal{L}$ ) with respect to  $\boldsymbol{\alpha}$  is carried out by an optimization procedure as represented schematically in Figure 2.4. The model parameters are updated using a quasi-Newton algorithm [Gill *et al.*, 1981] with finite difference approximations of the gradient of the likelihood function. Since this method requires  $N_\alpha + 1$  mutually independent runs of the Kalman filter, the optimization procedure is very suitable for parallel computing, speeding up the procedure by a factor that is approximately proportional to the number of computer processors. If parallel computing is not possible and computational costs are important, other optimization procedures may be more appropriate.

An alternative approach to the quasi-Newton algorithm is the variational or adjoint method [Bryson and Ho, 1975; Bennett *et al.*, 1996]. This method calculates the exact gradient, rather than obtaining the gradient with finite difference approximations. The adjoint method requires only one forward run and one backward run.

A derivative-free method that does not require evaluation of the likelihood function is the EM (expectation maximization) algorithm of Dempster *et al.* [1977].



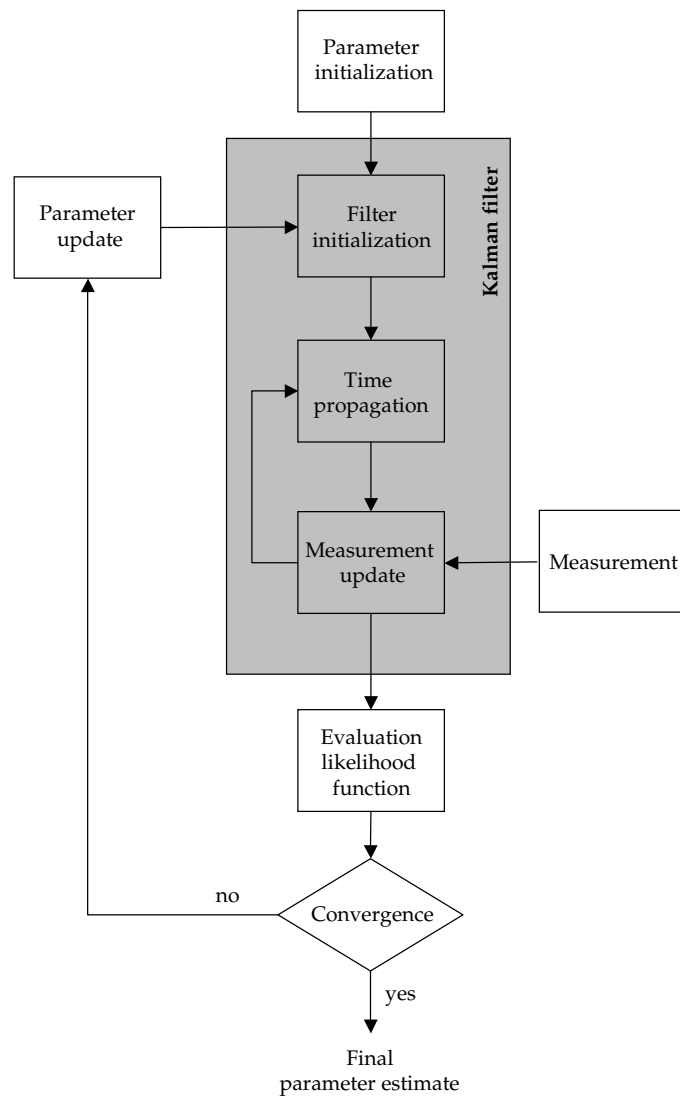


**Figure 2.4:** Flowchart of the optimization procedure; innovations obtained from the Kalman filter are evaluated using the log likelihood function

Basically, the procedure consists of two steps: an estimation and a maximization step, which are iterated to convergence. The maximization step calculates the maximum likelihood estimates of all unknown parameters conditional on a full data set. The estimation step constructs estimates of the statistics of the problem conditional on the observed data and the parameters. More details on this algorithm and its implementation can be found in *Wu et al.* [1996] and in *Shumway and Stoffer* [1982, 2000].

The accuracy of parameter estimates is expressed by the covariance matrix of the estimates. For a large amount of measurements, the maximum likelihood estimator is asymptotically efficient, in the sense that the bias of the estimate approaches zero and the covariance of the estimate approaches the Cramer-Rao lower bound, which equals the inverse of the second-order derivative of the likelihood function with respect to the parameters [*Kendall and Stuart*, 1979]:

$$R_C^{-1} = \frac{\partial^2 \log \mathcal{L}}{\partial \alpha \partial \alpha^T}, \quad (2.54)$$

where  $R_C$  is the Cramer-Rao lower bound. The second-order derivatives are approximated by finite differences.

## 2.8 Smoothing

In the filtering problem, the optimal estimate of the state at time  $t$  is based upon the knowledge of all measurements taken up to time  $t$ . However, a more accurate estimate of the state  $\mathbf{x}_t$  can be produced if at later time steps measurements are also available. The additional information contained in the measurements taken after time  $t$  can be exploited to provide this improvement in estimation accuracy. An estimate of  $\mathbf{x}_t$  based on all available information up to time  $T$  ( $T > t$ ), is referred to as the smoothed estimate of  $\mathbf{x}_t$ . There are basically three classes of smoothing algorithms: fixed-point smoothing, fixed-lag smoothing and fixed-interval smoothing.

Fixed-point smoothing is concerned with computing smoothed estimates of the state vector at some fixed point in time. For example, there may be a certain point in time at which the value of the system state is considered critical. Thus, one would desire an estimate of  $\mathbf{x}_t$  for fixed  $t$ , conditioned on more and more data as measurements become available:  $\hat{\mathbf{x}}_{t|s} = E(\mathbf{x}_t | \mathbf{Y}_s)$ , with  $s = t, t+1, \dots, T$ .

Fixed-lag smoothing computes smoothed estimates for a fixed delay. Thus, one is willing to delay the computation of the estimate of  $\mathbf{x}_t$  until  $t+s$ , where  $s$  is a fixed integer, to take advantage of additional information in these  $s$  measurements:  $\hat{\mathbf{x}}_{t|t+s} = E(\mathbf{x}_t | \mathbf{Y}_{t+s})$ , with  $t = 0, 1, \dots, T-s$ . Both of these algorithms can be applied in online situations.

Fixed-interval smoothing is concerned with computing smoothed estimates for a fixed span of data:  $\hat{\mathbf{x}}_{t|T} = E(\mathbf{x}_t | \mathbf{Y}_T)$ , with  $t = 0, 1, \dots, T$ . Hence it is an off-line technique which is used to obtain refined state estimates of better quality than that provided by online filters.

In this thesis, the fixed-interval smoother (FIS) is applied for interpolation over gaps in the data, as well as for extraction of estimated components such as trends. In addition, smoothed estimates of the initial state vector are obtained here in order to present model predictions of the calibrated model in a simple forecast mode (i.e. without Kalman filtering). It must be noticed that smoothing does not lead to better parameter estimates [Bryson and Frazier, 1962]. Hence, the FIS algorithm is applied merely as a post-processor of the optimization procedure in Figure 2.4.

There is a variety of FIS algorithms. The one considered here utilizes a backward filter, subsequent to application of the Kalman filter forward recursion of Equation 2.43 [Fraser and Potter, 1969]. The forward filter produces a state estimate  $\hat{\mathbf{x}}_{t|t}$  and error covariance  $\mathbf{P}_{t|t}$ . Let  $\hat{\mathbf{x}}_{b,t|t+1}$  and  $\mathbf{P}_{b,t|t+1}$  denote the state estimate and error covariance before incorporating measurement  $\mathbf{y}_t$  into the backward filter, respectively, and let  $\hat{\mathbf{x}}_{b,t|t}$  and  $\mathbf{P}_{b,t|t}$  be analogous quantities after incorporation. Because the backward filter is of inverse covariance form [Maybeck, 1979], it actually incorporates  $\mathbf{y}_t$  to generate  $\mathbf{P}_{b,t|t}^{-1}$  and  $\hat{\mathbf{z}}_{b,t|t} = \mathbf{P}_{b,t|t}^{-1} \hat{\mathbf{x}}_{b,t|t}$ , and then propagate backward in time to form  $\mathbf{P}_{b,t-1|t}^{-1}$  and  $\hat{\mathbf{z}}_{b,t-1|t} = \mathbf{P}_{b,t-1|t}^{-1} \hat{\mathbf{x}}_{b,t-1|t}$ .

The smoothed estimate of  $\mathbf{x}_t$ ,  $\hat{\mathbf{x}}_{t|T}$ , is generated by optimally combining the value of  $\hat{\mathbf{x}}_{t|t}$  from the forward filter and  $\hat{\mathbf{x}}_{b,t|t+1}$  from the backward filter. An optimal combination is accomplished by viewing  $\hat{\mathbf{x}}_{t|t}$  and  $\hat{\mathbf{x}}_{b,t|t+1}$  as two separate “observations” of  $\mathbf{x}_t$  and assigning relative weights according to their accuracy, indicated by  $\mathbf{P}_{t|t}$  and  $\mathbf{P}_{b,t|t+1}$ , respectively:

$$\begin{aligned} \hat{\mathbf{x}}_{t|T} &= \mathbf{P}_{t|T} \left[ \mathbf{P}_{t|t}^{-1} \hat{\mathbf{x}}_{t|t} + \mathbf{P}_{b,t|t+1}^{-1} \hat{\mathbf{x}}_{b,t|t+1} \right], \\ &= \mathbf{P}_{t|T} \left[ \mathbf{P}_{t|t}^{-1} \hat{\mathbf{x}}_{t|t} + \hat{\mathbf{z}}_{b,t|t+1} \right], \end{aligned} \quad (2.55)$$

$$\mathbf{P}_{t|T}^{-1} = \mathbf{P}_{t|t}^{-1} + \mathbf{P}_{b,t|t+1}^{-1}, \quad (2.56)$$

where  $\mathbf{P}_{t|T}$  is the smoothed error covariance matrix. Equation 2.56 indicates that

$$\mathbf{P}_{t|T} \leq \mathbf{P}_{t|t},$$

that is, the smoothed estimate is at least as good as the filtered estimate for all time. Figure 2.5 illustrates the difference between filtered and smoothed estimates.

Algebraic manipulation of Equations 2.55 and 2.56 yields a computationally efficient form to obtain smoothed estimates of  $\mathbf{x}_t$  and  $\mathbf{P}_t$ . First, the forward filter of Equation 2.43 is applied for  $t = 1, 2, \dots, T$  to produce  $\hat{\mathbf{x}}_{t|t}$  and  $\mathbf{P}_{t|t}$ . Subsequently, the inverse-covariance backward filter is applied for  $t = T, T-1, \dots, 2$ , with initial conditions

$$\hat{\mathbf{z}}_{b,T|T+1} = 0 \text{ and } \mathbf{P}_{b,T|T+1}^{-1} = 0. \quad (2.57)$$

Measurement updates are generated by

$$\hat{\mathbf{z}}_{b,t|t} = \hat{\mathbf{z}}_{b,t|t+1} + \mathbf{C}^T \mathbf{R}^{-1} \mathbf{y}_t, \quad (2.58a)$$

$$\mathbf{P}_{b,t|t}^{-1} = \mathbf{P}_{b,t|t+1}^{-1} + \mathbf{C}^T \mathbf{R}^{-1} \mathbf{C}. \quad (2.58b)$$

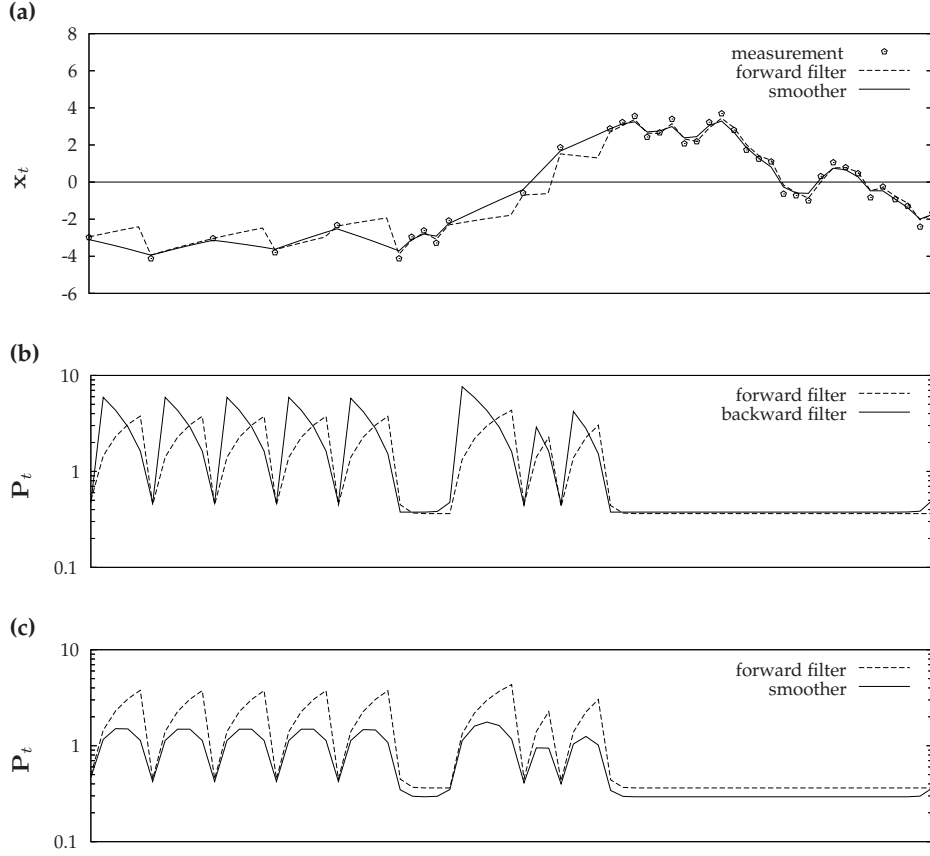


**Figure 2.5:** Typical smoothing problem; (a) unequally spaced measurements together with filtered estimate and smoothed estimate; (b) mean square estimation error of forward filter and backward filter; (c) mean square estimation error of forward filter and smoother

If no measurement is available, then

$$\hat{\mathbf{z}}_{b,t|t} = \hat{\mathbf{z}}_{b,t+1}, \quad (2.58c)$$

$$\mathbf{P}_{b,t|t}^{-1} = \mathbf{P}_{b,t+1}^{-1}. \quad (2.58d)$$

The estimate is propagated backward in time to the preceding measurement time via

$$\mathbf{J}_t = \mathbf{P}_{b,t|t}^{-1} \mathbf{G} \left[ \mathbf{G}^T \mathbf{P}_{b,t|t}^{-1} \mathbf{G} + \mathbf{Q}^{-1} \right]^{-1}, \quad (2.58e)$$

$$\mathbf{L}_t = \mathbf{I} - \mathbf{J}_t \mathbf{G}^T, \quad (2.58f)$$

$$\hat{\mathbf{z}}_{b,t-1|t} = \mathbf{A}^T \mathbf{L}_t \left[ \hat{\mathbf{z}}_{b,t|t} - \mathbf{P}_{b,t|t}^{-1} \mathbf{B} \mathbf{u}_{t-1} \right], \quad (2.58g)$$

$$\mathbf{P}_{b,t-1|t}^{-1} = \mathbf{A}^T \left[ \mathbf{L}_t \mathbf{P}_{b,t|t}^{-1} \mathbf{L}_t^T + \mathbf{J}_t \mathbf{Q}^{-1} \mathbf{J}_t^T \right] \mathbf{A}, \quad (2.58h)$$

where  $\mathbf{J}_t$  and  $\mathbf{L}_t$  are dummy matrices. At time  $t$ , the smoothed estimate is obtained by combining  $\hat{\mathbf{x}}_{t|t}$ ,  $\mathbf{P}_{t|t}$ ,  $\hat{\mathbf{z}}_{b,t|t+1}$  and  $\mathbf{P}_{b,t|t+1}^{-1}$  through

$$\mathbf{X}_t = \left[ \mathbf{I} + \mathbf{P}_{t|t} \mathbf{P}_{b,t|t+1}^{-1} \right]^{-1}, \quad (2.58i)$$

$$\mathbf{W}_t = \mathbf{P}_{t|t} \mathbf{X}_t^T, \quad (2.58j)$$

$$\mathbf{Y}_t = \mathbf{I} - \mathbf{W}_t \mathbf{P}_{b,t|t+1}^{-1}, \quad (2.58k)$$

$$\mathbf{P}_{t|T} = \mathbf{Y}_t \mathbf{P}_{t|t} \mathbf{Y}_t^T + \mathbf{W}_t \mathbf{P}_{b,t|t+1}^{-1} \mathbf{W}_t^T, \quad (2.58l)$$

$$\hat{\mathbf{x}}_{t|T} = \mathbf{X}_t \hat{\mathbf{x}}_{t|t} + \mathbf{P}_{t|T} \hat{\mathbf{z}}_{b,t|t+1}, \quad (2.58m)$$

with  $\mathbf{X}_t$ ,  $\mathbf{W}_t$  and  $\mathbf{Y}_t$  as dummy matrices.

For the nonlinear model of Equation 2.44, a smoothed estimate can be obtained by a run of the EKF (Equation 2.46) and a subsequent run of the following backward filter running from  $t = T, \dots, 1$ , with initial conditions of the Lagrange multipliers  $\lambda_T = 0$  and  $\Lambda_T = 0$  [Bryson and Ho, 1975; Krishnamurthy and Johnston, 1999]:

$$\hat{\mathbf{x}}_{t|T} = \hat{\mathbf{x}}_{t|t} - \mathbf{P}_{t|t} \frac{\partial \mathcal{F}^T}{\partial \mathbf{x}} \lambda_t, \quad (2.59a)$$

$$\lambda_{t-1} = (\mathbf{I} - \mathbf{P}_{t|t} \mathbf{S})^T \left[ \frac{\partial \mathcal{F}^T}{\partial \mathbf{x}} \lambda_t - \mathbf{C}^T \mathbf{R}^{-1} \nu_t \right], \quad (2.59b)$$

$$\mathbf{P}_{t|T} = \mathbf{P}_{t|t} - \mathbf{P}_{t|t} \frac{\partial \mathcal{F}^T}{\partial \mathbf{x}} \Lambda_t \frac{\partial \mathcal{F}}{\partial \mathbf{x}} \mathbf{P}_{t|t}, \quad (2.59c)$$

$$\Lambda_{t-1} = (\mathbf{I} - \mathbf{P}_{t|t} \mathbf{S})^T \frac{\partial \mathcal{F}^T}{\partial \mathbf{x}} \Lambda_t \frac{\partial \mathcal{F}}{\partial \mathbf{x}} (\mathbf{I} - \mathbf{P}_{t|t} \mathbf{S}) + \mathbf{S} (\mathbf{I} - \mathbf{P}_{t|t} \mathbf{S}), \quad (2.59d)$$

with  $\mathbf{S} = \mathbf{C}^T \mathbf{R}^{-1} \mathbf{C}$  and  $\nu_t$  the innovation vector defined in Equation 2.43c.



# 3

## Decoupling of modeling and measuring interval

---

**Abstract.** A state space representation of the transfer function-noise (TFN) model allows the choice of a modeling (input) interval that is smaller than the measuring interval of the output variable. Since in geohydrological applications the interval of the available input series (precipitation excess) is often smaller than the interval of the output series (groundwater head), the state space model opens the way to a more detailed description of the system. This chapter evaluates the influence of the reduction of the modeling interval on the performance of the state space model while keeping the measuring interval fixed. In order to obtain general conclusions of the relation between the modeling interval and the model performance, a large number of groundwater time series are generated and modeled with the state space model. The results show that a reduction of the modeling interval noticeably improves the model performance. The degree of improvement depends on aspects like the response time of the system, the length of the time series and the amount of noise. A case study illustrates the effect of reducing the modeling interval as well as that of adding high-frequency measurements to the time series.

---

*This chapter is adapted from Berendrecht, W.L., A.W. Heemink, F.C. van Geer, and J.C. Gehrels, Decoupling of modeling and measuring interval in groundwater time series analysis based on response characteristics, Journal of Hydrology, 278, 1–16, 2003*

THE STATE SPACE APPROACH described in the previous chapter allows for decoupling of the modeling interval – being equal to the interval of the input series – and the measuring interval, i.e, the interval of the output series. As a consequence, high-frequency input data of precipitation and evaporation, which are generally widely available, can be used to obtain more accurate estimates of groundwater fluctuations. In the Netherlands, for example, groundwater head is measured bimonthly on the 14th and 28th of each month. This means that the measuring interval varies between 14 and 17 days. Applying a state space model, the modeling interval can be set to 1 day and the groundwater time series can be modeled more accurately.

The objective of this chapter is to determine the influence of a reduction of the modeling interval on the performance of the state space model. In this context, performance is defined as how well the transfer function can be estimated and hence the fluctuations caused by the input series can be filtered out of the output series. For this purpose a large number of representative time series are generated, using a range of predefined transfer functions. Also, a stochastic component is added to the series to make the time series similar to real groundwater time series. Evaluation of the calibrated time series models for different measuring and modeling intervals shows that a reduction of the modeling interval generally improves the model. The rate of improvement depends on several variables, such as the system noise and the response time of the system. A real-world model of irregularly observed groundwater head data illustrates and confirms these results.

### 3.1 Modeling framework

This section briefly describes the modeling framework that is used in the experiments presented in Section 3.2. A state space form of the TFN model is applied to describe the groundwater system (see also Equation 2.28):

$$\begin{bmatrix} \mathbf{x}_{d,t} \\ \mathbf{x}_{s,t} \end{bmatrix} = \begin{bmatrix} \mathbf{A}_d & 0 \\ 0 & \mathbf{A}_s \end{bmatrix} \begin{bmatrix} \mathbf{x}_{d,t-1} \\ \mathbf{x}_{s,t-1} \end{bmatrix} + \begin{bmatrix} \mathbf{b}_d \\ 0 \end{bmatrix} u_t + \begin{bmatrix} 0 \\ \mathbf{g}_s \end{bmatrix} w_t, \quad (3.1a)$$

$$y_t = \begin{bmatrix} \mathbf{c}_d & \mathbf{c}_s \end{bmatrix} \begin{bmatrix} \mathbf{x}_{d,t} \\ \mathbf{x}_{s,t} \end{bmatrix} + y_r + v_t, \quad (3.1b)$$



with

$$\mathbf{A}_d = \begin{bmatrix} \delta_1 & 1 & 0 & \cdots & 0 \\ \delta_2 & 0 & \ddots & \ddots & \vdots \\ \vdots & \vdots & \ddots & \ddots & 0 \\ \delta_{r-1} & \vdots & & \ddots & 1 \\ \delta_r & 0 & \cdots & \cdots & 0 \end{bmatrix}, \mathbf{b}_d = \begin{bmatrix} \omega_0 \\ -\omega_1 \\ \vdots \\ -\omega_{r-2} \\ -\omega_{r-1} \end{bmatrix}, \mathbf{c}_d = \begin{bmatrix} 1 & 0 & \cdots & 0 \end{bmatrix}, \quad (3.2)$$

$$\mathbf{A}_s = \begin{bmatrix} \phi_1 & 1 & 0 & \cdots & 0 \\ \phi_2 & 0 & \ddots & \ddots & \vdots \\ \vdots & \vdots & \ddots & \ddots & 0 \\ \phi_{p-1} & \vdots & & \ddots & 1 \\ \phi_p & 0 & \cdots & \cdots & 0 \end{bmatrix}, \mathbf{g}_s = \begin{bmatrix} 1 \\ -\theta_1 \\ \vdots \\ -\theta_{p-2} \\ -\theta_{p-1} \end{bmatrix}, \mathbf{c}_s = \begin{bmatrix} 1 & 0 & \cdots & 0 \end{bmatrix}. \quad (3.3)$$

The parameters in the system matrices are unknown and defined as follows:  $\delta_i$  and  $\omega_j$  represent, respectively, the  $i$ th autoregressive parameter and the  $j$ th moving average parameter of the transfer model,  $\phi_k$  and  $\theta_l$  represent, respectively, the  $k$ th autoregressive parameter and the  $l$ th moving average parameter of the noise model. This set of parameters together with the variance of the system noise  $q$ , and the reference level  $y_r$ , will be referred to as the parameter set  $\alpha$ . The variance of the measurement noise,  $r$ , is assumed to be known.

Calibration of the model is achieved by embedding the model in the linear Kalman filter of Equation 2.43 on page 37. The log likelihood function is then constructed from the innovations and innovation variances calculated by the Kalman filter. In order to reduce the number of parameters to be estimated, *Harvey* [1989] suggests multiplication of the variances in the model by a scaling factor. If the scaling variance is

$$\sigma_*^2 = \text{var}(w_t), \quad (3.4)$$

then  $r$  is scaled to

$$r_* = \frac{\text{var}(v_t)}{\sigma_*^2}, \quad (3.5)$$

and

$$q_* = \frac{\text{var}(w_t)}{\sigma_*^2} = 1. \quad (3.6)$$

As a result, the dimension of  $\alpha$  reduces by 1. Writing down the log likelihood in terms of these newly defined parameters gives

$$\log \mathcal{L} = -\frac{N-n}{2} \log 2\pi - \frac{N-n}{2} \log \sigma_*^2 - \frac{1}{2} \sum_{t=n+1}^N \log F_t - \frac{1}{2\sigma_*^2} \sum_{t=n+1}^N \frac{\nu_t^2}{F_t}, \quad (3.7)$$

with  $n$  the number of time steps needed to initialize the Kalman filter (see Section 2.7 on page 40). The advantage of this is that Equation 3.7 can be maximized with respect to  $\sigma_*^2$  by setting the derivative to zero, resulting in

$$\sigma_*^2 = \frac{1}{N-n} \sum_{t=n+1}^N \frac{\nu_t^2}{F_t}. \quad (3.8)$$

When  $\sigma_*^2$  is substituted in Equation 3.7, the ‘reduced’ log-likelihood function is obtained:

$$\log \mathcal{L}_r = -\frac{N-n}{2} (\log 2\pi + 1) - \frac{1}{2} \sum_{t=n+1}^N \log F_t - \frac{N-n}{2} \log \sigma_*^2. \quad (3.9)$$

The simple linear model structure makes it possible to calculate the Jacobian of the parameter vector  $\alpha$  by evaluating the derivatives of  $F_t$  and  $\nu_t$  analytically (through differentiating Equation 2.43, running in parallel with the Kalman filter).

Several tests have to ensure that the fitted model adequately describes the time series under consideration. The main diagnostics are based on the innovations obtained by the Kalman filter. The whiteness of the innovations can be tested using the autocorrelation function of the innovations. *Harvey* [1989] gives an estimator of the autocorrelation function of innovations containing missing values:

$$r(k) = \left[ \sum_{t=n+1}^{N^\dagger} \frac{\tilde{\nu}_t^\dagger \tilde{\nu}_{t-k}^\dagger}{N(k)} \right] \left[ \sum_{t=n+1}^{N^\dagger} \frac{\tilde{\nu}_t^{\dagger 2}}{(N-n)} \right]^{-1}, \quad (3.10)$$

where  $k$  is the time lag,  $N^\dagger$  is the length of the series generated by the underlying model,  $N(k)$  is the number of non-zero cross-products of innovations in the numerator of the statistic, and  $\tilde{\nu}_t^\dagger$  denotes the standardized innovation defined by

$$\tilde{\nu}_t^\dagger = \frac{\nu_t}{F_t^{\frac{1}{2}}}, \quad t = n+1, \dots, N^\dagger, \quad (3.11)$$

if  $y_t$  is observed and is set to zero for all other values of  $t$  for  $t = n+1, \dots, N^\dagger$ . The cross-correlation between input series and innovations as well as the cross-correlation between input series and residuals (i.e. estimated stochastic component) provide useful information on the correctness of the model structure.

## 3.2 Description of experiment

The effect of reducing the modeling interval is evaluated using generated time series. The advantage of a generated series is that the relation (transfer function) between the input and output is exactly known, enabling an accurate evaluation of the model performance. This section describes how time series were generated. Also it describes the criteria that were used to evaluate the model results.

### 3.2.1 Generation of groundwater time series

Groundwater time series were generated by transferring a daily input series of precipitation excess, using a predefined transfer function described by the probability density function of a lognormal distribution:

$$\Psi(t) = \frac{c}{t\sigma\sqrt{2\pi}} \exp \left[ -\frac{1}{2} \left( \frac{\ln t - \mu}{\sigma} \right)^2 \right] \quad \sigma > 0, 0 < t < \infty, \quad (3.12)$$

where  $\mu$  and  $\sigma$  are the geometric mean and standard deviation of the distribution, respectively, and  $c$  is a scaling constant. The main reasons for choosing this function are its flexibility (continuous in time) and the fact that the response of many hydrological systems to precipitation can be described by an exponential function. The deterministic component  $z_t$  of the generated time series can thus be written as

$$z_t = \sum_{\tau=1}^{t-1} \Psi_{\tau} P_{e,t-\tau}. \quad (3.13)$$

Here,  $P_e$  is the precipitation excess [ $\text{LT}^{-1}$ ]:

$$P_e = P - f_c E_r, \quad (3.14)$$

where  $P$  is the precipitation [ $\text{LT}^{-1}$ ],  $E_r$  is the Makkink reference evaporation [ $\text{LT}^{-1}$ ], and  $f_c$  is a crop factor [-] which was set to a value of 0.8. Both precipitation and evaporation were obtained from daily observations at the main meteorological station of the Royal Netherlands Meteorological Institute at De Bilt, the Netherlands, in the period from July 1, 1957 to December 31, 1999.

In addition to the deterministic transfer function, a stochastic component was added to the system. This component represents the part of the system dynamics that is not related to the input signal. The stochastic component is assumed to be described by the following autoregressive model:

$$\xi_t = \phi \xi_{t-1} + a_t, \quad (3.15)$$

where  $a_t$  is normally distributed with zero mean and variance  $\sigma_a^2$ , which was set to 1 percent of the variance of the deterministic component. A number of 20 independent realizations of each stochastic component were generated to obtain a statistically correct experiment.

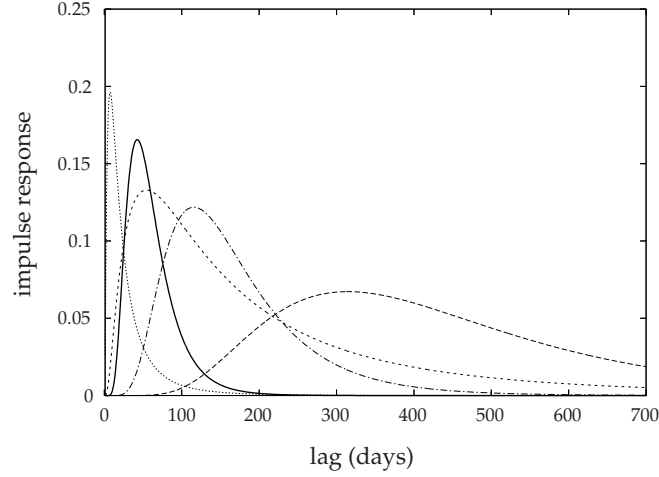


**Figure 3.1:** Examples of transfer functions applied to generate time series; the solid curve is used in this chapter

Using Equations 3.13 and 3.15 many different time series were generated, varying from fast responding systems (peak response within a couple of days) to very slow responding systems (peak response after one year). Figure 3.1 gives some transfer functions used in this experiment. This chapter only describes the results of the time series generated with the solid transfer curve in Figure 3.1, having a time of peak response  $t_p = 43$  days. Conclusions from this experiment are similar to those of the other analyzed transfer functions.

Each deterministic component was combined with two different stochastic components. Table 3.1 gives the parameters of this transfer function as well as the parameters of the stochastic component. Here, the ratio  $S_N$  is defined as

$$S_N = \frac{\text{var}(\xi_t)}{\text{var}(z_t)}, \quad (3.16)$$

where  $\text{var}(\xi_t)$  is the variance of the stochastic component, and  $\text{var}(z_t)$  is the variance of the deterministic component. Table 3.1 shows that, as a result of the higher value of  $\phi$ , the value of  $S_N$  of series S2 is higher.

Figure 3.2 shows one realization of time series S2. The time series was finally split into a calibration period (1957-1989) and a validation period (1990-1999) to validate the results obtained by the calibration.

**Table 3.1:** Parameters of predefined transfer function used to generate time series

Series	Deterministic component			Stochastic component	
	$\mu$	$\sigma$	$c$	$\phi$	$S_N$
S1	4.0	0.5	10	0	0.01
S2	4.0	0.5	10	0.99	0.37

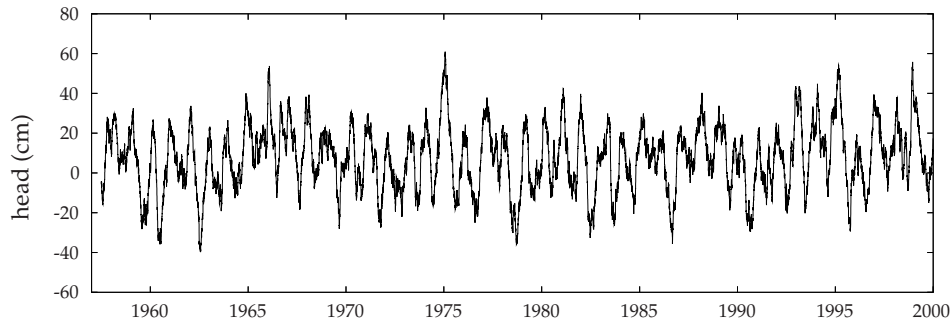


**Figure 3.2:** Realization of time series generated with a predefined transfer function (lognormal probability density function) and an autoregressive stochastic component corresponding to S2 in Table 3.1

### 3.2.2 Resampling of time series

A thorough analysis of the relation between modeling interval and model performance not only requires a range of transfer functions (as described in Section 3.2.1) but also a number of other variables that influence the relation between modeling interval and model performance. Table 3.2 gives an overview of the variables that were taken into account and the range of variation that was analyzed in this chapter. Basically, these time series were modeled with two different model forms: Model 1 has a modeling interval equal to the measuring interval; Model 2 has a modeling interval of 10 days.

### 3.2.3 Evaluation criteria

Before comparing models of different time series and with different modeling intervals, the number of parameters of each model needs to be selected. In practical applications, well-known criteria are the Akaike Information Criterion (AIC), Bayes Information Criterion (BIC) as well as the innovation variance of the calibrated and validated time series. In this experiment, with generated time series and a known deterministic component, the 'fit' of the calibrated deterministic component of the model to the real deterministic component can be calculated. A good measure of 'fit' (or 'error') is the mean absolute error (MAE) [L] of the deterministic component,

**Table 3.2:** Variation of variables applied for resampling of the time series

Variable	Range of variation
Measuring interval	10, 20, ..., 70 days
Length of time series	10, 20, ..., 100 % of maximum length (1957-1989)
Varying measuring interval	first fraction (0, 10, 20, ..., 100%) of time series has measuring interval of 70 days, last fraction a measuring interval of 10 days; modeling interval is 10 days

described as

$$\text{MAE} = \frac{1}{N-n} \sum_{t=n+1}^N |\hat{z}_t - z_t|, \quad (3.17)$$

where  $\hat{z}_t$  represents the estimated deterministic component. In other words, the MAE quantifies how well the deterministic component can be separated from the stochastic component. Based on the MAE, the optimal number of parameters was selected for each time series model. The MAE-criterion was also applied to compare the models of the time series given in Table 3.2. A second criterion was used to indicate the accuracy of the estimated transfer function. For this purpose, a useful parameter is the standard deviation of the gain of the transfer function  $s_G$  [ $L(LT^{-1})^{-1}$ ], where the gain  $G$  [ $L(LT^{-1})^{-1}$ ] represents the area under the impulse-response curve (see Equation 2.8 on page 29).

### 3.3 Comparison of model results for varying modeling and measuring interval

This section discusses the results of the experiment. First, the influence of modeling interval, measuring interval, and length of time series on the fit of the deterministic component is evaluated. Next, the influence of these aspects on the parameter accuracy is analyzed. Finally, the effect of adding high-frequency measurements to an existing time series of low-frequency measurements is demonstrated.

#### 3.3.1 Fit of deterministic component

Figure 3.3 shows the fit of the deterministic component expressed in terms of MAE, for four different cases and seven measuring intervals. For the calculation of the MAE only the errors at measurement points were used. The four cases are interpreted as follows:

1. S1 - Model 1:  $\phi = 0$ ;  $dt_{mod} = dt_{meas}$

Figure 3.3 shows that the performance of the model improves as the measuring interval decreases: from a mean absolute error of ca. 3.5 cm to an error of ca. 0.5 cm. A smaller measuring interval (and thus a smaller modeling interval) clearly allows for a finer discretization and hence a better approximation of the transfer function. The curve of MAE flattens from the moment the measuring interval becomes larger than the time of peak response  $t_p$ . From this point, a coarser discretization of the transfer function will hardly influence the model fit. This is directly related to the gradient of the transfer function. The rising limb of the transfer function is steep and requires a small interval, whereas the falling limb of the transfer function has a smaller gradient and can therefore be well approximated by a model with a large interval.

2. S1 - Model 2:  $\phi = 0$ ;  $dt_{mod} = 10$

In this case, the same time series S1 is modeled, but with the modeling inter-

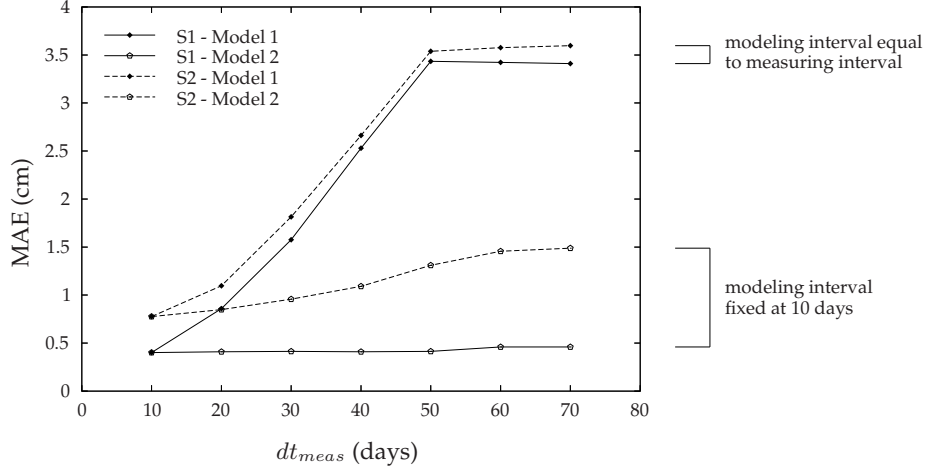


**Figure 3.3:** Fit of deterministic component (mean absolute error, MAE) as a function of measuring interval, for series S1 using 20 realizations of a white-noise stochastic component ( $\phi = 0$ ) and S2 using 20 realizations of an autoregressive stochastic component ( $\phi = 0.99$ ). Model 1 has a modeling interval equal to the measuring interval, whereas Model 2 keeps the modeling interval fixed at 10 days.

val fixed at 10 days. Figure 3.3 shows that the performance of this model is much better and in fact practically insensitive to the measuring interval. This is easily understood by realizing again that a smaller modeling interval gives a finer discretization of the transfer function, resulting in a better approximation.

3. S2 - Model 1:  $\phi = 0.99$ ;  $dt_{mod} = dt_{meas}$

The difference between series S1 and S2 is that the stochastic component of series S2 has an autoregressive part, resulting in a larger value of  $S_N$ . Consequently, the fit of the deterministic component of series S2 is not as good as for S1. The difference, however, is limited compared to the effect of the measuring interval.

4. S2 - Model 2:  $\phi = 0.99$ ;  $dt_{mod} = 10$

Again, a reduction of the modeling interval greatly improves the performance of the model. However, the MAE slowly increases as the measuring interval increases, whereas the curve of MAE flattens from the moment the measuring interval becomes larger than  $t_p$ . It can therefore be concluded that the influence of the modeling interval on MAE increases as the correlation length (i.e. the value of  $\phi$ ) of the stochastic component increases.

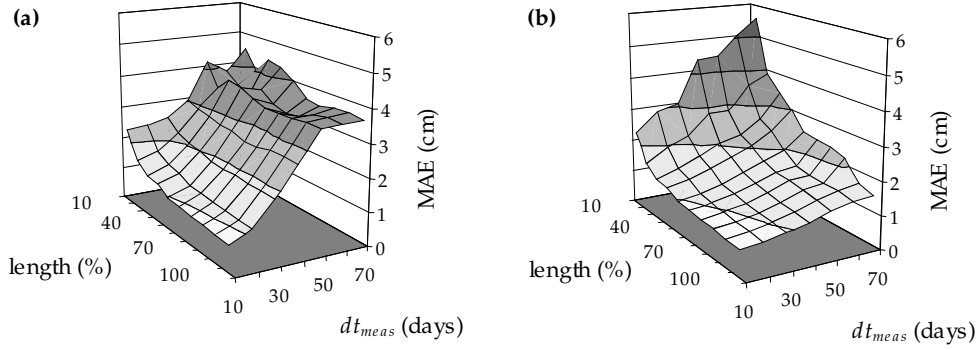


**Figure 3.4:** Fit of deterministic component (mean absolute error, MAE) as a function of measuring interval and length of the time series (as a percentage of the total length, i.e. 33 years), for series S2 and (a) Model 1 having a modeling interval equal to the measuring interval; and (b) Model 2 having a modeling interval of 10 days. The results are based on 20 realizations of the stochastic component.

Another important aspect that influences the fit of the deterministic component is the length of the time series. In Figure 3.3 the length of the time series was fixed at 33 years. In the context of this chapter an important question is whether a reduction of the modeling interval still improves the fit if the time series is short. Figure 3.4 shows the relation between the MAE and the length of the time series. Only the results for series S2 are presented, because this series has a large stochastic component.

For a length of 100% the curve of the MAE is the same as the curve in Figure 3.3. If the modeling interval is equal to the measuring interval (Figure 3.4a), the MAE first hardly increases as the length decreases. Only if the length is reduced to less than 50% (16.5 years) the increase becomes noticeable. The pattern of the curve becomes a little irregular for combinations of large measuring interval and short time series. Much more realizations would be necessary to obtain a smooth curve. These combinations of measuring interval and length of time series, however, result in datasets with an unrealistic small number of measurements. For example, the worst combination (measuring interval is 70 days and length is 10% of the full length) consists of only 16 measurements. For all other combinations, a reduction of the modeling interval clearly improves the fit of the deterministic component.

Bierkens *et al.* [1999] found as well (for a time series with  $t_p = 1$  day) that similar parameter values can be obtained for different measuring intervals as long as the measuring interval is smaller than the characteristic response time (i.e. time for which the response is only 5% of the peak response). On the basis of the present study more general statements can be made, summarized as follows:

1. A reduction of the modeling interval results in a better fit of the deterministic component, regardless the measuring interval;



2. The effect of a reduction of the modeling interval increases for larger measuring intervals;
3. For a small stochastic component, the fit is practically insensitive to the measuring interval if a small modeling interval (i.e. small with respect to the time of peak response) is used;
4. For a large stochastic component, the fit slightly decreases with increasing measuring interval if a small modeling interval is used.

The presented results are of great practical importance, because the models of existing groundwater time series can simply be improved by only reducing the modeling interval.

### 3.3.2 Parameter accuracy

The overall accuracy of the estimated parameters, expressed by the standard deviation of the gain ( $s_G$ ), is evaluated in relation to the measuring interval and the length of the time series. Figure 3.5 shows this relation for the same four cases as in the previous subsection. In this context, it is important to note that the estimated gain is ca.  $10 \text{ cm}(\text{mmday}^{-1})^{-1}$  ( $= c$  in Equation 3.12). The figures are interpreted as follows:

1. Figure 3.5a. S1 - Model 1:  $\phi = 0$ ;  $dt_{mod} = dt_{meas}$   
The figure shows that the standard deviation of the gain decreases considerably with decreasing measuring interval. This is not surprising because more measurements result in a more accurate estimation of the parameters. In addition, the curve of  $s_G$  has the same pattern as found for the MAE: a rather fast increase for measuring intervals smaller than  $t_p$  and a flattening of the curve for measuring intervals larger than  $t_p$ . Finally, the influence of the measuring interval increases with decreasing length of the time series. High standard deviations occur for short time series with large measuring interval.
2. Figure 3.5b. S1 - Model 2:  $\phi = 0$ ;  $dt_{mod} = 10$   
Similar to the results presented for the MAE, a fixed small modeling interval results in better models for all measuring intervals in the sense that the transfer function is estimated more accurately. However, a small increase of  $s_G$  can still be observed as the measuring interval increases. This is directly related to the fact that the number of measurements reduces as the measuring interval increases.
3. Figure 3.5c and d. S2 ( $\phi = 0.99$ ) - Model 1 ( $dt_{mod} = dt_{meas}$ ) and Model 2 ( $dt_{mod} = 10$ )  
The pattern of  $s_G$  is similar to the pattern of series S1. However, the influence of the measuring interval on  $s_G$  is small with respect to the influence of the stochastic component on  $s_G$ .

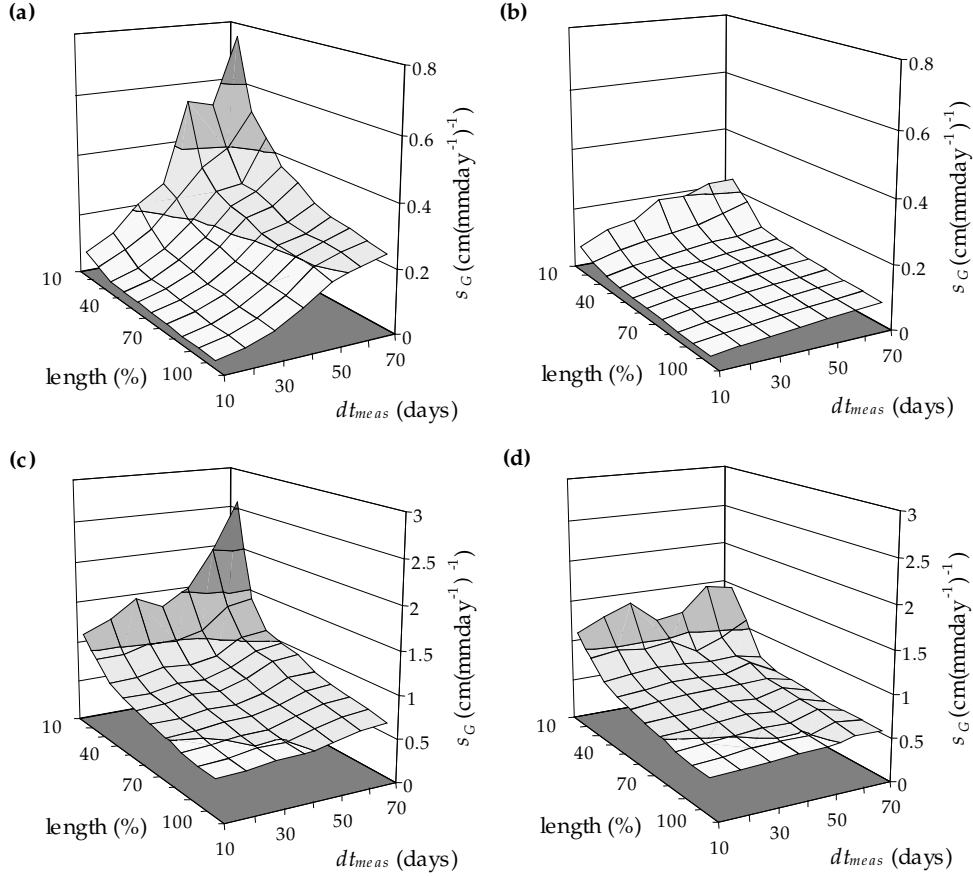


**Figure 3.5:** Relation between parameter accuracy, measuring interval and length of time series (relative to the original length of the time series (33 years)) for (a) series S1, Model 1; (b) series S1, Model 2; (c) series S2, Model 1; and (d) series S2, Model 2. The results are based on 20 realizations of the stochastic component.

Summarizing, a reduction of the modeling interval has a positive effect on the accuracy of the estimated transfer function. The relative improvement (improvement with respect to its original value) depends on the contribution of the stochastic component.

### 3.3.3 Adding high-frequency measurements

In practice, a large data set of groundwater measurements is often available. The previous sections have shown that a reduction of the modeling interval can improve the model performance considerably. Another way to improve the model performance is to extend the time series with a set of high-frequency measurements obtained with automatic data loggers. This section evaluates the influence of such an extension on the model performance. MAE and  $s_G$  are used again as evaluation

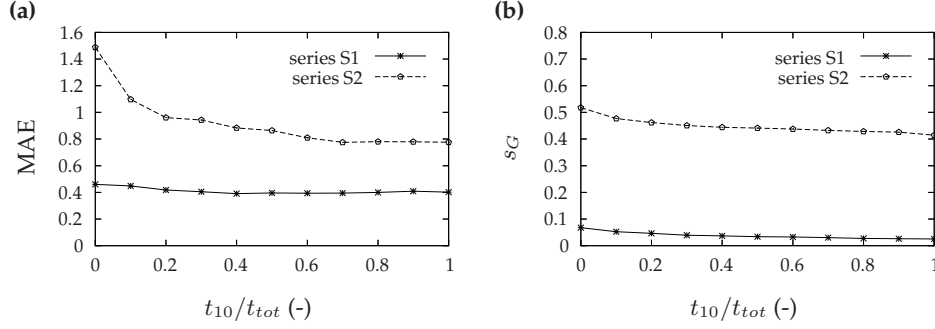


**Figure 3.6:** Influence of reducing the measuring interval from 70 days to 10 days in the final  $t_{10}/t_{tot}$  fraction of time series S1 and S2 on (a) the fit of the deterministic component MAE (cm); and (b) the parameter accuracy  $s_G$  ( $\text{cm}(\text{mmday}^{-1})^{-1}$ ). The modeling interval is 10 days and the length of the series is 33 years. The results are based on 20 realizations of the stochastic component.

criteria.

Figure 3.6 shows the effect of adding high-frequency measurements to the time series S1 and S2 used earlier. The horizontal axis represents the fraction of the time series that has a measuring interval of 10 days (instead of 70 days). Hence, if  $t_{10}/t_{tot} = 0$  the whole time series has a measuring interval of 70 days, whereas  $t_{10}/t_{tot} = 0.1$  means that the first 90% of the time series has a measuring interval of 70 days and the final 10% a measuring interval of 10 days. The MAE is calculated at each model time step to obtain a valid comparison between the models.

Figure 3.6a shows that the first high-frequency measurements (between 0% and 20% of the total length of the series) are the most effective in terms of an increase in the model performance, especially for series S2. This is very attractive, because it means that relatively few extra measurements are needed to reduce the MAE considerably. The curves of  $s_G$  (Figure 3.6b) are different: instead of a quick drop during the first 20%, the curves display a steady decrease of  $s_G$ . One of the reasons is that  $s_G$  depends more on the total number of measurements and length of the time series than on the measuring interval. The same experiment was applied to shorter time series, showing the same results.

Summarizing, the model performance can be further improved by extending (low-frequency) time series with high-frequency measurements. The effect of this extension becomes larger for time series with large stochastic components. This section only evaluated the influence of high-frequency measurements at the ending of a period, because there are already many time series with low-frequency measurements available. If one starts monitoring, however, it could be advantageous to start with high-frequency measurements. This topic will not be discussed in detail, but several calculations have shown that high-frequency measurements at the beginning of the period have more effect than at the end of the period.

### 3.4 Case study

#### 3.4.1 Description of the data set

Groundwater head data (1990-2000) were obtained from an observation well in the east of the Netherlands. The measuring frequency of this series was 24 observations per year. In 1999, the measuring frequency has been increased to one observation per day during a period of three months (which is about 2.5% of the total length of the time series). This time series is therefore a good example to examine the practical significance of the results reported in the previous sections. The series was split into a calibration series (from 1990 until June 1999, which is at the end of the daily measurements) and a validation series (from July 1999 until October 2000). The daily meteorological input data were obtained from two meteorological stations: the precipitation from a nearby station at Eerbeek (5 km distance) and the potential evapotranspiration from a station at De Bilt (65 km distance).

From this time series three different samples were selected:

1. Measuring interval = 14 days, modeling interval = 14 days,
2. Measuring interval = 14 days, modeling interval = 1 day,
3. Measuring interval = 14 days and 1 day, modeling interval = 1 day.

#### 3.4.2 Modeling results

Identification of the system resulted in the following model form for all three samples:

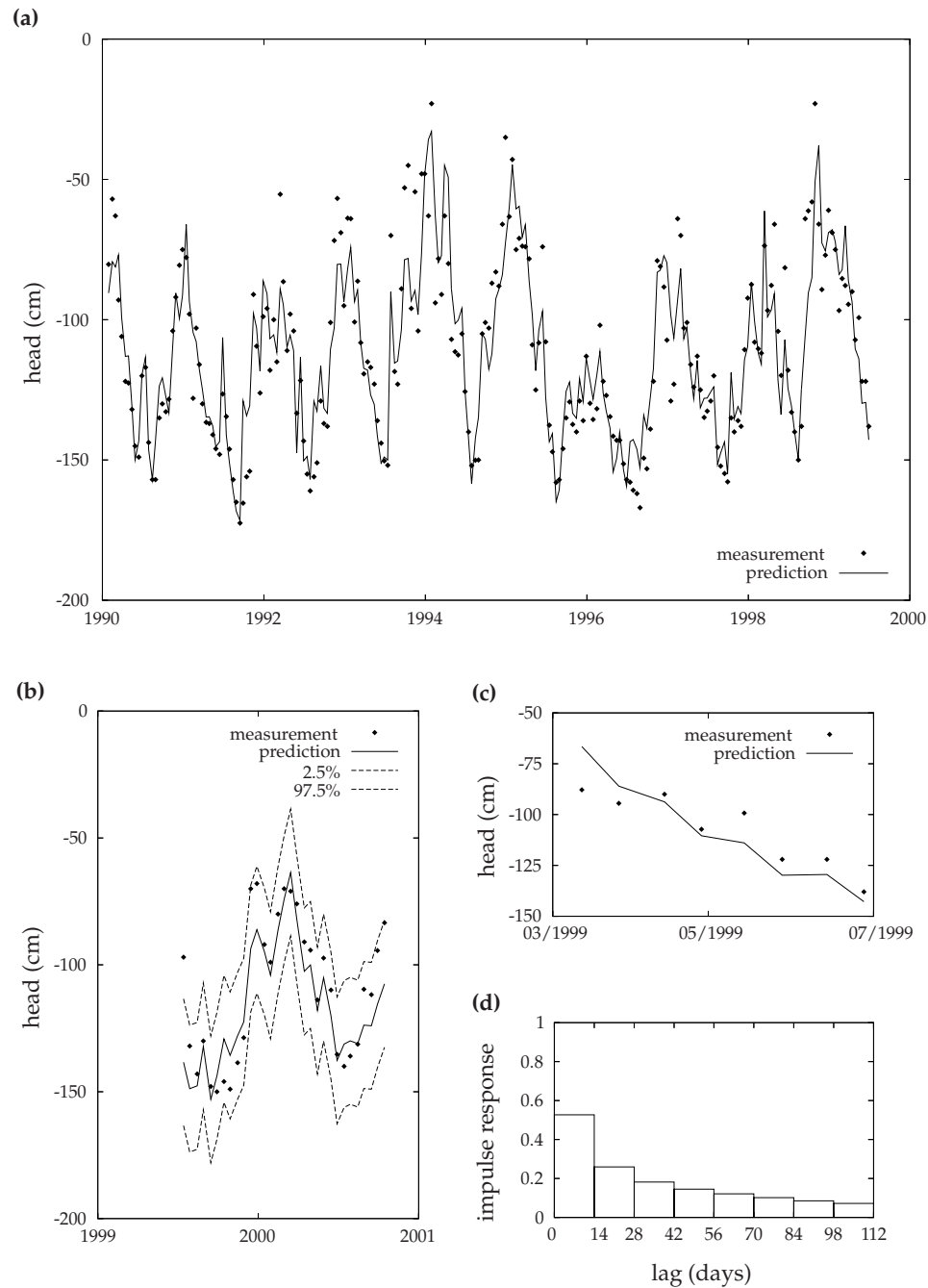
$$\begin{bmatrix} x_{d,1} \\ x_{d,2} \\ x_{s,1} \end{bmatrix}_t = \begin{bmatrix} \delta_1 & 1 & 0 \\ \delta_2 & 0 & 0 \\ 0 & 0 & \phi_1 \end{bmatrix} \begin{bmatrix} x_{d,1} \\ x_{d,2} \\ x_{s,1} \end{bmatrix}_{t-1} + \begin{bmatrix} \omega_0 \\ \omega_1 \\ 0 \end{bmatrix} u_t + \begin{bmatrix} 0 \\ 0 \\ 1 \end{bmatrix} w_t,$$

$$y_t = \begin{bmatrix} 1 & 0 & 1 \end{bmatrix} \begin{bmatrix} x_{d,1} \\ x_{d,2} \\ x_{s,1} \end{bmatrix}_t + y_r + v_t,$$

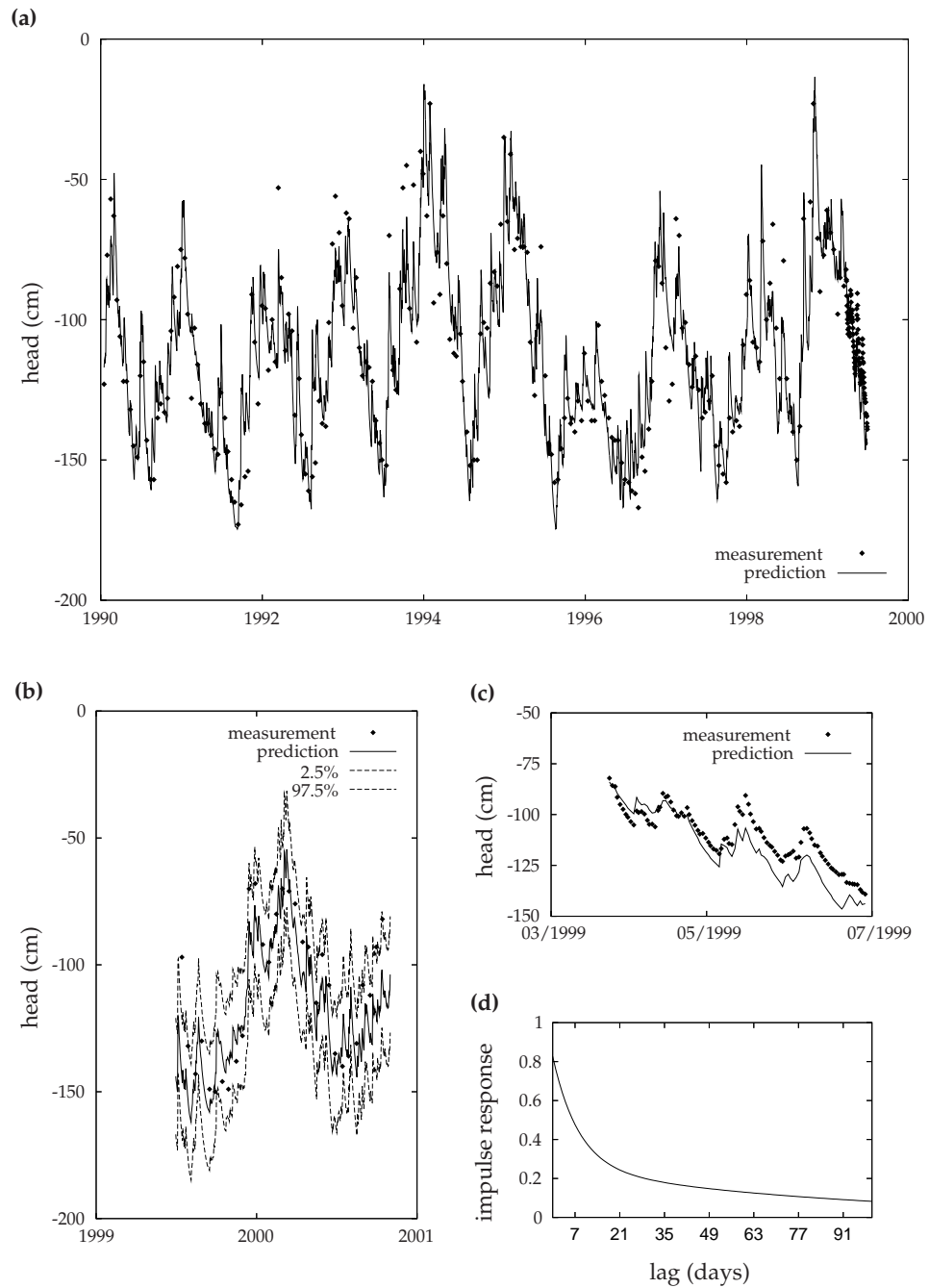
with elements as defined in Equation 3.1.

Table 3.3 lists the estimated parameters of the three models. The graphical output is given in Figures 3.7 and 3.8. Since the difference between the estimated deterministic parameters ( $\delta_1, \delta_2, \omega_0, \omega_1$ ) of series 2 and series 3 is not significant (see Table 3.3), the result of series 2 is omitted. Note that due to the extra measurements in series 3 the standard deviations of the parameters (except  $y_r$ ) decrease.

The results in both figures allow for some general statements. A small modeling interval enables a much better approximation to the peak response (compare Figures 3.7d and 3.8d). As a result, the extreme values of the time series are modeled clearly better (compare the peaks in 1994 and 1999 in Figures 3.7a and 3.8a).



**Figure 3.7:** Results of series 1; (a) measurements and predictions of the model for the calibration period; (b) measurements combined with the predictions and 95% prediction interval for the validation period; (c) measurements and predictions for the period of daily measurements (for comparison with Figure 3.8); and (d) estimated impulse response function



**Figure 3.8:** Results of series 3; (a) measurements and predictions of the model for the calibration period; (b) measurements combined with the predictions and 95% prediction interval for the validation period; (c) measurements and predictions for the period of daily measurements; and (d) estimated impulse response function

**Table 3.3:** Estimated parameters of the calibrated models; the standard deviation of the parameter estimation error is given in parentheses

	Series 1		Series 2		Series 3	
$dt_{meas}, d$	14		14		mixed	
$dt_{mod}, d$	14		1		1	
$\delta_1$	1.0438	(0.12)	1.8594	(0.015)	1.8729	(0.011)
$\delta_2$	-0.1698	(0.092)	-0.8609	(0.015)	-0.8742	(0.010)
$\phi_1$	0.3906	(0.044)	0.9417	(0.0068)	0.9578	(0.0044)
$\omega_0, \text{cm}(\text{mm} \cdot \text{d}^{-1})^{-1}$	7.377	(0.020)	0.8724	(0.035)	0.8264	(0.028)
$\omega_1, \text{cm}(\text{mm} \cdot \text{d}^{-1})^{-1}$	-4.066	(0.056)	-0.8317	(0.034)	-0.7905	(0.027)
$y_r, \text{cm}$	-138.6	(1.9)	-140.1	(1.6)	-139.8	(1.8)

Also, Figure 3.8c shows that the daily fluctuations of groundwater head are modeled rather well. Only a slight local trend is observed. A possible explanation of this trend is that the assumption of linearity is incorrect.

The difference in model performance has to be quantified by criteria such as the innovation variance of the calibrated series,  $\text{var}(n_{c,t})$ , the innovation variance of the validated series,  $\text{var}(n_{v,t})$ , and the standard deviation of the gain,  $s_G$ . As different modeling intervals are used, comparison of the variance of the system noise  $q = \text{var}(w_t)$  is not useful. Instead, the variance of the stochastic component is compared:

$$\text{var}(\xi_t) = \frac{q}{1 - \phi_1^2}. \quad (3.18)$$

Table 3.4 evaluates the model performance, using these criteria. Before comparing the results it is important to remark that the coefficient of determination,  $R_T^2$ , is based on all measurements. Hence, the value of  $R_T^2$  of series 3 is based on more measurements and thus not directly comparable to  $R_T^2$  of series 1 and 2. If the daily measurements of series 3 would be ignored in the calculation of  $R_T^2$ , then  $R_T^2 = 0.86$ .

Table 3.4 shows the following:

1. Reducing the modeling interval from 14 days to 1 day results in a reduction of  $\text{var}(\xi_t)$  of about 21%. The variance reduces another 3% if the daily measurements are added to the time series.
2. The gain  $G$  increases slightly if the modeling interval is reduced to 1 day, which means that the area under the impulse response function increases. This is also expressed by an increase of the coefficient of determination.
3. The accuracy of the estimated transfer function improves from series 1 to 2:  $s_G$  reduces by 22%. Adding daily measurements, however, does not result in a reduction of  $s_G$ . The reason for this is the relatively large stochastic component and short series of high-frequency measurements.

This case study confirms that adjusting the modeling interval to the response time of the system, improves the model significantly. The model especially de-

*Table 3.4: Comparison of criteria for the evaluation of the performance of the three different models*

	Series 1	Series 2	Series 3
$dt_{meas}, d$	14	14	mixed
$dt_{mod}, d$	14	1	1
$var(n_{c,t}), cm^2$	152.7	120.7	89.2
$var(n_{v,t}), cm^2$	118.2	116.7	114.8
$var(\xi_t), cm^2$	180.5	142.0	136.7
$G, cm(mm.d^{-1})^{-1}$	26.3	26.7	26.5
$s_G, cm(mm.d^{-1})^{-1}$	1.8	1.4	1.4
$R_T^2$	0.83	0.87	0.84

scribes the extremes in the time series much better. As a result, the system noise reduces considerably. The noise could be reduced even further by adding high-frequency measurements. The improvements due to the relatively short series of high-frequency measurements is, however, small. A longer high-frequency time series will probably lead to a further improvement.

### 3.5 Discussion and conclusions

The objective of this chapter was to determine the influence of a reduction of the modeling interval on the performance (i.e. 'fit' and accuracy of estimated transfer function) of the state space model. The fit can only be measured if the real transfer function is known. For this reason a large range of groundwater time series were generated. Calculations on several samples (with varying measuring and modeling intervals) of different time series show that the performance of transfer models can be increased by simply reducing the modeling interval. The degree of model improvement depends on several aspects.

First, the modeling interval itself relative to the time of peak response of the system is important. If the modeling interval is large with respect to the time of peak response, a reduction of the interval will greatly improve the performance. On the other hand, if the modeling interval is already small with respect to the time of peak response, a further reduction will not be very effective.

Second, the relative effect of a reduction of the modeling interval will be less if the stochastic component of the system (the part of the system dynamics that is not related to the input signal) is large.

Third, the effect of reducing the modeling interval becomes larger as the length of the time series increases. This reduction is especially observed for the fit of the deterministic component.

In addition to reducing the modeling interval, one could extend a time series with easily obtainable high-frequency measurements (i.e. a reduction of the *measuring* interval). The effect of such an extra set of high-frequency measurements again strongly depends on the stochastic component: high-frequency measurements are much more effective if the stochastic component is large. Moreover, the first high-frequency measurements have the greatest influence on the model performance. It is therefore attractive to add a small time period of high-frequency measurements



to the existing time series of low-frequency measurements.

The state space model has been used to model a real-world test case of which the measuring interval was reduced to one day for the last three months. The results of this case study support the results of the generated time series: a reduction of the modeling interval significantly improves the performance of the time series model. Due to the short period of high-frequency measurements in the test case (only three months), the improvement resulting from these high-frequency measurements was relatively moderate.

Further improvement of groundwater time series models can be achieved by including physical knowledge. The state space approach allows for extension of the model with unobserved states, such as unsaturated processes. This is the topic of the next chapter.



# 4

## Incorporation of a nonlinear root zone model

---

**Abstract.** A nonlinear state space model is developed for describing fluctuations of groundwater levels. Nonlinearity is introduced by modeling the (unobserved) degree of water saturation of the root zone. The nonlinear relations are based on physical concepts describing the dependence of the actual evapotranspiration and of the percolation rate on the degree of saturation of the root zone. Precipitation and reference evaporation are the input variables. Assuming gravity-driven flow, the recharge from the root zone is transferred to the water table by means of a linear reservoir model. Errors due to model assumptions and parameter uncertainties are modeled as a noise process. The parameters of the resulting stochastic model are calibrated on time series by combining an extended Kalman filter with a maximum likelihood criterion. The model was tested at two locations and compared with a linear time series model. It is shown that the nonlinear model estimated extreme groundwater levels better than the linear time series model. The variance of the stochastic component reduced significantly and, hence, the uncertainty of estimated trends reduced. Another advantage of the nonlinear model is that it also gives an indication of fluctuations in the degree of saturation in the root zone.

---

*This chapter is adapted from Berendrecht, W.L., F.C. van Geer, J.C. Gehrels, and A.W. Heemink, A nonlinear state space approach to model groundwater level fluctuations, submitted to Advances in Water Resources*

LINEAR TRANSFER FUNCTION-NOISE MODELS have been widely applied in hydrological and geohydrological applications. Many time series of groundwater level fluctuations have been successfully modeled with TFN models. However, there has always been a class of deep groundwater time series that could not be modeled satisfactorily with this linear type of model [Gehrels *et al.*, 1994]. The main problem encountered was that trends cannot be detected accurately. Although the residual variance (part that cannot be explained by the model input) is often small relative to the total variance of groundwater fluctuations, it is generally large relative to estimated trends. As a consequence, the estimated trend has a high level of uncertainty, hampering accurate evaluation of interventions.

One of the most important reasons that the TFN model fails to accurately describe the groundwater level fluctuations is that it assumes a linear relation between input (precipitation and evapotranspiration) and output (groundwater level). Physical knowledge shows that the response of a groundwater system to precipitation and evapotranspiration can be strongly nonlinear [e.g. Feddes *et al.*, 1988]. It is well known that the degree of water saturation of the root zone determines in a nonlinear way the hydraulic conductivity, and as a result, the percolation to the groundwater table. Also, the degree of saturation influences the water uptake by roots and thus the actual evapotranspiration.

A well-known type of model that incorporate these nonlinear relations is the physical-mechanistic model [Neuman *et al.*, 1974; Belmans *et al.*, 1983; Van Dam, 2000]. A disadvantage of this type of models, however, is that they generally require a lot of parameters. In practical applications, there is often insufficient data to estimate these parameters. Stochastic models such as TFN models are generally more parsimonious. Moreover, the stochastic form of the model makes it possible to model unknown disturbances, errors due to model assumptions, errors due to parameter uncertainty and errors in model inputs. Besides, the stochastic model can be easily used for online processing if it is written in state space form. Several stochastic models were already applied for estimating soil water content [e.g. Or and Hanks, 1992; Parlange *et al.*, 1992, 1993; Wu *et al.*, 1997; Hoeben and Troch, 2000; Wu *et al.*, 2001]. Furthermore, Bierkens [1998] developed a nonlinear stochastic model for describing shallow groundwater level fluctuations. This model, however, cannot be applied for modeling deep groundwater level fluctuations.

The aim of this chapter is to develop a parsimonious state space model capturing the most relevant physical processes needed to describe groundwater level fluctuations. The model incorporates the saturation of the root zone as a separate variable (which may be unobserved). In this way, the model can estimate the temporal variation of actual evapotranspiration and percolation, and thus groundwater recharge, more accurately. The model is based on well-known physical concepts like Richards' equation and Darcy's law. The intention is to use these physical relations in a simple, conceptual way rather than to include a detailed description of unsaturated processes in the subsoil. The state equation is combined with an extended Kalman filter algorithm to calibrate its parameters to observed time series of groundwater levels. Although this chapter only describes a single time series model, it is straightforward to extend the state space model for modeling multiple time series simultaneously.

The presented model is tested on two time series of groundwater level data observed in the center of the Netherlands. For comparison, a linear TFN model is calibrated to both time series. Results show that the nonlinear model performs better than the linear TFN model in the sense that it further reduces the noise variance. Hence, the uncertainty of estimated trends reduces. Reduction of the noise variance also enables a more accurate prediction of groundwater level fluctuations. In addition, the nonlinear model gives a reasonably good estimate of the degree of water saturation in the root zone.

The chapter is organized as follows. Section 4.1 presents the conceptual background of the nonlinear model. Subsequently, Section 4.2 rewrites the model into state space form and describes how the system state and model parameters are estimated. Section 4.3 uses two real-world examples to test the model. The results are compared with a linear TFN model. Finally, Section 4.4 gives some concluding remarks.

## 4.1 A nonlinear reservoir model

A widely applied schematization of a groundwater system is the reservoir model as illustrated in Figure 4.1. The first (upper) reservoir is the root zone. Here, the input variables enter the system. The second reservoir is the percolation zone, describing the downward flux from the root zone to the third reservoir, the saturated zone. This last reservoir is the lower boundary of the model and represents the observed groundwater level.

### 4.1.1 Root zone

The main parameter of the root zone is the effective degree of water saturation  $S_e$  [-],  $0 < S_e \leq 1$ , described by the following differential equation:

$$\frac{dS_e}{dt} = \frac{1}{D_e} (P_e - E_a - R_p). \quad (4.1)$$

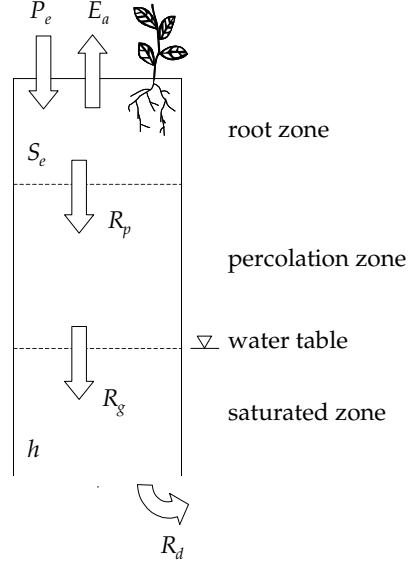


Figure 4.1: Schematization of groundwater system

Here,  $D_e = D(\theta_s - \theta_r)$  is the effective thickness of the root zone [L], with  $D$  the root zone depth [L],  $\theta_s$  the saturated soil water content [-], and  $\theta_r$  the residual soil water content [-].  $P_e$  is the net precipitation [ $LT^{-1}$ ], which is assumed to be related to the observed gross precipitation  $P_G$  [ $LT^{-1}$ ] as

$$P_e = f_i P_G, \quad (4.2)$$

where  $f_i$  is an interception factor [-].  $E_a$  is the actual evapotranspiration [ $LT^{-1}$ ] and depends on the degree of water saturation and the potential evapotranspiration  $E_p$  [ $LT^{-1}$ ], which is a linear function of the observed Makkink reference evaporation  $E_r$  [ $LT^{-1}$ ]:

$$E_p = f_c E_r, \quad (4.3)$$

where  $f_c$  is an empirical crop factor [-] relating the rate of evapotranspiration to the type of vegetation. The relation between  $E_a$ ,  $E_p$  and the degree of water saturation  $S_e$  is derived from the relation between  $E_a/E_p$  and the soil moisture pressure head  $\psi$  described by Feddes *et al.* [1978] and given in Figure 4.2a. Here,  $\psi_o$  is the 'anaerobiosis point', at which deficient aeration conditions exist,  $\psi_r$  is the 'reduction point', at which water uptake by the roots starts to reduce, and  $\psi_w$  is the 'wilting point', at which water uptake is zero. The relation between  $E_a/E_p$  and  $\psi$  can be transformed into a relation between  $E_a/E_p$  and the degree of saturation  $S_e$  following [Van Genuchten, 1980]

$$S_e(\psi) = \left[ \frac{1}{1 + |\alpha\psi|^n} \right]^m, \quad (4.4)$$

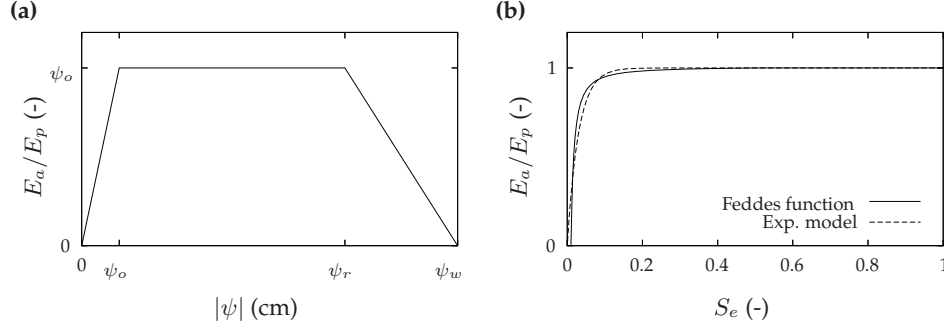


**Figure 4.2:** (a) Actual evapotranspiration rate as a function of the absolute value of the soil moisture pressure head  $|\psi|$  after Feddes et al. [1978]; and (b) actual evapotranspiration rate as a function of the degree of water saturation using the “Feddes function” and Equation 4.4 with  $\psi_o = 0$ , and an approximation using the “Exponential model” ( $S_r = 0.2$ )

where  $\alpha$ ,  $n$  and  $m = 1 - \frac{1}{n}$  are empirical factors. A typical example of this relation is shown in Figure 4.2b (solid line). Here,  $\psi_o$  is assumed to be equal to zero. Since this relation is rather complex to evaluate in state space form, a more simple but effective approximation is used (Figure 4.2b, dashed line). This approximation has been adopted from geostatistics and is generally referred to as the Exponential model [Isaaks and Srivastava, 1989]:

$$E_a(S_e) = \left[ 1 - \exp\left(-\frac{3S_e}{S_r}\right) \right] E_p, \quad (4.5)$$

with  $S_r$  a shape factor defined as the degree of saturation where  $E_a(S_r) \approx 0.95E_p$ .

The downward flux after passage through the root zone,  $R_p$  [ $LT^{-1}$ ], is described by Darcy’s law [Feddes et al., 1988]:

$$R_p(S_e) = K(S_e) \left( \frac{d\psi}{dz} + 1 \right), \quad (4.6)$$

where  $K(S_e)$  denotes the unsaturated hydraulic conductivity [ $LT^{-1}$ ] as a function of the degree of water saturation, and  $d\psi/dz$  is the hydraulic head gradient, taken positive downward. For large unsaturated zones, the movement of soil water below the root zone is mainly governed by gravity. Therefore it can be assumed that the pressure head remains constant with depth, so that Equation 4.6 reduces to

$$R_p(S_e) = K(S_e). \quad (4.7)$$

The unsaturated hydraulic conductivity and thus  $R_p$  is described according to Van Genuchten [1982]:

$$R_p(S_e) = K_s S_e^\lambda \left[ 1 - \left( 1 - S_e^{1/m} \right)^m \right]^2, \quad (4.8)$$

where the constant  $K_s$  denotes the saturated hydraulic conductivity [ $LT^{-1}$ ] and  $\lambda$  and  $m$  are empirical shape factors [-], with  $\lambda m \geq -2$  ensuring  $dR_p/dS_e \geq 0$  for  $0 < S_e \leq 1$ .

#### 4.1.2 Percolation zone

Basically, the percolation zone redistributes the incoming flux  $R_p$  into an outgoing flux  $R_g$  [ $LT^{-1}$ ]. This redistribution is calculated using a transfer function that is based on the general form of a convolution integral [e.g. *Gehrels, 1999*]:

$$R_g(t) = \int_0^\infty R_p(t - \tau)F(\tau)d\tau, \quad (4.9)$$

where  $F(\cdot)$  is a transfer function representing the percolation zone. *Gehrels* [1999] shows that linearization of the well-known Richards' equation gives an expression for  $F(\cdot)$  that is analogous to the linear convection-dispersion Equation [*Maas, 1994*].

#### 4.1.3 Saturated zone

**Drainage** The saturated zone is fed from the percolation zone with a flux  $R_g$ . The lower boundary consists of a drainage flux  $R_d$  [ $LT^{-1}$ ], which is assumed to have a linear relation with the groundwater level:

$$R_d = \frac{h_d}{\gamma}, \quad (4.10)$$

where  $h_d$  is the groundwater level above some reference level [L], and  $\gamma$  is the drainage resistance [T]. The groundwater fluctuation is then described by the following reservoir function [*Knotters and Bierkens, 2000*]:

$$\varphi \frac{dh_d}{dt} = R_g - R_d, \quad (4.11)$$

where  $\varphi$  is a storage coefficient [-].

**Large-scale groundwater withdrawal** In many situations, large-scale withdrawal of groundwater has a significant influence on the groundwater level. If a large number of spatially distributed extraction wells are present, it is virtually impossible to estimate a transfer function for each individual well. Therefore the individual wells are lumped into one representative drawdown. For a groundwater withdrawal  $Q$  [ $LT^{-3}$ ] in a semi-confined aquifer  $i$  at distance  $r_Q$  [L] from the observation point, the drawdown  $s$  [L] after a time lag  $t$  [T] is calculated as [*Huisman, 1972*]

$$s_{i,t} = -\frac{Q}{4\pi T} W\left(u_i^2, \frac{r_Q}{\sqrt{T_i c_i}}\right), \quad (4.12)$$

with

$$u_i^2 = \frac{\varepsilon}{4T_i} \frac{r_Q^2}{t}, \quad (4.13)$$



$\varepsilon$  is the specific yield [-],  $T_i$  [ $L^2T^{-1}$ ] is the transmissivity and  $c_i$  [T] is the resistance of the semi-impervious layer for aquifer  $i$ . The function  $W$  is a logarithmic integral:

$$W\left(u^2, \frac{r_Q}{\sqrt{Tc}}\right) = \int_{u^2}^{\infty} \frac{1}{\nu} \exp\left(-\nu - \frac{r_Q^2}{4Tc\nu}\right) d\nu. \quad (4.14)$$

For each well, the drawdown at the observation point is calculated with Equation 4.12. The representative drawdown in aquifer  $i$  is then written as

$$s_{r,i} = \sum_k s_{k,i}, \quad (4.15)$$

where  $s_{k,i}$  is the drawdown caused by the  $k$ th well. Finally, the estimated drawdown at the observation well is calculated as a summation of the drawdown in each aquifer  $i$ , scaled by a factor  $\beta_i$  [-]:

$$s_{obs} = \sum_i \beta_i s_{r,i}. \quad (4.16)$$

The factor  $\beta_i$  is introduced for two reasons. First, the contribution of each aquifer to the drawdown may be not the same. Second, the representative drawdown in aquifer  $i$  is only an approximation of the drawdown. A correction factor enables one to improve this approximation during calibration.

**Groundwater level** The observed groundwater level can now be written as a superposition of the reference level  $z_r$ ,  $h_d$  from Equation 4.11, and  $s_{obs}$  from Equation 4.16:

$$z = z_r + h_d + s_{obs}, \quad (4.17)$$

with  $z$  the observed groundwater level [L].

## 4.2 State space representation of the nonlinear reservoir model

In order to calibrate the described model to a groundwater time series, it is written as the nonlinear discrete state space representation given in Equation 2.44:

$$\mathbf{x}_t = \mathcal{F}[\mathbf{x}_{t-1}, \mathbf{u}_t] + \mathbf{g}w_t, \quad (4.18)$$

with  $\mathcal{F}[\cdot, \cdot]$  a function of state and input. The terms of Equation 4.18 will be discussed below.

The vector  $\mathbf{u}_t$  represents the system input and is written as

$$\mathbf{u}_t^T = \begin{bmatrix} P_{G,t} & E_{r,t} \end{bmatrix}. \quad (4.19)$$

The nonlinear function  $\mathcal{F}[\cdot, \cdot]$  relates the state at the previous time step,  $\mathbf{x}_{t-1}$ , and the input at the current time step,  $\mathbf{u}_t$ , to the state at the current time step,  $\mathbf{x}_t$ . Basically, the vector  $\mathbf{x}_t$  consists of the three components described in the previous section: the root zone, percolation zone, and saturated zone.

The discretization of Equation 4.1 describing the root zone is rather straightforward. Only one provision is required to bound the degree of saturation between 0 and 1. This is because Equation 4.8 only has a solution for  $0 < S_e \leq 1$ . Therefore the function  $\tilde{S}_e$  is introduced, which is continuous and differentiable in  $\mathbb{R}$ :

$$\tilde{S}_e = \begin{cases} 0.05 \exp(20S_e - 1), & S_e < 0.05 \\ 1 - 0.05 \exp(19 - 20S_e), & S_e > 0.95 \\ S_e, & \text{otherwise.} \end{cases} \quad (4.20)$$

The first element of the state equation is then written as

$$S_{e,t} = S_{e,t-1} + \frac{\Delta t}{D_e} \left( f_i P_{G,t} - E_a(\tilde{S}_{e,t-1}) - R_p^{t-1} \right), \quad (4.21)$$

with

$$R_p^{t-1} = K_s \tilde{S}_{e,t-1}^\lambda \left[ 1 - \left( 1 - \tilde{S}_{e,t-1}^{1/m} \right)^m \right]^2, \quad (4.22)$$

and  $E_a(\cdot)$  as defined in Equation 4.5.

Equation 4.9 describing the percolation zone is written as the following discrete form of the linear reservoir model, which is a well-known discretization of the convection-dispersion equation:

$$\begin{bmatrix} R_{1,t} \\ R_{2,t} \\ R_{g,t} \end{bmatrix} = \begin{bmatrix} \delta_{p,1} R_{1,t-1} + (1 - \delta_{p,1}) R_p^{t-1} \\ \delta_{p,2} R_{2,t-1} + (1 - \delta_{p,2}) R_{1,t-1} \\ \delta_{p,3} R_{g,t-1} + (1 - \delta_{p,3}) R_{2,t-1} \end{bmatrix}, \quad (4.23)$$

where  $\delta_{p,i}$  is the autoregressive parameter of the  $i$ th state of the percolation zone [-]:  $0 \leq \delta_{p,i} < 1$ . At every time step, an impulse of the flux from the root zone  $R_p$  enters at  $R_1$  and is damped while passing through the states. Note that the gain of each equation is equal to 1. Obviously, the number of states can be reduced or extended depending on the length of the percolation zone, but in most practical applications satisfactory results have been obtained with the use of three states.

Equation 4.11, describing the saturated zone, is rewritten as

$$h_{d,t} = \delta_s h_{d,t-1} + \omega R_{g,t-1}, \quad (4.24)$$

with  $\delta_s = \exp(-1/\varphi\gamma)$ , and  $\omega = \gamma(1 - \delta_s)$ .

Fluctuations of the groundwater level that cannot be described by the previous states are described by a stochastic or ‘residual’ component  $\xi$ , written as the following autoregressive model:

$$\xi_t = \phi \xi_{t-1} + w_t, \quad (4.25)$$

where  $\phi$  is an autoregressive parameter [-]:  $0 \leq \phi < 1$ , and  $w_t$  is a zero-mean white-noise process with covariance  $q$ . The vector  $\mathbf{g}$  relates  $w_t$  to the state  $\xi$  (residual component):

$$\mathbf{g}^T = \begin{bmatrix} 0 & 0 & 0 & 0 & 0 & 1 \end{bmatrix}. \quad (4.26)$$

In addition to the noise term in the residual component, noise may enter the model in the root zone as well. However, tests (using Equation 2.50 on page 39) have shown that this additional noise term leads to a poor filter performance. Hence, we describe the system noise only by the residual component of Equation 4.25. This component thus accounts for all model errors and unknown disturbances.

The elements of the state vector

$$\mathbf{x}_t^T = \begin{bmatrix} S_{e,t} & R_{1,t} & R_{2,t} & R_{g,t} & h_{d,t} & \xi_t \end{bmatrix} \quad (4.27)$$

are not observed directly. Instead, the measurement  $z_t$  is observed, which is a function of  $\mathbf{x}_t$  (Equation 4.17), the reference level  $z_r$ , the drawdown  $s_{obs,t}$ , and the measurement noise  $v_t$ :

$$z_t = \mathbf{c}\mathbf{x}_t + z_r + s_{obs,t} + v_t, \quad (4.28)$$

where  $\mathbf{c} = [0 \ 0 \ 0 \ 0 \ 1 \ 1]$ , and  $v_t$  is a zero-mean white-noise process with variance  $r$  representing the measurement error. Extension of the measurement equation with other observations (e.g. soil moisture data) is straightforward.

The unknown parameters in the equations given above need to be estimated and will be referred to as the vector  $\boldsymbol{\alpha} = [f_i, f_c, S_r, m, D_e, K_s, \lambda, \delta_p, \varphi, \gamma, \beta, z_r, \phi, q, r]$ . Usually, the variance of the measurement error  $r$  is assumed to be known. In addition, the parameters  $f_i$ ,  $f_c$ ,  $S_r$ , and  $m$  can be obtained from field data. Maximum-likelihood estimates of  $\boldsymbol{\alpha}$  are calculated by embedding the extended Kalman filter of Equation 2.46 on page 38 in the optimization procedure described in Section 2.7.

### 4.3 Example applications

The nonlinear state space model was applied at two locations in the center of the Netherlands. At the first location ("Ermelo"), the groundwater level was moderately deep (ca. 10-13 m below surface level). The second location ("Kootwijk") had a deeper groundwater level (16-20 m below surface level). Both depths were large enough to justify the assumption of gravity-driven flow in the percolation zone. Since at both locations the available amount of data was too small for creating a validation set, this section evaluates the prediction performances using the data that were also used for model calibration (generally referred to as verification).

#### 4.3.1 Description of the data sets

**Location Ermelo** The first test case is a groundwater time series (period 1960-1999,  $N = 819$ ) with a frequency of observation of twice a month. The water table

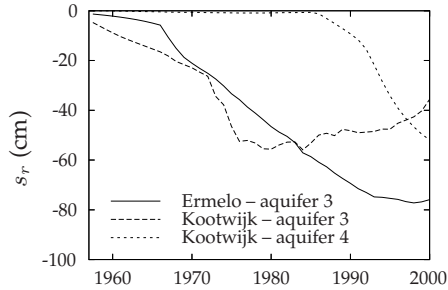


**Figure 4.3:** Representative drawdown for Ermelo and Kootwijk; for Kootwijk, a drawdown is observed in two aquifers

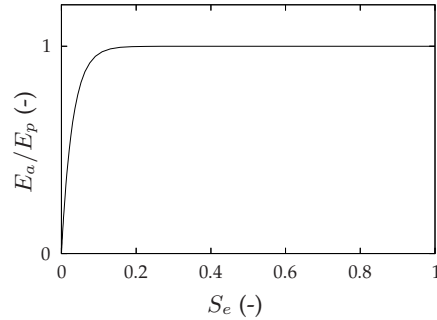


**Figure 4.4:** Water uptake function ( $S_r = 0.2$ ) for Ermelo and Kootwijk, based on a soil water retention curve for sand soils and a reduction point of  $\psi_r = -100$  cm

fluctuated between 10 - 13 m below surface level. The dominating vegetation was forest. Corresponding values for the interception factor and the crop factor are  $f_i = 0.8$  and  $f_c = 0.7$ , respectively [Feddes, 1987]. Descriptions of the soil profile showed that this location consists of a sand soil.

**Location Kootwijk** The second groundwater time series (period 1957-1999,  $N = 1002$ ) also had a frequency of observation of twice a month. The water table was deeper than that at location Ermelo: 16 - 20 m below surface level. At this location the dominating vegetation was purple moor grass. Gehrels [1999] reports a value of  $f_c = 1.0$  for this type of vegetation. The interception factor was set to  $f_i = 1.0$ . The soil mainly consists of sand.

**Meteorological data** Since accurate modeling of the root zone requires a small modeling interval, daily observations of the input variables were used. Gross precipitation was obtained by spatial interpolation of observations from surrounding meteorological stations, whereas the reference evapotranspiration was obtained from the main meteorological station of the Royal Netherlands Meteorological Institute at De Bilt.

**Groundwater withdrawal** The number of wells was ca. 500, with a maximum total withdrawal of ca.  $300 \times 10^6 \text{ m}^3 \cdot \text{y}^{-1}$ . Figure 4.3 shows the representative draw-

**Table 4.1:** Parameters for location Ermelo and Kootwijk that are not estimated

Parameter	Ermelo	Kootwijk
$f_i$	0.8	1.0
$f_c$	0.7	1.0
$S_r$	0.2	0.2
$m$	0.4	0.4
$r, \text{cm}^2$	1.0	1.0

**Table 4.2:** Maximum likelihood estimates of the parameters for location Ermelo of nonlinear model and linear model with associated first-order estimates of error standard deviation

Parameter	Nonlinear model		Linear model	
	Estimate	Standard deviation	Estimate	Standard deviation
$D_e$ , cm	29.4	2.18		
$K_s$ , cm.day <sup>-1</sup>	0.532	0.0414		
$\lambda$	-3.74	0.206		
$\delta_r$			0.990	0.000623
$\delta_p$	0.661	0.0297	0.292	0.173
$\varphi$	0.263	0.00561	0.284	0.0115
$\gamma$ , day	2882	109	2688	109
$\beta$	0.659	0.0655	0.627	0.0737
$z_r$ , cm	620	10.4	636	10.3
$\phi$	0.9978	0.000405	0.9975	0.000440
$q$ , cm <sup>2</sup>	0.312	0.0146	0.492	0.0207
$\text{var}(\xi_t)$ , cm <sup>2</sup>	69.4	13.1	100.1	17.9

down at both locations. At Ermelo only one aquifer was influenced by groundwater abstractions, whereas at Kootwijk two aquifers were influenced.

#### 4.3.2 Calibration and evaluation

A number of model parameters was not calibrated, but a priori set at a fixed value. Table 4.1 gives these parameters with their associated fixed values. The interception factor  $f_i$ , the crop factor  $f_c$  and the shape factor  $m$  were taken directly from the field data (Section 4.3.1). The shape factor  $S_r$  was set to a value of 0.2. In this way, the exponential model describing  $E_a/E_p$  as a function of  $S_e$  (Equation 4.5) approximates the water uptake curve for a sand soil (Figure 4.4). Furthermore, the variance of the measurement error was assumed to be equal to 1 cm<sup>2</sup>.

In order to determine the influence of the introduced nonlinearities, the time series were also modeled with a linear state space model. The only difference with the nonlinear model is that the linear model replaces the nonlinear Equation 4.21 with a linear equation that is equivalent to a state equation in the percolation zone (Equation 4.23). The autoregressive parameter in the linear root zone is referred to as  $\delta_r$ .

##### Location Ermelo

Table 4.2 shows the calibrated parameters with error standard deviations for both the nonlinear model and the linear model. Estimation of the parameters of the percolation zone ( $\delta_{p,1}$ ,  $\delta_{p,2}$  and  $\delta_{p,3}$ ) showed that these parameters were highly correlated. The same results were obtained when all three parameters were set to the same value, i.e., only one parameter was estimated ( $\delta_p$  in Table 4.2). Note that the calibrated parameters for the saturated zone ( $\varphi$  and  $\gamma$ ), the parameter for the draw-down ( $\beta$ ), the reference level  $z_r$ , and the autoregressive parameter of the residual component ( $\phi$ ) of both models are not significantly different (given the estimated standard deviation of estimation errors). On the other hand, the system noise variance  $q$  shows a reduction of 37% with respect to the variance  $q$  of the linear model.

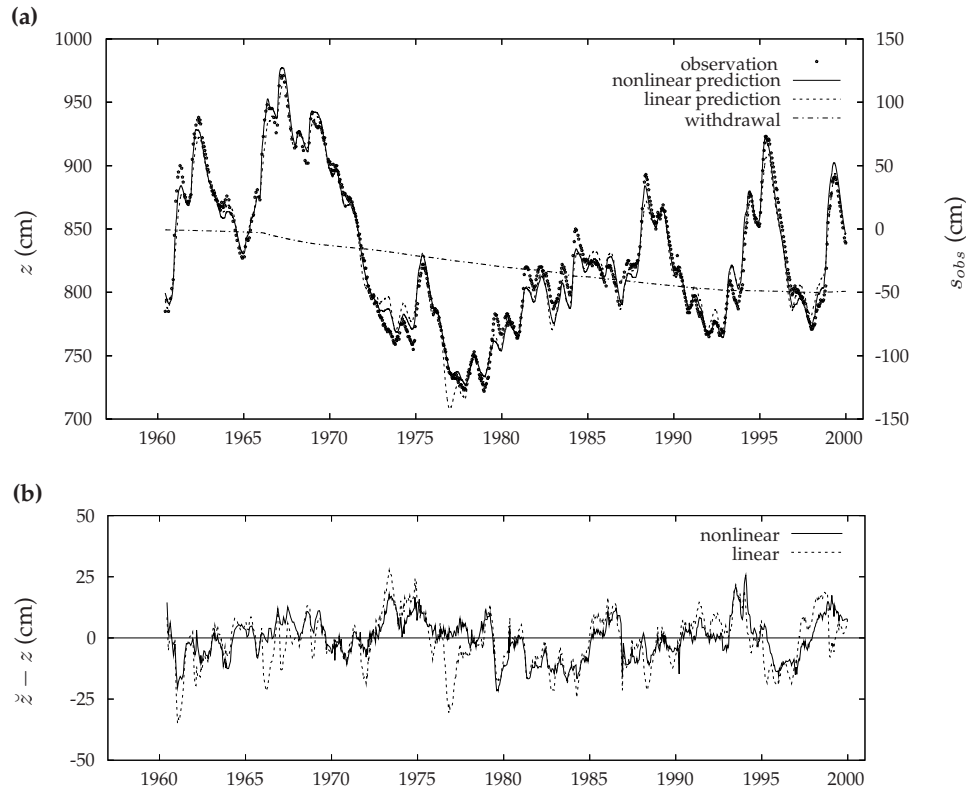


**Figure 4.5:** (a) Prediction of nonlinear model and that of linear model, effect of groundwater withdrawal (effects of both models do not differ significantly), together with the observations at location Ermelo; and (b) prediction error (residual component) of nonlinear model and linear model for location Ermelo

This means that the prediction uncertainty of the nonlinear model is much smaller.

Figure 4.5a shows the prediction  $\hat{z}$  (i.e. the deterministic component) of the calibrated nonlinear model and of the calibrated linear model together with the measurements  $z$ . Since the estimated effect of groundwater withdrawal is almost equal for both models, the figure only plots the effect as estimated by the nonlinear model. Figure 4.5b shows the prediction error of the deterministic component, i.e. the predicted groundwater level minus the measured one. Overall, both models perform well. The nonlinear model, however, generally predicts local extremes better than the linear model. This is best observed in Figure 4.5b. Especially for the very dry year of 1976, the linear model predicted a groundwater level that is ca. 30 cm lower than the observed one. The nonlinear model, on the other hand, predicted the observed decline well.

In addition to the parameter estimates, Table 4.2 gives the variance of the resid-

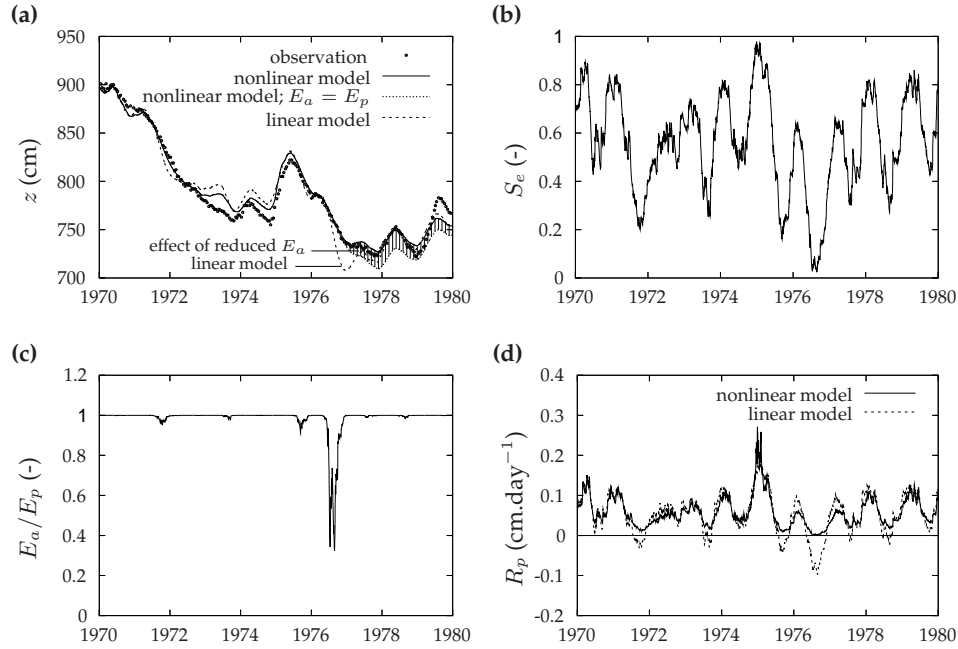


**Figure 4.6:** (a) Prediction of groundwater level, with the shaded area representing the effect of the nonlinear relation between  $E_a$  and  $S_e$ ; (b) degree of water saturation in nonlinear root zone; (c) ratio between actual and potential evapotranspiration for the nonlinear model; and (d) percolation flux for the nonlinear and linear model for the period 1970-1980

ual component for both the nonlinear and linear model, calculated as

$$\text{var}(\xi_t) = \frac{q}{1 - \phi^2}. \quad (4.29)$$

In addition, standard deviations of the estimated residual variances are given. These standard deviations are based on the standard deviations of  $q$  and  $\phi$ . The figures show that by incorporating the nonlinear root zone, we have reduced the residual variance by approximately 31%.

Since the nonlinear root zone is the only difference between the nonlinear and the linear model, it is interesting to determine what part of the nonlinearity – actual evapotranspiration or the percolation flux – is responsible for the increase in model accuracy. For this purpose, Figure 4.6 plots for the period 1970-1980 the predicted groundwater level together with the following quantities of the root zone: the degree of water saturation  $S_e$  (i.e. the first state of the state vector  $\mathbf{x}_t$ ), the ratio between the actual and potential evapotranspiration (derived from  $S_e$  using Equation 4.5), and the percolation flux for both the nonlinear model (derived from  $S_e$  using Equation 4.22) and the linear model (first state of the state vector). As can be seen from the figure, most of the time, actual evapotranspiration  $E_a$  equals

**Table 4.3:** Maximum likelihood estimates of the parameters for location Kootwijk of nonlinear model and linear model with associated first-order estimates of error standard deviation

Parameter	Nonlinear model		Linear model	
	Estimate	Standard deviation	Estimate	Standard deviation
$D_e$ , cm	41.2	6.54		
$K_s$ , cm.day <sup>-1</sup>	0.671	0.0904		
$\lambda$	-3.54	0.578		
$\delta_r$			0.992	0.00300
$\delta_{p,1}$	0.990	0.000943	0.992	0.00299
$\delta_{p,2}$	0.840	0.111		
$\delta_{p,3}$	0.834	0.117		
$\varphi$	0.267	0.0101	0.274	0.0109
$\gamma$ , day	7986	1103	5672	672
$\beta_1$	0.399	0.586	1.51	0.461
$\beta_2$	1.34	0.268	0.532	0.367
$z_r$ , cm	2062	125	2315	68.3
$\phi$	0.9989	0.000390	0.9990	0.000288
$q$ , cm <sup>2</sup>	0.682	0.0260	0.803	0.0290
$\text{var}(\xi_t)$ , cm <sup>2</sup>	310.2	34.5	401.7	53.7

potential evapotranspiration  $E_p$ . In 1976,  $E_a/E_p$  dropped to a value of 0.4. For that period, the cumulative difference between  $E_a$  and  $E_p$  is ca. 9 cm. The effect of the reduced evapotranspiration on the groundwater level is denoted by the shaded area in Figure 4.6a. The area represents the difference between the groundwater level predicted with the calibrated nonlinear model and that predicted with the nonlinear model assuming full evapotranspiration ( $E_a = E_p$ ). First, the figure shows that the reduction of the evapotranspiration rate affects the groundwater level considerably: the maximum difference between both predictions is almost 20 cm, and, due to the slow response time of the system, the effect is still present after a couple of years. Second, the figure shows that the underestimation of the groundwater level for 1976 by the linear model mainly results from neglecting the other nonlinear relation, namely the relation between percolation flux  $R_p$  and the degree of water saturation  $S_e$ . This is further illustrated in Figure 4.6d. Here the percolation flux is plotted as a function of time for both the linear and nonlinear model. The figure clearly demonstrates why the groundwater level decline was overestimated: during a half-year period, the percolation flux in the linear model is negative, i.e. an upward flux of at most 0.1 mm.day<sup>-1</sup>. This is quite unrealistic for a groundwater level that is ca. 10 m below surface level. The same phenomenon is observed for 1971: the linear estimate of the percolation flux becomes negative, so that the groundwater level decline is overestimated.

Summarizing, the nonlinear model predicts extremes in groundwater level fluctuations better than the linear model. As a result, it has a much lower noise variance  $q$  and residual variance  $\text{var}(\xi_t)$ . The example showed that most of the improvement is caused by the nonlinear relation between the percolation flux  $R_p$  and the degree of water saturation  $S_e$ , producing a more realistic estimate of the percolation flux.



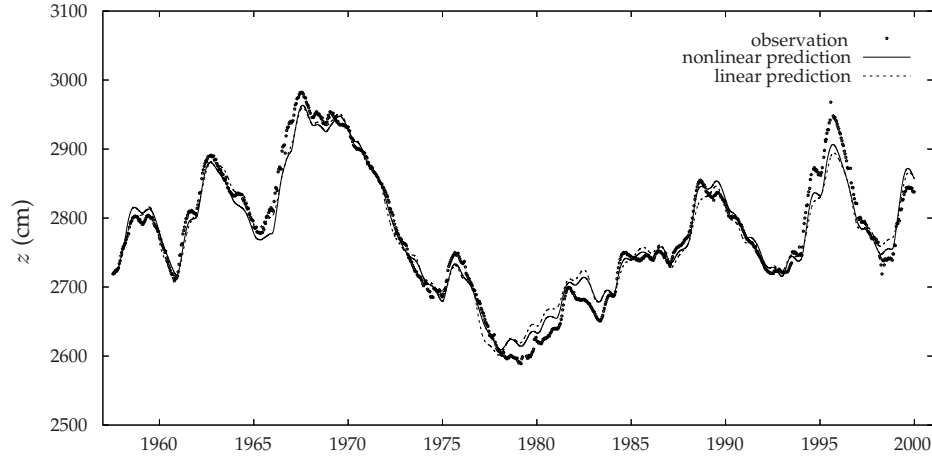


**Figure 4.7:** Prediction of nonlinear model and that of linear model compared with observations at location Kootwijk

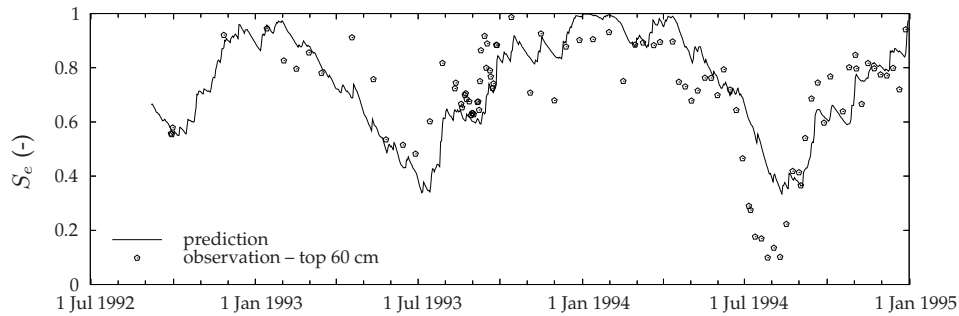
#### Location Kootwijk

Table 4.3 gives the calibrated parameters with associated error standard deviations of the nonlinear model. Like the table for location Ermelo, it compares the results with those of a linear model. Note that the groundwater time series is short relative to the response time of the system. Based on the parameters of the percolation zone and saturated zone, the characteristic response time of the system is 17 years, which is ca. 40% of the length of the time series. Consequently, the error standard deviations of the estimated parameters are relatively high (e.g.,  $\beta_1$  and  $\beta_2$ ). Also, the linear model could estimate only one significant parameter for describing the percolation zone.

Figure 4.7 shows the prediction of the models together with observations. The difference between the nonlinear predictions and the linear ones is less distinct than for location Ermelo. The reason for this is that, due to the slower response of the groundwater level to the percolation flux, the influence of the root zone at location Kootwijk is less than that for location Ermelo. Nevertheless, the variance of the system noise  $q$  and the residual variance  $\text{var}(\xi_t)$  of the nonlinear model are still significantly smaller than those of the linear model, indicating that the nonlinear model predicts the groundwater level fluctuations more accurately than the linear model.

The applicability of the state space model would be extended if it could not only be used to predict groundwater fluctuations, but also to estimate the average soil water content in the root zone (by using the first element of the state vector in Equation 4.27). From the soil water content, actual evapotranspiration and the percolation rate can be derived. Below, the results of the nonlinear model are compared with the results of field experiments.

During the 1990s, *Gehrels* [1999] investigated groundwater fluctuations in the



**Figure 4.8:** Prediction of the degree of water saturation compared with the degree of water saturation derived from soil water content measurements averaged over the top 60 cm for the period July 1992 until January 1995 (measurements adapted from Gehrels [1999]).

area around Kootwijk. Part of his study consisted of modeling of soil water movement, estimation of percolation rates, and estimation of groundwater recharge. For this purpose, several field investigations were carried out, such as tracer methods for recharge estimation and capacitance probe soil water measurements. A detailed description of these methods, the way they were used, and the results are given in Gehrels [1999].

The soil water content predictions of the nonlinear model were compared with the soil water measurements described in Gehrels [1999]. Soil water content was monitored at several depths ranging from 4 cm to 300 cm below surface. Measurements were available for September 1992 to December 1994. The measuring interval varied from daily to weekly. In order to compare the measurements with model predictions, the actual degree of saturation was derived from the measurements and averaged over the top 60 cm. Figure 4.8 shows the measured degree of saturation averaged over the depth interval, together with the predicted degree of water saturation. From the figure it follows that the nonlinear model predicts the average degree of saturation reasonably well.

Other quantities that can be derived from the model are actual evapotranspiration and the percolation rate. Figure 4.9 shows the annual actual evapotranspiration and the annual percolation rate. Actual evapotranspiration is remarkably constant through time, with an average of  $528 \text{ mm.y}^{-1}$ . In contrast, the percolation rate has a high temporal variability, which is the result of the temporal variability of precipitation. The average annual percolation rate is  $352 \text{ mm.y}^{-1}$ . From a chloride mass balance, Gehrels [1999] calculated an average percolation rate of  $360 \text{ mm.y}^{-1}$ . Furthermore, he calculated the average annual percolation rate from a chloride mass balance and an oxygen-18 tracer test for the period 1993-1995. The methods provided an estimate of the annual percolation rate of  $510 \text{ mm.y}^{-1}$  and  $459 \text{ mm.y}^{-1}$ , respectively. For the same period, the state space model gives an average annual percolation rate of  $523 \text{ mm.y}^{-1}$ .

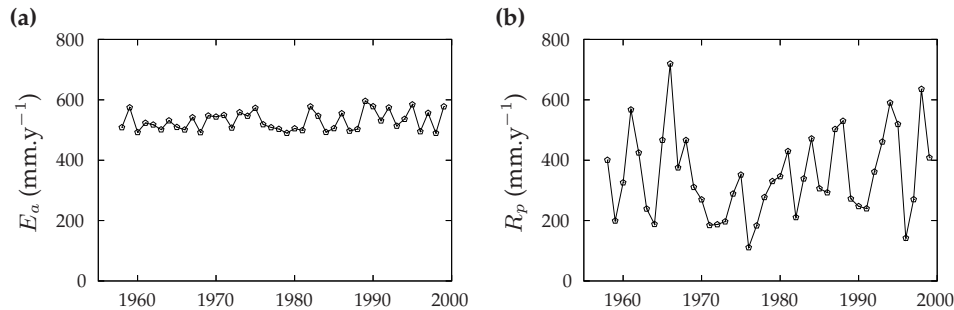


**Figure 4.9:** Annual values as calculated with the nonlinear model of (a) actual evapotranspiration and (b) percolation rate

#### 4.4 Summary and conclusions

This chapter presented a nonlinear time series model for analyzing time series of groundwater level data. The model incorporates the unobserved degree of water saturation of the root zone to model actual evapotranspiration and groundwater recharge. Model parameters were calibrated by applying an extended Kalman filter together with a maximum likelihood criterion. On the basis of two test cases and comparison of results with those of a linear transfer function-noise model, some general conclusions are drawn.

The main conclusion is that the nonlinear model predicts groundwater level fluctuations more accurately than the linear TFN model. In particular, extremes in the time series (very wet or dry periods) are described better by the nonlinear model. As a result, temporal trends can be estimated with higher certainty. Another interpretation is that, given a requested level of certainty, trends can be detected within a shorter space of time.

The first test case showed that the increase in model accuracy mainly results from the improved description of the percolation flux. As a consequence of the introduced nonlinearity, the variance of the residual component was 31% lower. In the second test case the unsaturated zone was larger, resulting in a smaller influence of the root zone on the water table. The variance of the residual component was 23% lower for the nonlinear model.

The nonlinear model does not only incorporate nonlinear conceptual relations in the root zone (our primary goal), it also predicts the degree of water saturation in the root zone fairly well. The model could predict the degree of saturation even more accurately if it were calibrated using measurements of the degree of saturation. Finally, actual evapotranspiration and the percolation rate were derived from the model. It was shown that these quantities were close to water balance results obtained from field experiments.



# 5

## State space modeling in switching regimes

---

**Abstract.** A nonlinear state space model is developed for describing groundwater fluctuations in systems that are influenced by drains. As drains are only active if the water table is above drainage level, the regime of the system switches at the drainage level. The groundwater level is related to observations on precipitation and evapotranspiration, regional groundwater flow, and drainage flux. The drainage flux is a nonlinear function of the groundwater level in the sense that it switches from a constant (zero) flux if the water table is below drainage level to a flux that is linearly related to the groundwater level if the water table is above drainage level. The system noise is also nonlinearly related to the groundwater level. The model is calibrated on a time series of groundwater level data using a maximum likelihood criterion. For this purpose the model is processed through a truncated first-order filter. To increase filter performance, the strong nonlinear relation between the groundwater level and the drainage flux is smoothed. The state space model was tested at two locations. It is shown that the model performs well. Moreover, it is superior to commonly applied linear transfer function-noise models. The applications illustrate the suitability of the state space model for estimating the effects of interventions, for characterizing the groundwater system, and for simulation and prediction.

---

*This chapter is adapted from Berendrecht, W.L., A.W. Heemink, F.C. van Geer, and J.C. Gehrels, State space modeling of water table fluctuations in switching regimes, Journal of Hydrology, 292, 249–261, 2004*

**S**WITCHING REGIMES are regularly found in hydrology. Well-known examples are stream flow in rivers with a weir and groundwater fluctuations in systems with different drainage levels. *Knotters and De Gooijer* [1999] already applied a threshold autoregressive self-exciting open-loop (TARSO) model [Tong, 1990] to describe this type of system. The previous chapters, however, showed that the state space approach is more attractive for several reasons. The state space model can incorporate physical knowledge easily, giving more insight into the hydrological processes. This is advantageous when the model is applied to support water management and decision making.

The aim of this chapter is therefore to develop a state space threshold model for hydrological applications. Although the model concept is general, this chapter focuses on nonlinearity in groundwater systems due to drainage. Such systems can be found in lowland areas with shallow water tables (less than 2 m below ground surface). Changes in the regime are caused by temporary activation of drains in periods of high water levels. The state space model describes the observed groundwater level using precipitation and evapotranspiration as input. Due to the physical basis, effects of interventions can easily be incorporated into the model. Model parameters, including the threshold value (drainage level), are estimated using a maximum likelihood criterion combined with a truncated first-order filter.

The model is tested on two time series of groundwater level data. Results show that the state space model describes the groundwater fluctuations very well. Moreover, the performance of the model is superior to that of common linear transfer function-noise models. This chapter also demonstrates that the state space model can be used for characterization of the groundwater system.

## 5.1 Water balance of a nonlinear phreatic groundwater system

Figure 5.1 shows a typical schematization of a groundwater system that is dominated by drainage. A water balance for this system is given by

$$\varphi \frac{dh_t}{dt} = f_i P_t - f_c E_{r,t} - q_{b,t} - q_{v,t} - q_{l,t}, \quad (5.1)$$

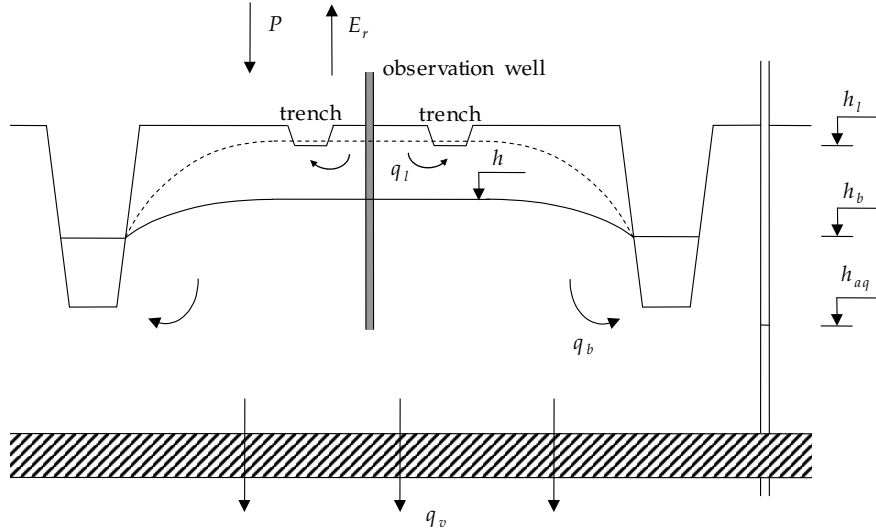


**Figure 5.1:** Schematization of the groundwater system; the dashed line represents a typical water table during winter, the solid line represents a typical water table during summer.

where  $h_t$  is the groundwater level at the observation well [L],  $P_t$  is the precipitation [ $\text{LT}^{-1}$ ],  $E_{r,t}$  is the Makkink reference evapotranspiration [ $\text{LT}^{-1}$ ] [Winter *et al.*, 1995],  $f_i$  is an interception factor [-],  $f_c$  is a crop factor [-] [Feddes, 1987],  $\varphi$  is a storage coefficient [-],  $q_{b,t}$  is the flux to the main drainage system [ $\text{LT}^{-1}$ ],  $q_{v,t}$  is the vertical flux representing downward seepage [ $\text{LT}^{-1}$ ], and  $q_{l,t}$  is the flux to the local drainage system [ $\text{LT}^{-1}$ ]. The vertical flux,  $q_{v,t}$  is assumed to be related to the groundwater level as

$$q_{v,t} = \frac{h_t - h_{aq,t}}{\gamma_v}, \quad (5.2)$$

where  $h_{aq,t}$  is the head in the underlying semi-confined aquifer [L], and  $\gamma_v$  is the resistance of the semi-confining layer [T]. Similarly, the flux to the main drainage system is written as

$$q_{b,t} = \frac{h_t - h_{b,t}}{\gamma_b}, \quad (5.3)$$

where  $h_{b,t}$  represents the drainage base level [L], and  $\gamma_b$  represents the resistance between the observation well and the main drainage system [T]. The drainage base level is assumed to be exogenous (i.e., independent of system variables). As a result, water exfiltrates if the groundwater level is higher than the drainage base level, and infiltrates if it is lower.

Since both  $q_{v,t}$  and  $q_{b,t}$  are linearly related to the groundwater level  $h_t$ , they are

added together in a variable  $q_{r,t}$ , representing the “regional” flow [ $\text{LT}^{-1}$ ]:

$$q_{r,t} = \frac{h_t - h_{r,t}}{\gamma_r}, \quad (5.4)$$

where  $h_{r,t}$  [L] and  $\gamma_r$  [T] can be defined in terms of Equations 5.2 and 5.3, depending on the boundary conditions. For example, one of the following sets of boundary conditions can be applied:

1. a prescribed head (Dirichlet condition) for both  $h_{b,t}$  and  $h_{aq,t}$ :

$$\gamma_r = \frac{\gamma_b \gamma_v}{\gamma_b + \gamma_v} \quad \text{and} \quad h_{r,t} = \frac{\gamma_b h_{aq,t} + \gamma_v h_{b,t}}{\gamma_b + \gamma_v}, \quad (5.5)$$

2. a prescribed head (Dirichlet condition) for  $h_{b,t}$  and a constant flux (Neumann condition) for  $q_v$ :

$$\gamma_r = \gamma_b \quad \text{and} \quad h_{r,t} = h_{b,t} - \gamma_b q_v. \quad (5.6)$$

The essential part of the groundwater system depicted in Figure 5.1 is the local drainage system represented by the trenches. In the situation of Figure 5.1, where the water table is lower than the local drainage level  $h_l$  [L], the drainage system is not active. However, as the water table rises and becomes higher than the threshold  $h_l$  (dashed line), groundwater is discharged through the trenches. The drainage flux  $q_{l,t}$  [ $\text{LT}^{-1}$ ] is therefore described by the following equations:

$$q_{l,t} = \begin{cases} 0 & h_t \leq h_l, \\ \frac{h_t - h_l}{\gamma_l} & h_t > h_l, \end{cases} \quad (5.7)$$

where  $\gamma_l$  is the local drainage resistance [T].

Equation 5.1 can now be written as the following ordinary differential equation:

$$\frac{dh_t}{dt} = \frac{1}{\varphi} \left[ f_i P_t - f_c E_{r,t} - \frac{h_t - h_{r,t}}{\gamma_r} - q_{l,t} \right]. \quad (5.8)$$

## 5.2 State space model of the phreatic system

The model described by Equation 5.8 is calibrated to a groundwater time series by combining a maximum likelihood criterion with a nonlinear filter. For this purpose, Equation 5.8 is written as (see Equation 2.47):

$$h_t = \mathcal{F}[h_{t-1}, \mathbf{u}_t] + \mathcal{G}[h_{t-1}] w_t, \quad (5.9a)$$

$$z_t = h_t + v_t, \quad (5.9b)$$

where  $h_t$  is the system state at time  $t$  representing the groundwater level at the observation well,  $z_t$  is the observation at time  $t$  allowing for an observation error



$v_t \simeq N(0, \sigma_v^2)$ ,  $w_t \simeq N(0, \sigma_w^2)$  represents system noise containing errors in model inputs and errors due to model assumptions, and  $\mathbf{u}_t$  is a vector containing the input data at time  $t$  written as

$$\mathbf{u}_t = \begin{bmatrix} P_t \\ E_{r,t} \end{bmatrix}. \quad (5.10)$$

The vector  $\mathbf{u}_t$  can easily be extended with more input data, such as data describing interventions. For instance, if the reference level  $h_r$  changes over time, the input vector can be augmented with an input series of fluctuations  $\Delta h_{r,t}$ , so that  $h_{r,t}$  is written as

$$h_{r,t} = h_r + \beta \Delta h_{r,t}, \quad (5.11)$$

where  $\beta$  is a scaling factor [-] depending on the source of fluctuations (e.g.,  $h_b$  or  $h_{aq}$ ) and the type of boundary condition (see Equations 5.5 and 5.6).

For  $h_t \leq h_l$  ( $q_{l,t} = 0$ ), Equation 5.8 is approximated by the following discrete form:

$$h_t = h_{t-\Delta t} e^{-\Delta t / \varphi \gamma_r} + \int_{t-\Delta t}^t e^{-(t-\tau) / \varphi \gamma_r} \frac{1}{\varphi} \left( f_i P_t - f_c E_{r,t} + \frac{h_{r,t}}{\gamma_r} \right) d\tau. \quad (5.12)$$

Assuming that  $P_t$  and  $E_{r,t}$  are constant between  $t - \Delta t$  and  $t$ , the following equation is obtained:

$$h_t = h_{t-\Delta t} e^{-\Delta t / \varphi \gamma_r} + \gamma_r \left( 1 - e^{-\Delta t / \varphi \gamma_r} \right) \left( f_i P_t - f_c E_{r,t} + \frac{h_{r,t}}{\gamma_r} \right), \quad (5.13)$$

or

$$h_t = \delta_r h_{t-\Delta t} + \omega_r (f_i P_t - f_c E_{r,t}) + \mu_{r,t}, \quad (5.14)$$

with

$$\delta_r = e^{-\Delta t / \varphi \gamma_r} \quad [-], \quad (5.15)$$

$$\omega_r = \gamma_r (1 - \delta_r) \quad [\text{T}], \quad (5.16)$$

$$\mu_{r,t} = h_{r,t} (1 - \delta_r) \quad [\text{L}]. \quad (5.17)$$

Similarly, Equation 5.8 for  $h_t > h_l$  is written as

$$h_t = \delta_s h_{t-\Delta t} + \omega_s (f_i P_t - f_c E_{r,t}) + \mu_{s,t}, \quad (5.18)$$

with

$$\delta_s = e^{-\Delta t / \varphi \Gamma} \quad [-], \quad (5.19)$$

$$\omega_s = \Gamma (1 - \delta_s) \quad [\text{T}], \quad (5.20)$$

$$\mu_{s,t} = H_t (1 - \delta_s) \quad [\text{L}], \quad (5.21)$$

and (similar to Equation 5.5) lumping  $h_l$ ,  $h_{r,t}$ ,  $\gamma_l$  and  $\gamma_r$  into

$$\Gamma = \frac{\gamma_l \gamma_r}{\gamma_l + \gamma_r} \text{ [T]} \text{ and } H_t = \frac{\gamma_r h_l + \gamma_l h_{r,t}}{\gamma_l + \gamma_r} \text{ [L]}. \quad (5.22)$$

Equations 5.14 and 5.18 can also be written in terms of the local drainage flux  $q_{l,t}$ :

$$h_t = \delta_r h_{t-\Delta t} + \omega_r (f_i P_t - f_c E_{r,t} - q_{l,t}) + \mu_{r,t}. \quad (5.23)$$

For  $h_t \leq h_l$ ,  $q_{l,t} = 0$ , while for  $h_t > h_l$ ,  $q_{l,t}$  can be calculated by substituting Equation 5.18 into Equation 5.23 and isolating  $q_{l,t}$ :

$$q_{l,t} = \frac{1}{\omega_r} [(\delta_r - \delta_s) h_{t-\Delta t} + (\omega_r - \omega_s) (f_i P_t - f_c E_{r,t}) + \mu_{r,t} - \mu_{s,t}]. \quad (5.24)$$

Since  $q_{l,t}$  and thus  $h_t$  is non-differentiable at  $h_t = h_l$ , Equation 5.24 needs to be smoothed. For this purpose,  $q_{l,t}$  is transformed into the function  $q_{l,t}^*$ , which is differentiable in  $\mathbb{R}$  up to the second order:

$$q_{l,t}^* = \begin{cases} \frac{2\lambda e^{2(q_{l,t}-\lambda)/\lambda}}{1+e^{2(q_{l,t}-\lambda)/\lambda}} & \text{for } q_{l,t} < \lambda, \\ q_{l,t} & \text{for } q_{l,t} \geq \lambda, \end{cases} \quad (5.25)$$

with  $\lambda$  ( $\lambda > 0$ ) a small value (e.g.  $\lambda = 0.01$ ) and  $q_{l,t}$  as defined in Equation 5.24. At  $q_{l,t} = \lambda$  the function  $q_{l,t}^*$  switches from a linear function to an exponential function that is positive definite. In this way,  $q_{l,t}$  asymptotically approaches zero if the water table is lower than the local drainage level  $h_l$ . A larger value of  $\lambda$  gives a smoother function but one that approximates the original function less well. Hence, the choice of  $\lambda$  is a trade-off between filter performance and model correctness.

The influence of the system noise  $w_t$  (see Equation 5.9a) may change as the regime switches. For this reason, we write the stochastic part of Equation 5.9a,  $\xi_t = \mathcal{G}[h_{t-1}] w_t$ , as the following smooth function:

$$\xi_t = \left[ 1 + (g - 1) \frac{e^{\kappa(h_l - h_{t-\Delta t})}}{1 + e^{\kappa(h_l - h_{t-\Delta t})}} \right] w_t, \quad (5.26)$$

where  $\kappa$  is a scaling factor determining the smoothness of Equation 5.26, and  $g$  determines the influence of the system noise below the local drainage level. Above the drainage level,  $\xi_t$  is asymptotically equal to  $w_t$ , and below the drainage level,  $\xi_t$  is asymptotically equal to  $g w_t$ .

The complete state space model can now be written by combining Equations 5.23, 5.25 and 5.26, with  $\Delta t = 1$ :

$$h_t = \delta_r h_{t-1} + \omega_r (f_i P_t - f_c E_{r,t} - q_{l,t}^*) + \mu_{r,t} + \xi_t, \quad (5.27a)$$

$$z_t = h_t + v_t. \quad (5.27b)$$

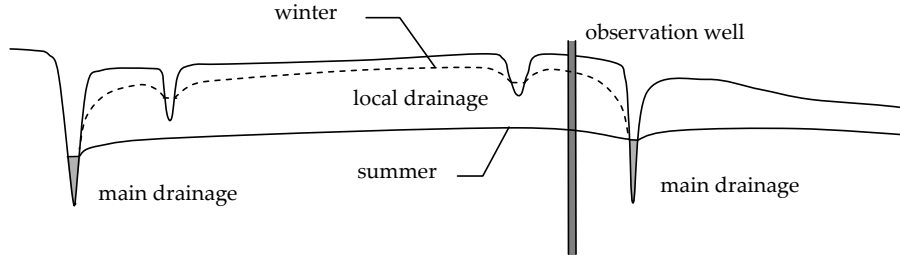


Figure 5.2: Schematization of the “Mortelen” site (well 1)

The unknown parameters in Equation 5.27 need to be estimated and will be referred to as the vector  $\alpha = [f_i, f_c, \gamma_l, h_l, \varphi, \gamma_r, h_r, \beta, g, \sigma_w^2]$ . The variance of the measurement error  $\sigma_v^2$  is assumed to be known. Besides, the parameters  $f_i$  and  $f_c$  are obtained from field data. Maximum-likelihood estimates of  $\alpha$  are calculated by embedding the truncated filter-order filter of Equation 2.48 in the optimization procedure described in Section 2.7.

### 5.3 Application and evaluation of the nonlinear model

The model was tested on two time series. At both locations, the groundwater level was influenced by local drainage. The calibration results will be discussed separately. The end of the section compares the performance of the state space model with that of a linear transfer function-noise (TFN) model.

#### 5.3.1 Observation well 1

The first time series was obtained from a well at the site “Mortelen” in the southern part of the Netherlands. Observations on groundwater levels were available for September 1967 with an average observation frequency of twice a month. The variance of the measurement noise was assumed to be  $\sigma_v^2 = 0.5 \text{ cm}^2$ . Data on daily precipitation were obtained from the meteorological station of Dinther at 14 km distance from the well site. Data on daily reference evapotranspiration were estimated as an average of daily observations at two main meteorological stations in De Bilt and Beek. The dominant land use was pasture. Corresponding values for the interception factor and crop factor are, respectively,  $f_i = 1.0$  and  $f_c = 1.0$  [Feddes, 1987]. Figure 5.2 gives a schematization of the site. During winter, the groundwater level rises above the local drainage level, whereas during summer, the trenches run dry as a result of a low groundwater level. In 1988, the bottom of the left ditch of the main drainage system was lowered by ca. 75 cm. Since the exact date of this intervention was unknown, it was assumed that the reference level decreased linearly from  $h_r$  in 1988 to  $h_r - \beta \Delta h_r$  in 1989, with  $\Delta h_r$  is 1 cm. The parameter  $\beta$  [-] was estimated.

In order to be able to validate the calibrated model, the time series was split into a calibration set (1975-2000) and a validation set (1967-1975). The first period was

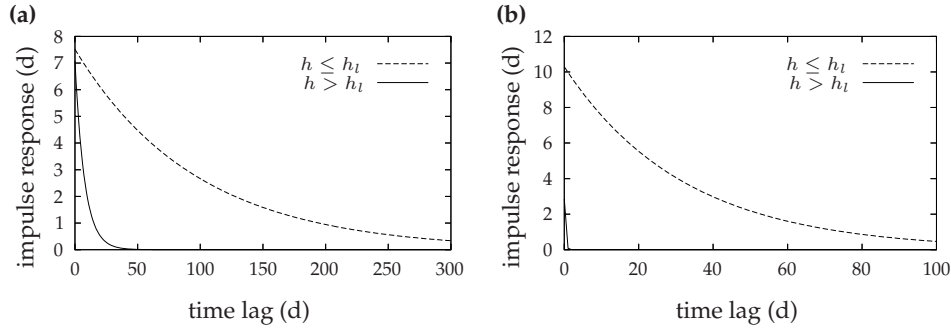


**Figure 5.3:** Impulse response functions for (a) observation well 1, and (b) observation well 2. The solid lines represent the response function for  $h > h_l$ ; the dashed lines represent the response function for  $h \leq h_l$ . Note the different scales.

used for validation instead of the last to estimate the effect of the intervention more accurately.

Table 5.1 gives the calibrated model parameters together with standard deviations. Both the level and the resistance of the local drainage system were estimated reasonably certain (standard deviations are 0.4 cm and 4 days, respectively). The lowering of the reference level, estimated at  $\beta\Delta h_r = 40$  cm, was significantly less than 75 cm. Finally, note that the weighting of the system noise for  $h_t > h_l$  (represented by  $g$  in Equation 5.26) does not significantly differ from the influence of the system noise for  $h_t \leq h_l$ :  $g$  is not significantly larger than 1.

From the model parameters, impulse-response functions could be derived. Figure 5.3a shows these functions for the two regimes (that above and that below the local drainage level). The figure clearly demonstrates the influence of the local drainage system on the response time.

Figure 5.4 depicts the prediction ( $w_t = 0$ ) of groundwater levels for the calibration period (1975-2000). The model predicted the groundwater level very well. Also, the influence of the intervention on the system can be seen. Before the intervention, the water table exceeded the local drainage level ( $h_l = -66.4$  cm) every year. After the intervention the frequency of exceedance was less. In 1996, the

**Table 5.1:** Calibrated parameters with associated error standard deviation of the state space model fitted to the time series of observation well 1

Parameter	Estimate	Standard deviation
$\gamma_l$ , d	62.4	4.10
$h_l$ , cm	-66.4	0.366
$\varphi$	0.131	0.00158
$\gamma_r$ , d	724.	44.5
$h_r$ , cm	-95.2	1.93
$\beta$	39.6	2.55
$g$	1.07	0.0562
$\sigma_w^2$ , cm <sup>2</sup>	10.4	0.967

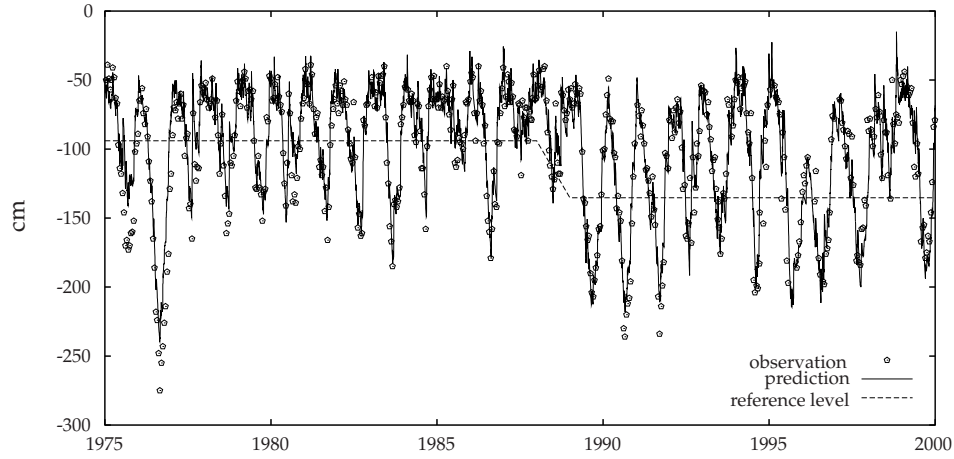


**Figure 5.4:** Predicted ( $w_t = 0$ ) and observed groundwater levels for observation well 1 for the calibration period 1975-2000; the step in the reference level represents the estimated effect of the intervention in 1988

water table even remained below the local drainage level. Also, the intervention increased the amplitude of water table fluctuations.

Figure 5.5 shows the prediction of groundwater levels for the validation period (1967-1975). The 2.5% and 97.5% prediction intervals were estimated from a set of 1000 series of simulated groundwater levels. These samples were simulated using daily input data, the calibrated model parameters, and 1000 samples of a zero-mean white-noise process with variance  $\sigma_w^2 = 10.4 \text{ cm}^2$ . The figure demonstrates that the prediction interval is smaller for water tables above the local drainage level than for water tables below local drainage level. The fraction of observations outside the prediction interval equals 0.063 (which is close to the theoretical value of 0.05). Summarizing, the verification results (comparison of predictions and measurements for the calibration period) and validation results for observation well 1 are satisfactory, indicating that the state space model gives a good representation of the groundwater system.

### 5.3.2 Observation well 2

Well 2 was situated in “De Meetkerkse Moeren”, a location near the border between Belgium and the Netherlands. The dominant land use was pasture. The interception factor and crop factor were  $f_i = 1.0$  and  $f_c = 1.0$  [Feddes, 1987]. Daily observations on groundwater level were available for December 2000 and onwards. Since the time series was short, all data were used for calibration. Hence, the calibrated model could not be validated. Similar to well 1, for well 2 the variance of the measurement noise was assumed to be  $\sigma_v^2 = 0.5 \text{ cm}^2$ . The reference level  $h_r$  was assumed to be constant over time. Daily input data were obtained from the nearby meteorological station of Vlissingen. Figure 5.6 gives a schematic representation of the site. Several ditches and trenches were present in the neighborhood of the well.

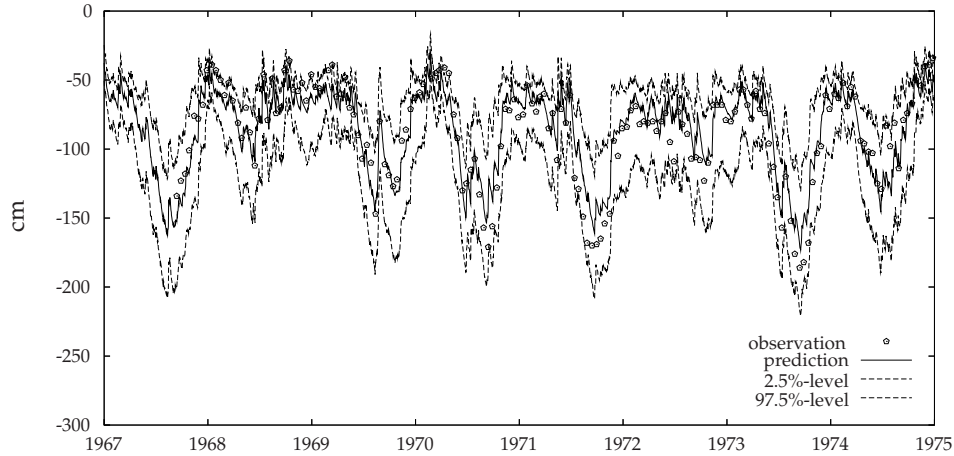


**Figure 5.5:** Predicted groundwater levels, observed groundwater levels, and 95% prediction interval (dashed lines) for observation well 1. The prediction interval was estimated from a set of 1000 simulated groundwater levels. The model was calibrated for 1975-2000

During wet periods, water was discharged through these trenches.

The results of the calibration are presented in Table 5.2. The estimated local drainage level was 1.2 cm below surface. As a result, the local drainage resistance was very small: ca. 3 days. This is illustrated in Figure 5.3b. An impulse of input is almost instantaneously discharged through the local drainage system. Also notice that, in contrast to well 1, the parameter  $g$  significantly differs from 1:  $g = 1.8$ . This means that the influence of the system noise for  $h_t \leq h_l$  is 1.8 times larger than for  $h_t > h_l$ .

Figure 5.7 shows the prediction of groundwater levels together with the observations. The model predictions follow the seasonal pattern remarkably well. From late autumn to early spring, the water level is controlled by the local drainage system. By way of illustration, Figure 5.8a shows the daily drainage flux together with daily precipitation excess ( $=f_i P_t - f_c E_{r,t}$ ). The trenches immediately discharge most of the peaks of precipitation excess. On average, ca. 50% of the precipitation excess

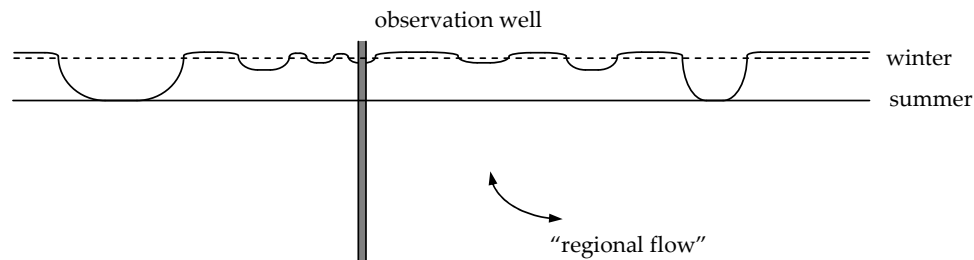


**Figure 5.6:** Schematization of the site "De Meetkerkse Moeren" (well 2)

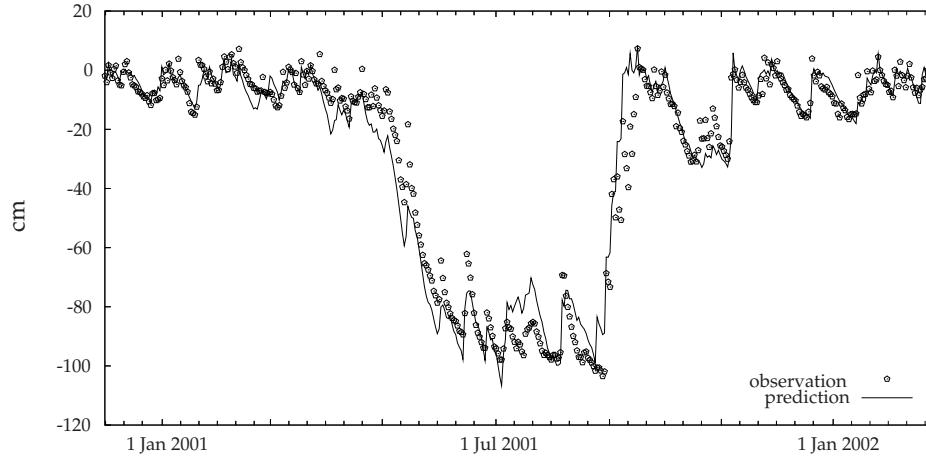


Figure 5.7: Predicted ( $w_t = 0$ ) and observed groundwater levels for observation well 2

is discharged through the trenches in this period. From mid spring until late summer, the trenches are dry. In May, the groundwater level sharply declines with almost 1 m. During summer, the groundwater level remains low. The reference level  $h_r = -34.7$  cm is then higher than the water table, resulting in a considerable infiltration of water into the system of ca.  $1.5 \text{ mm.d}^{-1}$  (Figure 5.8b). At the end of the summer, the direction of the regional flux switches and groundwater is being discharged with ca.  $1 \text{ mm.d}^{-1}$ .

Since a validation set was not available, other criteria were needed to check model correctness. A useful check is the whiteness of the innovations. Figure 5.9a shows the innovations with 2.5 and 97.5 percentiles calculated with the truncated first-order filter as  $\pm 1.96\sqrt{f_t}$ . The fraction innovations outside these limits equals 0.052, which is close to the theoretical value of 0.05. The variation of the percentiles demonstrates the influence of the parameter  $g$ : the 2.5 and 97.5 percentiles become smaller when the water table level becomes higher than the local drainage level. Figure 5.9b shows the autocorrelations of the innovations with the 2.5 and 97.5 percentiles. As there is no significant autocorrelation, it is likely that the calibrated model gives a statistically correct description of the system.

Table 5.2: Calibrated parameters with associated error standard deviation of the state space model fitted to the time series of observation well 2

Parameter	Estimate	Standard deviation
$\gamma_l, \text{d}$	2.96	0.403
$h_l, \text{cm}$	-1.20	0.130
$\varphi$	0.0957	0.00317
$\gamma_r, \text{d}$	337.	39.1
$h_r, \text{cm}$	-34.7	4.03
$g$	1.80	0.160
$\sigma_w^2, \text{cm}^2$	3.94	0.644

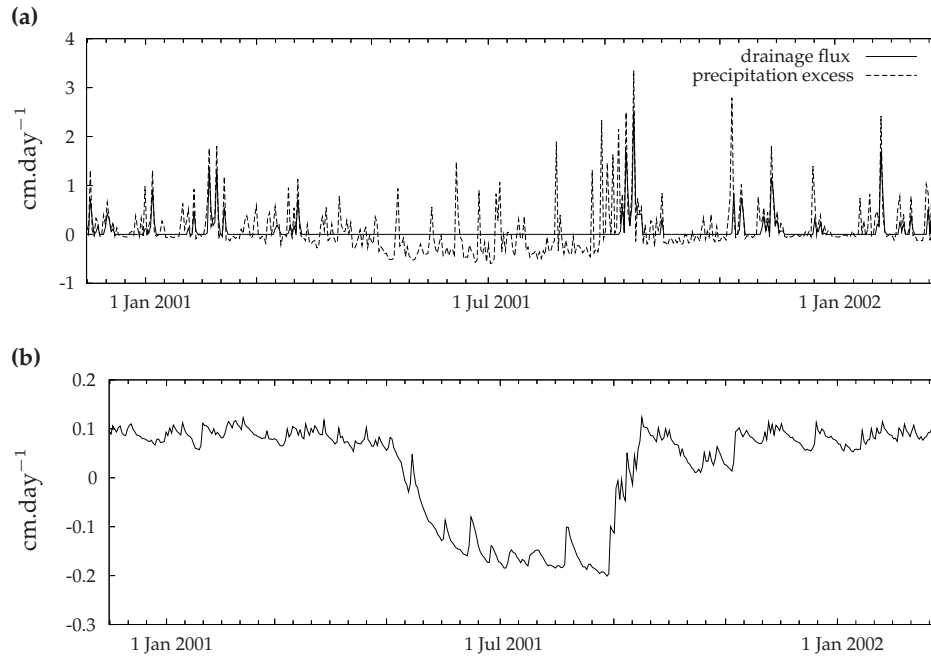


**Figure 5.8:** (a) local drainage flux with precipitation excess and (b) regional drainage flux as estimated for observation well 2

A useful application of the model is to characterize the groundwater system on the basis of some univariate statistics such as mean, standard deviation, and percentiles. Since the length of the observed time series was too short for calculating these statistics, 1000 samples were simulated for the period 1957-2003 using the calibrated model parameters and daily input data (precipitation and evaporation). From these samples univariate statistics were calculated as an average over time and realizations. Table 5.3 gives an overview of the statistics. The cumulative probability of the groundwater level is represented by a graph of the frequency of exceedance (Figure 5.10a). This graph can be used for the purpose of risk analysis. For example, one can derive from the graph that 24 days per year, the water table is expected to be above surface level. Figure 5.10b shows the frequency of exceedance as a function of time. The bold line (median) represents the groundwater level that is exceeded once per 2 years. Similarly, only once every 10 years the water table is higher than the upper line (90 percentile), and only once in that period it is lower than the lowest line (10 percentile). The figure demonstrates that for summer, the uncertainty (bandwidth) is larger than for winter.

### 5.3.3 Comparison with linear model

Table 5.4 presents statistics that evaluate the predictive performance of the state space model both for well 1 and well 2. The verification (prediction for same pe-



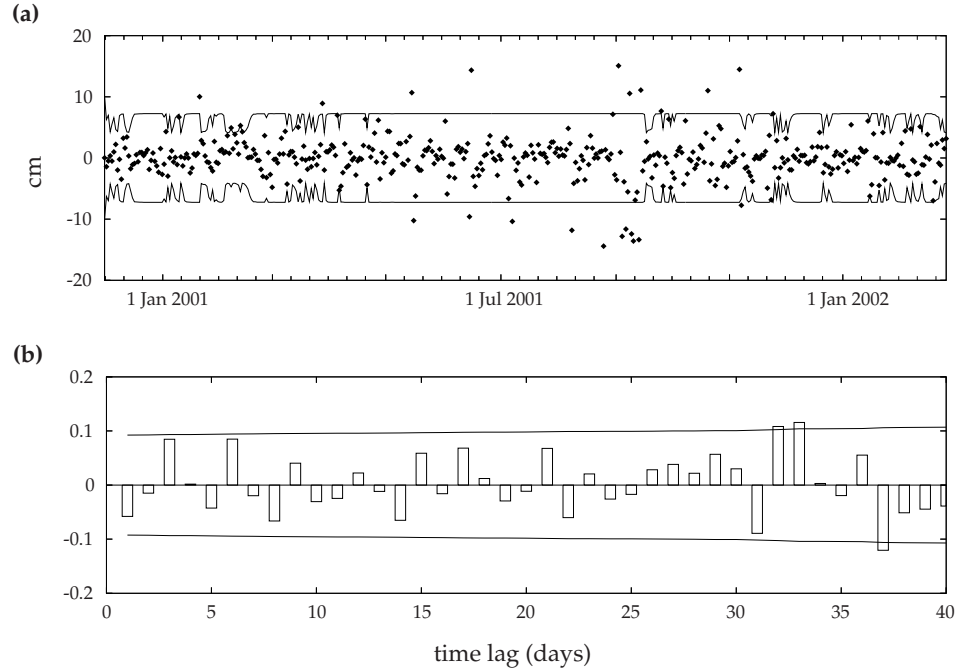


**Figure 5.9:** (a) Innovations with 2.5 and 97.5 percentiles and (b) autocorrelations of the innovations with 2.5 and 97.5 percentiles

riod as that used for calibration) and validation (prediction for another period than that used for calibration) results of the nonlinear model are compared with the calibration and validation results of a linear transfer function-noise (TFN) model of the form

$$h_t = \delta h_{t-1} + \omega (f_i P_t - f_c E_{r,t}) + \mu + w_t, \quad (5.28)$$

where  $\delta$  is an autoregressive parameter [-],  $\omega$  is a moving-average parameter [T],  $\mu$  is a reference level [L], and  $w_t$  is a zero-mean white-noise process. The TFN model predicts the groundwater level through a linear relation between input (precipitation and evapotranspiration) and output (groundwater level). Consequently, it does not take the local drainage system into account.

The statistics given in Table 5.4 are defined as follows. The mean prediction

**Table 5.3:** Univariate statistics of groundwater levels (cm) at well 2 for the period 1957-2003 on the basis of the calibrated model (calibration period from December 2001 until February 2003)

Statistic	Value
Mean	-32.0
Standard deviation	34.0
25 percentile	-59.1
50 percentile	-28.4
75 percentile	-8.6

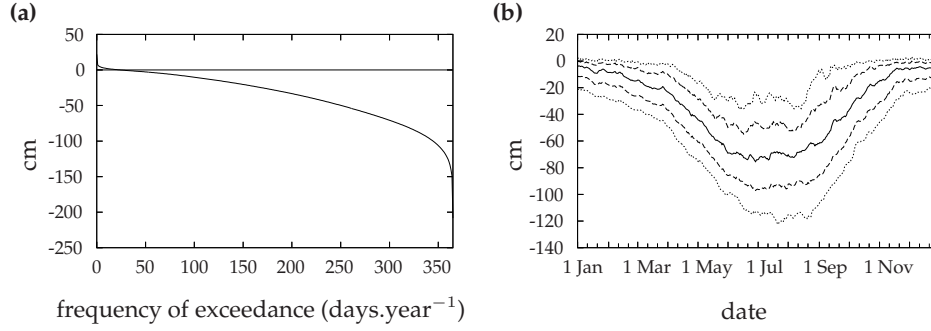


**Figure 5.10:** (a) Frequency of exceedance of groundwater level at well 2; and (b) for every day of the year the median and 10, 25, 75, and 90 percentiles. The curves are based on 1000 simulations for 1957-2000, using the calibrated model

error (ME) measures the systematic error of the prediction:

$$\text{ME} = \frac{1}{N} \sum_{i=1}^N (z_i - \check{z}_i), \quad (5.29)$$

with  $\check{z}_i$  the predicted ( $w_t = 0$ ) groundwater level [L]. The mean absolute error (MAE) and the root mean square error (RMSE) measure the accuracy:

$$\text{MAE} = \frac{1}{N} \sum_{i=1}^N |z_i - \check{z}_i|, \quad (5.30)$$

$$\text{RMSE} = \sqrt{\frac{1}{N} \sum_{i=1}^N (z_i - \check{z}_i)^2}. \quad (5.31)$$

The percentage of observations outside the 95% prediction interval ( $p$ ) measures how well the prediction errors are modeled. Ideally,  $p$  should be equal to 0.05.

The verification results for both well 1 and well 2 show that the nonlinear state space model gives a better fit than the linear TFN model. When the nonlinearity is incorporated, the MAE is 21% smaller for well 1 and even 42% for well 2. Validation of the nonlinear state space model gives satisfactory results. The MAE and RMSE of the predictions for the validation period are even smaller than those for the

**Table 5.4:** Verification and validation results for nonlinear state space (SS) model and linear transfer function-noise (TFN) model for well 1 and 2.

Well	Model	Verification			Validation			$p$
		ME	MAE	RMSE	ME	MAE	RMSE	
1	SS	-2.69	11.33	15.46	-1.32	10.11	12.83	0.063
1	TFN	0.44	15.17	19.59	10.97	15.64	17.99	0.011
2	SS	0.14	5.06	7.37				
2	TFN	0.30	9.99	12.60				

ME, MAE and RMSE are in centimeters,  $p$  is dimensionless.

calibration period. Also, the value of  $p$  is close to the theoretical value of 0.05 (see also Section 5.3.1). The linear TFN model clearly performs worse in the validation period. First, the mean error ME is 11 cm, indicating that the calibrated TFN model overfits the data in the calibration period. The TFN model is not able to determine the reference level and the effect of the intervention correctly. Second, the percentage of observations outside the prediction interval,  $p$ , is much smaller than 0.05. This results from the fact that the TFN model overestimates the noise variance for periods where the water table level is higher than the local drainage level.

## 5.4 Summary and conclusions

This chapter developed a nonlinear state space model for describing water table fluctuations in a nonlinear groundwater system. Nonlinearity was introduced to model a local drainage system that is only active when the water table is above the drainage level. Although this chapter only discussed systems with one local drainage level, the state space model can easily be extended with more drainage levels (more regimes).

The model was tested on two time series of groundwater levels. The length of the first time series was ca. 33 years with bimonthly observations. During the observation period an intervention took place, resulting in a change of the regional flow component. Calibration and validation of the state space model showed that the model described the water table fluctuations accurately. Also the effect of the intervention was estimated accurately. The second time series had a length of only 1.5 years with an observation interval of 1 day. Since all data were needed for calibration, the model could not be validated. Nevertheless, checks on whiteness of the innovations indicated that the model was statistically correct.

Comparison of the results with those of a commonly used linear transfer function-noise model demonstrated that the nonlinear state space model performs better. Particularly the validation results showed that predictions of the TFN model were biased and less accurate. Furthermore, the TFN model could not describe the prediction errors well.

The main conclusion therefore is that for systems with switching regimes, the state space model is a powerful tool for accurately describing water table fluctuations in shallow groundwater systems with various drainage levels. The approach may be of great support for water management in the sense that it helps to identify the system, describes the effect of interventions, and can be used for online processing and forecasting of groundwater levels.



# 6

## Multiple time series modeling

---

**Abstract.** This chapter provides an approach for large-scale modeling of multiple time series of groundwater head data. The model is based on the vector transfer-function noise (VTFN) model. Correlation among time series is described by the noise component. A common problem with multiple time series models is that the dimension of the parameter space increases exponentially with the number of time series. This chapter applies reduction techniques so that larger data sets can be analyzed. Reduction is carried out by describing the correlation among time series with common factors. The reduced VTFN model is embedded in a Kalman filter. Unknown parameters are estimated with a likelihood criterion. The technique is illustrated using two data sets. Results show that the reduced model produces a description of the system that is similar to that of the full (i.e., less parsimonious) model. Consequently, larger systems, which cannot be modeled with a full model, can be efficiently modeled with the reduced model. In addition, the factor model makes it possible to split the stochastic component into specific (“local”) noise and common (“regional”) noise. Also, it can be used to estimate common trends in time series.

---

*This chapter is adapted from Berendrecht, W.L., A.W. Heemink, J.C. Gehrels, and F.C. van Geer, Multiple time series modeling of groundwater head fluctuations, submitted to Water Resources Research*

THE STATISTICAL ANALYSIS of multiple time series has been, and still is, an important topic in many research areas. Generally, multivariate analysis focuses on interaction analysis, forecasting, interpolation, and intervention or trend analysis. Well-known multiple time series models are vector autoregressive (VAR) models [Shea, 1987; Aoki, 1990; Lütkepohl, 1991], contemporaneous autoregressive moving-average (CARMA) models [Camacho *et al.*, 1985, 1987; Hipel and McLeod, 1994], and space-time autoregressive moving-average models [Pfeifer and Deutsch, 1980; Deutsch and Pfeifer, 1981]. In geohydrology, multiple time series modeling has been applied mainly for the purpose of interpolation. Van Geer and Zuur [1997] spatially interpolate the Box-Jenkins transfer function-noise (TFN) model to estimate groundwater head between observation wells. Basically, they construct a multiple-output model using the correlation among noise series obtained by single-output transfer function-noise models. In Bierkens *et al.* [2001] and Knotters and Bierkens [2001] a regionalized autoregressive exogenous variable (RARX) model is applied for space-time prediction of water table depths. Here the temporal variation is modeled with an ARX model whose parameters are a continuous function of location and whose noise components are spatially colored. Besides for interpolation of groundwater head, multiple time series models are also very useful for optimizing monitoring networks. For instance, the model can be used for online prediction of groundwater head, making it possible to reduce the observation frequency. Furthermore, multiple time series models are, more than single-output time series models, effective in detecting interventions and outliers.

A major problem of multiple time series models is that the number of model parameters dramatically increases with the number of output series. System identification and estimation may then become difficult and reduction techniques need to be applied to overcome this problem. An effective method for reducing the dimension of the parameter space focuses on the correlation structure among the multiple time series and is referred to as dynamic factor analysis. Dynamic factor models have been used in statistics, psychometrics, and econometrics for a long time [Watson and Engle, 1983; Molenaar, 1985; Heij *et al.*, 1997; Forni *et al.*, 2000; Debrand and Patrat, 2001; Molenaar and Nesselroade, 2001]. More recently, Zuur *et al.* [2003] introduced dynamic factor analysis in environmental science for modeling common trends in multiple time series. The purpose of factor analysis is to de-

scribe the variation among many variables in terms of a few underlying but unobserved random variables called factors. Together these factors account for all correlations among the original variables. In this sense, the method differs from another reduction technique called principal component analysis, where the principal components are assumed to describe the entire variance-covariance matrix [see e.g. *Basilevsky, 1994*]. From a physical point of view, factors may be viewed as estimates of physical influences which have given rise to the observed correlations. However, factors may also contain common noise due to model assumptions or to errors in input data.

This chapter proposes a reduced vector transfer-function noise (VTFN) model for modeling multiple time series of groundwater head data. The VTFN model is a well-known and straightforward extension of the single-output TFN model described in many textbooks [*Box and Jenkins, 1970; Hipel and McLeod, 1994*]. Although many forms of the VTFN model exist, this chapter assumes that all correlation among the time series can be described within the noise model. Reduction of the VTFN model is carried out by writing the noise component of the VTFN model as a factor model. Two different noise models are discussed: the first-order vector autoregressive model, which describes the correlation among time series within the matrix of autoregressive parameters, and the first-order contemporaneous autoregressive model, which describes the correlation among time series within the white-noise vector. In the first case, the reduced autoregressive model is written as a dynamic factor model. In the latter, reduction is achieved by writing the white-noise vector as a static factor model. The most important result of using a factor model is that the number of parameters increases linearly with the number of time series, while the number of parameters of a full model increases quadratically.

In Section 6.1, the reduced VTFN model is developed. In Section 6.2, this model is tested on a set of five time series of groundwater head data and compared with a full model. In addition, the various components of the reduced model are analyzed. Section 6.3 presents a case study with 10 time series. Some of the time series have a temporal trend. Using reduction techniques, the number of model parameters can be reduced. The study also shows that spatial correlation in the stochastic component can be used to accurately estimate common trends. Finally, Section 6.4 discusses of the reduced model and gives some conclusions.

## 6.1 Development of multiple-output state space model

The general state space representation of a multi-input multi-output (MIMO) time series model is described by the following set of equations (see Equation 2.21):

$$\mathbf{x}_t = \mathbf{A}\mathbf{x}_{t-1} + \mathbf{B}\mathbf{u}_t + \mathbf{G}\mathbf{w}_t, \quad (6.1a)$$

$$\mathbf{y}_t = \mathbf{C}\mathbf{x}_t + \mathbf{v}_t, \quad (6.1b)$$

where  $\mathbf{x}_t$  is an  $n \times 1$  vector of unobserved system states,  $\mathbf{u}_t$  is a  $r \times 1$  vector representing the input of the system (e.g., precipitation and evapotranspiration),  $\mathbf{y}_t$  is a

$m \times 1$  vector of groundwater head observations at time  $t$ ,  $\mathbf{w}_t$  is a  $q \times 1$  disturbance vector (system noise) and  $\mathbf{v}_t$  is a  $m \times 1$  disturbance vector (measurement noise), with  $\mathbf{w}_t$  and  $\mathbf{v}_t$  serially and mutually uncorrelated with noise processes with mean zero and covariance matrix  $\mathbf{Q}$  ( $q \times q$ ) and  $\mathbf{R}$  ( $m \times m$ ), respectively. The system matrices are  $\mathbf{A}$  ( $n \times n$ ),  $\mathbf{B}$  ( $n \times r$ ),  $\mathbf{G}$  ( $n \times q$ ) and  $\mathbf{C}$  ( $m \times n$ ). As groundwater head is generally observed with respect to some reference level, the observation vector  $\mathbf{y}_t$  is decomposed into

$$\mathbf{y}_t = \mathbf{y}'_t + \mathbf{y}_r, \quad (6.2)$$

with  $\mathbf{y}_r$  a  $m \times 1$  vector of (unknown) reference levels.

Following the theory of Chapter 2, the state space model is assumed to be a linear combination of two components: a deterministic component  $\mathbf{x}_t^d$  describing the part of the system that is related to the input series, and a stochastic (noise) component  $\mathbf{x}_t^s$  describing the residual part of the system:

$$\begin{bmatrix} \mathbf{x}_t^d \\ \mathbf{x}_t^s \end{bmatrix} = \begin{bmatrix} \mathbf{A}^d & 0 \\ 0 & \mathbf{A}^s \end{bmatrix} \begin{bmatrix} \mathbf{x}_{t-1}^d \\ \mathbf{x}_{t-1}^s \end{bmatrix} + \begin{bmatrix} \mathbf{B}^d \\ 0 \end{bmatrix} \mathbf{u}_t + \begin{bmatrix} 0 \\ \mathbf{G}^s \end{bmatrix} \mathbf{w}_t, \quad (6.3a)$$

$$\mathbf{y}_t = \begin{bmatrix} \mathbf{C}^d & \mathbf{C}^s \end{bmatrix} \begin{bmatrix} \mathbf{x}_t^d \\ \mathbf{x}_t^s \end{bmatrix} + \mathbf{v}_t. \quad (6.3b)$$

### 6.1.1 Deterministic component

Since it is assumed that all correlation among time series is described by the stochastic component, the deterministic component of the transition matrix  $\mathbf{A}$  is block diagonal:

$$\mathbf{A}^d = \begin{bmatrix} \mathbf{A}_1^d & & \mathbf{0} \\ & \ddots & \\ \mathbf{0} & & \mathbf{A}_p^d \end{bmatrix}. \quad (6.4)$$

The dynamic relation between input (precipitation and evapotranspiration) and output (groundwater head) is described by a linear reservoir model, written as

$$\begin{aligned} x_{1,t} &= \delta_1 x_{1,t-1} + \omega (P_t - f_c E_t), \\ x_{2,t} &= \delta_2 x_{2,t-1} + (1 - \delta_2) x_{1,t}, \\ &\vdots \\ x_{p,t} &= \delta_p x_{p,t-1} + (1 - \delta_p) x_{p-1,t}, \end{aligned} \quad (6.5)$$

where  $P_t$  is precipitation,  $E_t$  is evapotranspiration,  $\delta_i$  is the  $i$ th autoregressive (AR) parameter,  $\omega$  and  $f_c$  are a scaling factor and a crop factor, respectively. In most applications the number of reservoirs  $p$  is smaller than 4.



Equation 6.5 can be written in the following vector notation, for  $l = 1, \dots, m$ :

$$\mathbf{x}_{l,t}^d = \mathbf{A}_l^d \mathbf{x}_{l,t-1}^d + \mathbf{B}_l^d \mathbf{u}_t, \quad (6.6)$$

with

$$\mathbf{A}_l^d = \begin{bmatrix} a_{l,11} & 0 & \cdots & 0 \\ \vdots & \ddots & \ddots & \vdots \\ \vdots & & \ddots & 0 \\ a_{l,p1} & \cdots & \cdots & a_{l,pp} \end{bmatrix}, \quad \mathbf{B}_l^d = \begin{bmatrix} b_{l,11} & b_{l,12} \\ b_{l,21} & b_{l,22} \\ \vdots & \vdots \\ b_{l,p1} & b_{l,p2} \end{bmatrix}, \quad (6.7)$$

where, for  $i = 1, \dots, p$  and  $j = 1, \dots, i$ ,

$$a_{l,ij} = \delta_{l,j} \prod_{s=j+1}^i (1 - \delta_{l,s}), \quad (6.8)$$

$$b_{l,i1} = \omega_l \prod_{s=2}^i (1 - \delta_{l,s}), \quad b_{l,i2} = -f_{c,l} b_{l,i1}. \quad (6.9)$$

The associated observation matrix  $\mathbf{C}^d$  is written as the following  $m \times mp$  matrix:

$$\mathbf{C}^d = \mathbf{I}_m \otimes \begin{bmatrix} 0 & \cdots & 0 & 1 \end{bmatrix}, \quad (6.10)$$

where  $\otimes$  is the Kronecker product.

Identification of the reservoir model is straightforward. First, a number of states (reservoirs) is assumed. Subsequently, the model parameters are estimated. Based on the calculated variances of the estimated AR-parameters, the significance of the estimated AR-parameters is evaluated. The number of states needed to describe the transfer function is then equal to the number of significant AR-parameters.

### 6.1.2 Stochastic component

Generally, the stochastic component of a single groundwater time series model can be described by a first-order autoregressive model. Two important subsets of the multiple autoregressive model are discussed here: a model that describes the correlation among time series within the transition matrix  $\mathbf{A}^s$ , and a model that describes the correlation within the noise covariance matrix  $\mathbf{Q}$ . The first model is referred to as a vector autoregressive (VAR) model; the latter one as a contemporaneous autoregressive (CAR) model.

Reduction of the VAR model is carried out by rewriting the VAR model into a dynamic factor model. Basically, dynamic factor models [Geweke, 1977; Engle and Watson, 1981] incorporate an a priori structure of the off-diagonal elements of the transition matrix  $\mathbf{A}^s$ . This is done by assuming that a set of  $m$  variables depends on  $k < m$  unobserved common dynamic factors (CDFs) and on  $m$  specific dynamic

factors (SDFs). In this way, the stochastic component of Equation 6.3 is written as

$$\mathbf{x}_t^s = \begin{bmatrix} \Phi & \mathbf{0} \\ \mathbf{0} & \Psi \end{bmatrix} \mathbf{x}_{t-1}^s + \begin{bmatrix} \boldsymbol{\eta}_t \\ \boldsymbol{\varepsilon}_t \end{bmatrix}, \quad (6.11a)$$

$$\mathbf{y}_t^s = \begin{bmatrix} \mathbf{I}_p & \Gamma \end{bmatrix} \mathbf{x}_t^s + \mathbf{v}_t, \quad (6.11b)$$

with

$$(\mathbf{x}_t^s)^\top = \begin{bmatrix} s_{1,t} & \cdots & s_{m,t} & f_{1,t} & \cdots & f_{k,t} \end{bmatrix}, \quad (6.12)$$

where  $s_{1,t}, \dots, s_{m,t}$  are the *specific dynamic factors* (SDFs),  $f_{1,t}, \dots, f_{k,t}$  are the *common dynamic factors* (CDFs),  $\Phi$  is a  $m \times m$  diagonal matrix with  $\phi_1, \dots, \phi_m$  the AR-parameters of the specific part of  $\mathbf{x}^s$ ,  $\Psi$  is an  $k \times k$  diagonal matrix with  $\psi_1, \dots, \psi_k$  the AR-parameters of the common part of  $\mathbf{x}^s$ ,  $\Gamma$  is a  $m \times k$  matrix of dynamic-factor loadings, which are coefficients relating the dynamic factors to each time series. Both  $\boldsymbol{\eta}_t$  ( $m \times 1$ ) and  $\boldsymbol{\varepsilon}_t$  ( $k \times 1$ ) are white-noise processes with  $\text{var}(\boldsymbol{\eta}_t) = \Sigma$  ( $m \times m$ ) and  $\text{var}(\boldsymbol{\varepsilon}_t) = \mathbf{I}_k$ :

$$\mathbf{Q} = \begin{bmatrix} \Sigma & \mathbf{0} \\ \mathbf{0} & \mathbf{I}_k \end{bmatrix}, \quad (6.13)$$

i.e., all common dynamic factors are mutually uncorrelated and have unit variance. Since the elements of  $\boldsymbol{\eta}_t$  are uncorrelated, the covariance matrix  $\Sigma$  is diagonal. Finally, the specific dynamic factors and common dynamic factors are assumed to be mutually uncorrelated.

The reduction of the CAR model is very similar to that of the VAR model. The difference is that the factors are now white-noise processes instead of dynamic AR-processes. Consequently, the stochastic component of Equation 6.3 is written as

$$\mathbf{x}_t^s = \Phi \mathbf{x}_{t-1}^s + \begin{bmatrix} \mathbf{I}_q & \Upsilon \end{bmatrix} \begin{bmatrix} \boldsymbol{\eta}_t \\ \boldsymbol{\varepsilon}_t \end{bmatrix}, \quad (6.14a)$$

$$\mathbf{y}_t^s = \mathbf{x}_t^s + \mathbf{v}_t, \quad (6.14b)$$

where  $\Upsilon$  denotes a  $q \times s$  matrix of noise-factor loadings,  $\boldsymbol{\eta}_t$  contains the *specific noise* terms, and  $\boldsymbol{\varepsilon}_t$  contains the *common noise* terms. The noise covariance matrix of  $\boldsymbol{\eta}_t$  and  $\boldsymbol{\varepsilon}_t$  is defined as in Equation 6.13, with the subscript  $k$  replaced by  $s$ , referring to the number of specific noise factors. Note that in Equation 6.14b, the observation matrix  $\mathbf{C}^s$  is an identity matrix:  $\mathbf{C}^s = \mathbf{I}_m$ . Equations 6.11 – 6.14 show that the main difference between both reduced models is the matrix  $\Psi$ , containing the autoregressive parameters of the common dynamic factors. Due to this matrix, the CDFs may have an autocorrelation that differs from that of the SDFs.

**Table 6.1:** Overview of the different model forms of the stochastic component

	$\mathbf{A}_{\text{diag}}^s$	$\mathbf{A}_{\text{full}}^s$	$\mathbf{A}_{\text{fac}}^s$
$\mathbf{Q}_{\text{diag}}$	univariate	VAR	DF
$\mathbf{Q}_{\text{full}}$	CAR	-	-
$\mathbf{Q}_{\text{fac}}$	SF	-	-

Table 6.1 gives an overview of the model forms discussed in this section. Since models with correlation in both  $\mathbf{A}^s$  and  $\mathbf{Q}$  are not suitable for use in practical applications [Hipel and McLeod, 1994], they are not given in Table 6.1. The univariate model (no correlation among time series) is given in order to complete the table. The reduced VTFN with factorized matrix  $\mathbf{A}^s$ , i.e. the reduced VAR model (Equation 6.11), will be referred to as a vector transfer-function noise with dynamic-factor (VTFN-DF) model. The VTFN with factorized matrix  $\mathbf{Q}$ , i.e. the reduced CAR model (Equation 6.14), will be referred to as a vector transfer-function noise with static-factor (VTFN-SF) model.

The unknown elements of the matrices  $\mathbf{A}^d$ ,  $\mathbf{B}^d$ ,  $\mathbf{A}^s$ ,  $\mathbf{Q}$ , and, depending on whether CDFs or SDFs are used,  $\Gamma$  or  $\Upsilon$ , need to be estimated and will be referred to as the parameter vector  $\alpha$ . Maximum-likelihood estimates of  $\alpha$  are calculated by embedding the Kalman filter of Equation 2.43 in the optimization procedure described in Section 2.7.

An attractive feature of the VTFN-DF model is that the common dynamic factors appear as separate states in the state equation. As a result, the stochastic component can be decomposed into two parts: the *regional noise*, represented by the CDFs, and the *local noise*, represented by the SDFs (see Equation 6.11). The Kalman filter provides the best estimate of  $\mathbf{x}_t$  based on all observations through time  $t$  in a recursive manner. However, the additional information contained in the observations after time  $t$  can be exploited to provide an improvement in estimation accuracy. An estimate of  $\mathbf{x}_t$  that is based on all observations ( $t = 1, \dots, T$ ) is referred to as a smoothed estimate of  $\mathbf{x}_t$ . The smoothed estimate of  $\mathbf{x}_t$  is generated by applying the fixed-interval smoothing algorithm described in Section 2.8.

## 6.2 Evaluation of the reduced VTFN model: two case studies

### 6.2.1 Description of data set and definition of the models

The reduced VTFN model was tested on a set of five time series of groundwater head data obtained from observation wells in the southern part of the Netherlands. Since the number of time series is rather small, results of the reduced model could be compared with results of a full model. All observation screens were situated in the same aquifer consisting of very fine sands covered by a clay layer with a resistance of ca. 5000 days. The time series (see Figure 6.1) had an average observation interval of 14 days. Monitoring of the groundwater head started in 1980. Daily observations of precipitation and evapotranspiration were obtained from a nearby meteorological station.

Table 6.2 gives an overview of the models that were applied to analyze the set

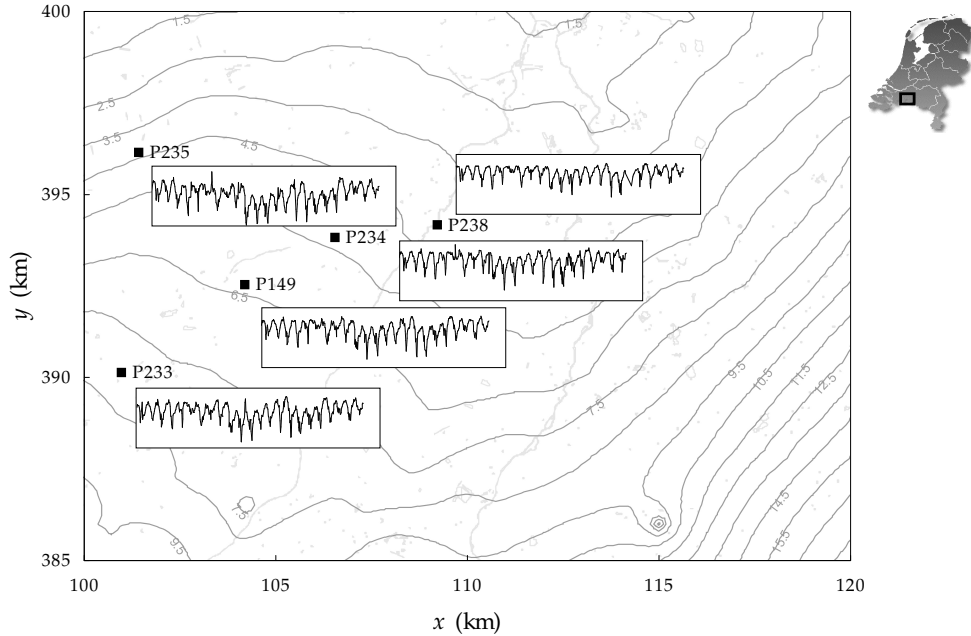


**Figure 6.1:** Time series of groundwater head observations; the average observation interval is 14 days; the vertical scale has a range of 500 cm. In the background, main surface water and contours of the average groundwater head are given.

of time series. The three models only differ in the way in which they describe the correlation in the stochastic component. The form of the deterministic component is the same for all models. The first noise model is a CAR model. Correlation among the time series enters the model via the system noise covariance matrix  $\mathbf{Q}$ . The matrix  $\mathbf{Q}$  is a full symmetric  $5 \times 5$  matrix. Hence, it contains 15 unknown parameters. The stochastic component of the system matrix,  $\mathbf{A}^s$ , is diagonal, containing 5 unknown parameters. The second model is a VTFN-SF model approximating Model 1 by assuming that the correlation structure in the system noise can be described by a common noise factor (see Equation 6.14). In this way the number of unknown parameters in the stochastic component is reduced from 20 to 15. The last model, the VTFN-DF model, assumes that the system noise is uncorrelated. Instead, the correlation among the time series is described by the transition matrix  $\mathbf{A}$  using one

**Table 6.2:** Form of system matrices  $\mathbf{A}^s$  and  $\mathbf{Q}^s$  of the tested models; the factorized matrices contain one common factor

Model	$\mathbf{A}^s$	$\mathbf{Q}^s$	$\dim \alpha^{s(1)}$
1	diagonal	full	20
2	diagonal	factorized	15
3	factorized	diagonal	16

<sup>(1)</sup>number of unknown parameters in the stochastic component

**Table 6.3:** Calibrated parameters of the deterministic component and reference level for Model 1 (full covariance matrix), Model 2 (factorized noise covariance matrix) and Model 3 (factorized transition matrix)

	Model 1				Model 2				Model 3			
	$\omega$	$\delta_1$	$\delta_2$	$y_r$	$\omega$	$\delta_1$	$\delta_2$	$y_r$	$\omega$	$\delta_1$	$\delta_2$	$y_r$
P233	.901	.986	.764	610.3	.896	.986	.762	610.1	.860	.987	.768	609.8
P234	.932	.983	.687	403.7	.927	.983	.683	403.6	.864	.984	.696	403.4
P235	.873	.988	.537	219.6	.868	.988	.536	219.2	.837	.989	.530	219.4
P238	.818	.981	.777	368.6	.808	.982	.772	368.4	.762	.983	.770	368.5
P149	.952	.984	.805	485.5	.948	.984	.804	485.3	.889	.985	.810	485.6

common dynamic factor (see Equation 6.11). This model has 16 unknown parameters in the stochastic component. Attempts to calibrate a VTFN model with a VAR(1) model for the stochastic component (i.e, a full system matrix  $\mathbf{A}^s$ ) failed. Although  $\mathbf{A}^s$  was reparameterized to enforce stationarity [Ansley and Kohn, 1986], the optimization routine did not converge. Obviously, too many correlated parameters needed to be estimated.

Finally, two assumptions were made. First, the measurement errors were assumed to be mutually uncorrelated, having a variance equal to  $1 \text{ cm}^2$ . Second, the crop factors  $f_c$  in the deterministic component were all set equal to 1.

### 6.2.2 Calibration and evaluation

Identification of the models pointed out that only two states (for each time series) were needed to describe the transfer function of the deterministic component. Hence, for each time series only three parameters were needed (15 parameters in total). Table 6.3 presents for the three models the calibrated parameters of the deterministic component and the reference levels. The table shows that the parameter estimates of Model 1 and 2 do not differ significantly. Model 3, however, gives lower values for the parameter  $\omega$ . The variance of the time series explained by the deterministic component is lower for Model 3 than for Model 1 and 2.

Table 6.4 gives an overview of the calibration results for the stochastic component. The prediction error covariance matrix

$$\mathbf{F}_\infty = \lim_{t \rightarrow \infty} \mathbf{F}_t \quad (6.15)$$

and the prediction error correlation matrix  $\Xi$  can be used to compare the variance-covariance structure and the correlation structure described by the three different models. Note that the autoregressive parameters ( $\mathbf{A}^s$ ) of Model 1 and Model 2 are practically the same. Since the deterministic component of Model 1 and 2 are also equal, the noise covariance structures of both models have to be the same. This is confirmed by the prediction error covariance matrices of Model 1 and 2, which are almost identical. Hence, the parsimonious Model 2 (having 5 parameters less than Model 1) gives practically the same description of the system as Model 1. In other words: the fact that only one common noise factor can describe most of the correlation in the noise vector suggests that there is redundancy in the full covariance

**Table 6.4:** Calibrated parameters of the stochastic component for Model 1 (full covariance matrix), Model 2 (factorized noise covariance matrix) and Model 3 (factorized transition matrix), and the prediction error covariance matrix  $\mathbf{F}_\infty$

	Model 1					Model 2					Model 3				
$\mathbf{A}^s$	.956	0	0	0	0	.957	0	0	0	0	.967	0	0	0	0
	0	.932	0	0	0	0	.934	0	0	0	0	.000	0	0	0
	0	0	.963	0	0	0	0	.963	0	0	0	0	.975	0	0
	0	0	0	.947	0	0	0	0	.949	0	0	0	0	.919	0
	0	0	0	0	.945	0	0	0	0	.946	0	0	0	0	.000
$\Upsilon^T$															
$\mathbf{Q}$	75.0					14.6					12.5				
	65.7	113.				0	37.5				0	205.			
	60.9	67.2	96.5			0	0	37.2			0	0	30.7		
	48.1	59.1	47.8	53.5		0	0	0	12.9		0	0	0	17.7	
	69.0	76.1	67.3	56.2	85.4	0	0	0	0	7.24	0	0	0	0	65.3
$\Gamma^T$						0	0	0	0	0	1	0	0	0	0
$\mathbf{F}_\infty$	865.8					867.3					1085.				
	599.6	858.0				615.5	866.0				853.7	1019.			
	761.9	652.4	1317.			746.0	649.3	1323.			916.7	873.2	1549.1		
	506.6	501.8	541.6	518.7		523.3	471.5	558.1	527.2		696.2	663.1	712.1	653.9	
	712.8	637.1	746.0	535.0	799.8	710.7	644.5	756.0	540.0	805.0	900.5	857.8	921.1	699.5	970.1
$\Xi$	1.000					1.000					1.000				
	.6966	1.000				.7102	1.000				.8120	1.000			
	.7135	.6137	1.000			.6965	.6067	1.000			.7070	.6952	1.000		
	.7559	.7522	.6553	1.000		.7739	.6978	.6684	1.000		.8264	.8125	.7075	1.000	
	.8565	.7691	.7268	.8306	1.000	.8506	.7719	.7327	.8289	1.000	.8776	.8630	.7514	.8783	1.000

matrix of Model 1. This will be discussed in more detail below.

Model 3 uses a common dynamic factor (CDF) instead of a common noise factor to represent the covariance structure of the stochastic component. The model gives larger prediction error variances than Model 1 and 2, which is in agreement with the smaller variance of the deterministic component of Model 3. Nevertheless, it shows that a part of the deterministic component may also be represented by the stochastic component or the other way round. A more detailed evaluation of the correlation structure is required to determine which model best represents the system. For this purpose, we analyze the eigenvalues of the prediction error correlation matrix  $\Xi$ :

$$\Xi = \mathbf{U}\mathbf{\Lambda}\mathbf{U}^T. \quad (6.16)$$

The eigenvalues  $\lambda_i$  ( $i = 1, \dots, m$ ) are placed as the elements of a diagonal matrix  $\mathbf{\Lambda}$  and the eigenvectors are collected as columns into the matrix  $\mathbf{U}$ . Figure 6.2 shows these eigenvalues for Model 1 through 3. Furthermore, Table 6.5 gives the total

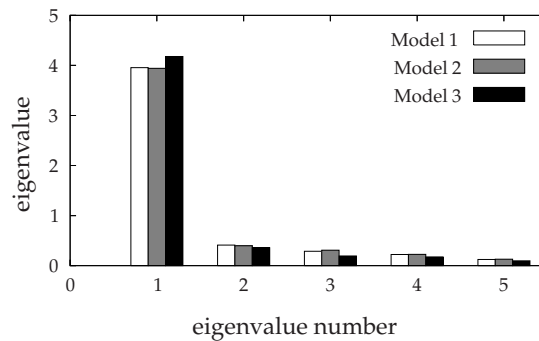
**Table 6.5:** Parameters for evaluating the calibration results of Model 1, 2 and 3

	Model 1	Model 2	Model 3
Total variance $\text{tr}(\mathbf{F}_\infty)$	4359.3	4388.1	5277.0
Variance described by $\lambda_1$	3417.5	3430.7	4354.9
Remaining variance	941.8	957.4	922.1
$\log \mathcal{L}$	-49373	-49406	-48789

noise variance, which is the trace of  $\mathbf{F}_\infty$  (i.e., the sum of the diagonal elements), the variance of the first eigenvalue  $\lambda_1$ , and the log-likelihood value  $\log \mathcal{L}$  (see Equation 2.53).

Several criteria exist for choosing the number of factors based on the eigenvalues of the correlation matrix. *Jobson* [1992] discusses some important criteria and tests in detail. The most simple criterion is the ‘eigenvalue 1 criterion’, which says that the number of factors is at least as large as the number of eigenvalues that exceed one. Another test, known as the ‘scree test’, determines the number of factors by evaluating the pattern of the eigenvalues. The typical shape of a scree graph consists of two parts: a rapidly downward sloping first part with an exponential shape followed by a second part which is almost a horizontal line. The almost horizontal part is viewed as random variation around a constant. These small eigenvalues correspond to specific factors, which are not required to explain the correlations among the variables. The large eigenvalues represent variation explained by the common factors. The correct number of factors corresponds to the eigenvalue number to the immediate left of the beginning of the scree.

Figure 6.2 clearly explains why Model 2 can describe the same correlation structure as Model 1 (even though Model 2 has 5 unknown parameters less). The reason is that the stochastic component of Model 1 has only one dominant eigenvalue that accounts for most of the correlation. As a result, the correlation among the noise processes can be well described by a common noise factor. A physical interpretation is that there is a driving force other than precipitation and evapotranspiration that influences the groundwater head simultaneously at all observation points. The common noise factor may also represent errors in model input and model concept.

**Figure 6.2:** Eigenvalues of the prediction error correlation matrix  $\Xi$  of Model 1, 2 and 3

The first eigenvalue of Model 3 is 4.18, which is larger than the first eigenvalue of Model 1 and 2. Hence, the CDF of Model 3 produces a higher correlation in the stochastic component than Model 1 and 2. Although the total prediction error variance of Model 3 is higher (Table 6.5), the total variance of the remaining eigenvalues is lower than for Model 1 and 2. This shows that the correlation structure of Model 3 better fits the system than the correlation structure of Model 1 and 2, and that Model 1 and 2 overfit the deterministic component. This is also reflected in the absolute value of  $\log \mathcal{L}$ , which is smallest for Model 3. Further, notice that the eigenvalue decomposition of Model 3 justifies the use of one CDF for reducing the VAR model. Also, it shows that a full VAR model is highly overparameterized, which explains its estimation problems.

### 6.2.3 Decomposition of time series

As described in Section 6.1.2, the VTFN-DF model can easily be decomposed into several components: the deterministic component describing groundwater fluctuations resulting from the model input (precipitation and evapotranspiration), the common dynamic factors representing the regional noise components, and the specific dynamic factors representing the unique, local noise. As an example, Figure 6.3 shows smoothed estimates of these components for observation well P149. Figure 6.3a shows the observed groundwater head time series. The deterministic component is plotted in Figure 6.3b using the calibrated parameters of Table 6.3. The variance described by the deterministic component is 69.3%. Figure 6.3c and 6.3d show the stochastic component decomposed into the regional noise (common dynamic factor) and the local noise (specific factor). The results show that most of the stochastic component can be described by the common dynamic factor. The variance explained by the common dynamic factor (usually referred to as the communality) is 96.7% of the total variance of the stochastic component. Only a small amount of the stochastic component (3.3%) is specific for location P149. The correlation among the deterministic component and the CDF is 0.08 (with an asymptotic 95% significance level of 0.07). This is low, but subscribes the conclusions in the previous section that a small part of the noise can be described by the deterministic component as well (as was done by Model 1 and 2).

### 6.2.4 Interpretation of the common dynamic factor

The common dynamic factor as shown in Figure 6.3 represents a regional fluctuation of the groundwater level that is not explained by the deterministic component. Nevertheless, the CDF contains natural fluctuations caused by precipitation and evapotranspiration. Since all time series were modeled with the same input, errors in the input and errors in the transfer function (e.g., neglecting nonlinearities) result in common errors in the deterministic component, which are accounted for by the CDF.

The CDF does not only describe the regional noise due to input errors; it also has a distinct pattern of short, strong lowerings of the groundwater level. It is



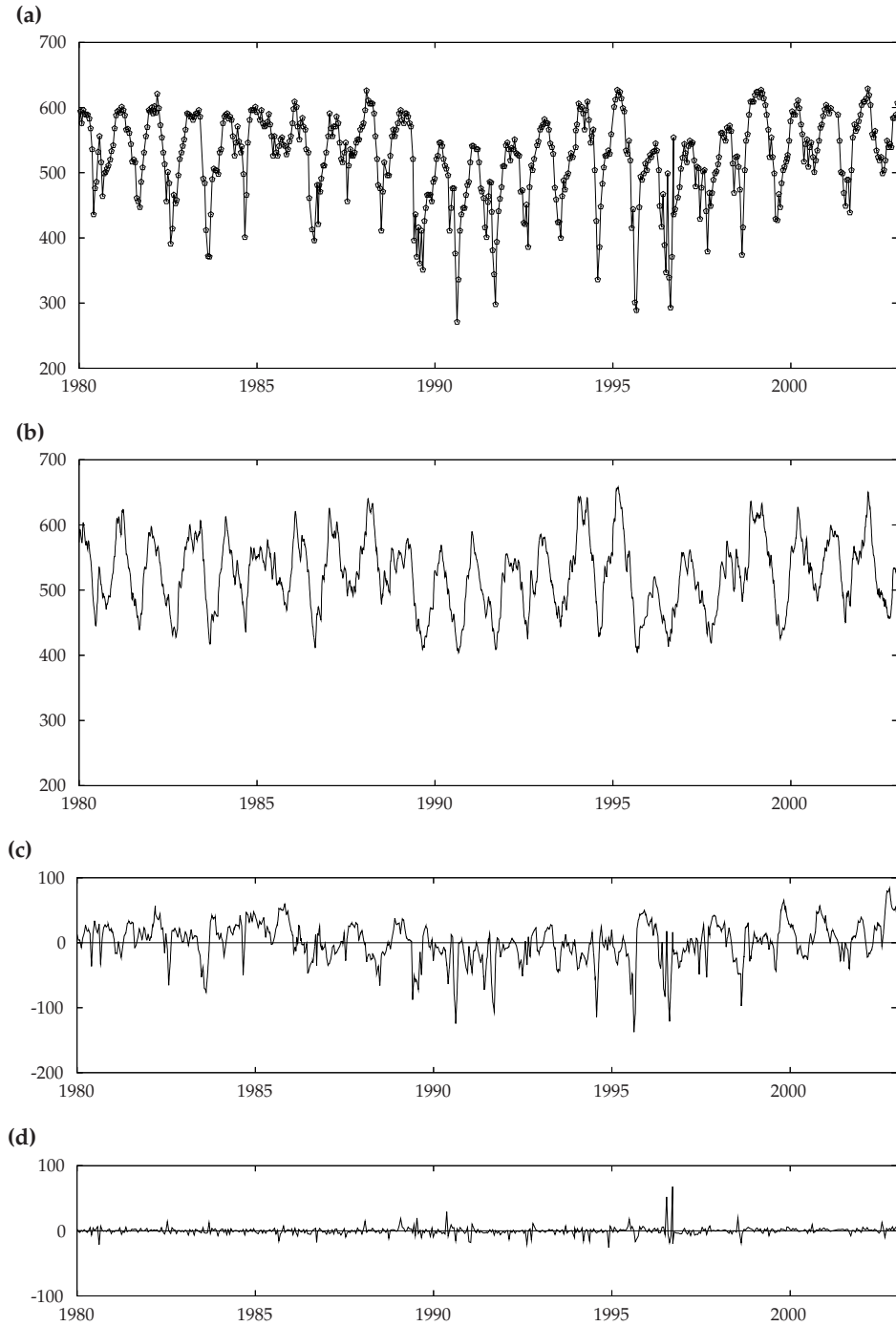


**Figure 6.3:** Decomposition of one of the five time series of groundwater head (P149) using the calibrated VTFN-DF model (Model 3) with (a) observations; (b) deterministic component; (c) common dynamic factor; and (d) specific dynamic factor

**Table 6.6:** Correlation among specific dynamic factors

	P233	P234	P235	P238	P149
P233	1.000				
P234	-.367 <sup>(1)</sup>	1.000			
P235	.079	-.205 <sup>(1)</sup>	1.000		
P238	-.287 <sup>(1)</sup>	.123	-.124	1.000	
P149	-.092	-.254 <sup>(1)</sup>	-.052	-.317 <sup>(1)</sup>	1.000

<sup>(1)</sup>Significant at 95% confidence level

known that these short-time fluctuations in this area are caused by small, temporary groundwater abstractions for irrigation purposes during summertime. The abstraction wells are scattered all over the area resulting in regional fluctuations of the groundwater level. Since in a short period a large amount of groundwater is abstracted, the drawdown is short-term but large (ca. 1 m).

### 6.2.5 Analysis of the specific dynamic factors

The specific dynamic factors represent local fluctuations of the groundwater level that have no relation with fluctuations observed at other observation wells. Figure 6.4 shows smoothed estimates of the specific factors. The vertical scale of the charts is the same as that applied in Figure 6.1. At all locations, the specific noise is small. Peaks in the specific noise may be interpreted as local deviations from the regional noise pattern or observation errors. The specific factor of location P235 has a small low-frequency fluctuation which may be the result of nearby abstraction from a well for drinking water.

The dynamic factor model assumes that all correlation is described by the CDF. Table 6.6 therefore evaluates the correlation among the SDFs. Only among some factors there is a significant but small correlation. No spatial pattern is observed in the correlation matrix, in the sense that there is no higher correlation among locations close to each other.

### 6.2.6 Cross validation of the VTFN-DF model

Once the VTFN-DF model is calibrated, it can be used to extrapolate one or more time series. For instance, short time series can be extended, or gaps in time series can be filled. Also, monitoring networks can be optimized, which means that at some

**Table 6.7:** Cross validation statistics of the VTFN-DF Model

	$p$	ME	MAE	RMSE
P233	0.039	-2.47	11.59	15.00
P234	0.035	0.22	7.31	13.34
P235	0.022	0.31	18.68	22.94
P238	0.025	1.26	6.40	10.27
P149	0.018	-0.30	3.93	7.21
Average	0.028	-0.20	9.58	13.75

ME, MAE and RMSE are in cm,  $p$  is dimensionless

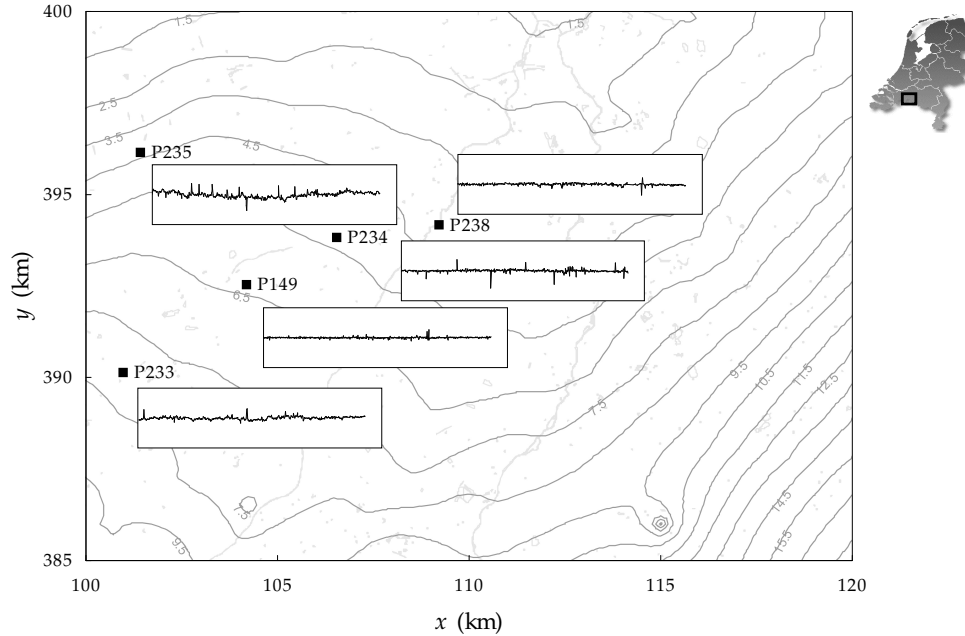


**Figure 6.4:** Spatial representation of the specific dynamic factors; vertical scale of the charts is between -250 cm and 250 cm. In the background main surface water and contours of the average groundwater head are given.

locations, the observation frequency is reduced. At other locations, groundwater head is predicted using the time series of the frequent observation locations.

In order to test the applicability of the calibrated VTFN-DF for this purpose, we needed to validate the correlation structure. Therefore, the following cross validation test was carried out. The time series were cut off at 1991 one at a time. The sequence from 1991 until 2002 was then estimated by one run of the Kalman filter using the calibrated VTFN-DF model. This was repeated for all five time series. Comparison of the predictions with the observations gave the prediction error. The following statistics were calculated: the mean error (ME) measuring the bias of the prediction error, the mean absolute error (MAE) measuring the prediction accuracy, the root mean square error (RMSE) which also measures the prediction accuracy but is more sensitive to outlying values, and the fraction of observations outside the 95% prediction interval,  $p$ . Statistics of the prediction error are given in Table 6.7. On average, the bias of the prediction error is small. The largest bias occurs at P233, where  $ME = -2.47$  cm. The accuracy of the prediction error also varied among the locations. The largest error found is ca. 19 cm for the well that showed low-frequency fluctuations in Figure 6.4 (P235). The average fraction of observations outside the 95% prediction interval is 0.028, which is close to the expected value of 0.05.

Obviously, the prediction error is closely related to the specific factor at a location. The larger the specific variance, the larger the expected prediction error.

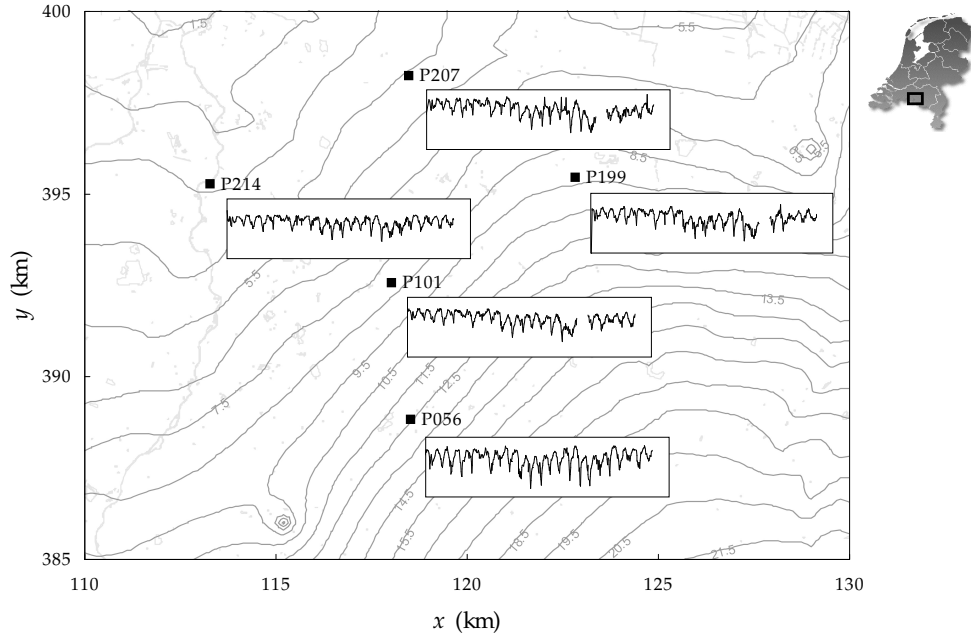


**Figure 6.5:** Locations of five additional observation wells, together with the time series of groundwater head data; average observation interval is 14 days. At P101, P207 and P199, data for a period of ca. 1 year are missing. In the background, main surface water and contours of the average groundwater head are given.

Hence, in the context of optimization of existing monitoring networks, it can be concluded that locations with the smallest specific variance are least sensitive to reduction of the observation frequency (or even removal of the observation well).

### 6.3 Estimation of common trends

Groundwater monitoring networks are often designed for detection of temporal trends in groundwater head. Very often, trends are caused by groundwater withdrawal. If only one abstraction well is present, the drawdown can be simply estimated with a TFN model, using abstraction rates as input. Generally there is more than one abstraction well and detailed data on abstraction rates are not always available. Trends may also be caused by structural changes in the hydrological system. In those situations, trends need to be modeled by the stochastic component. The spatial correlation in trends in groundwater levels is generally high. Using the spatial correlation structure will therefore improve the estimation of trends. The VTFN-DF model is very well suited for this purpose as it allows the frequency of the common factors to be different from the frequency of the specific factors (see Section 6.1.2). This section briefly discusses a case study where trends in groundwater time series were estimated with a VTFN-DF model.

The data set of the previous section was extended with five more time series of

**Table 6.8:** Calibrated parameters of the stochastic component for the VTFN-DF model using two CDFs.  $\Gamma_1$  and  $\Gamma_2$  represent the vectors of factor loadings of CDF1 and CDF2, respectively.

	$\text{diag}(\mathbf{A}^s)$	$\text{diag}(\mathbf{Q})$	$\Gamma_1$	$\Gamma_2$
P233	.954	14.5	-.066	6.25
P234	.001	206.	.187	5.87
P235	.972	32.3	.054	6.37
P238	.906	19.6	.234	4.74
P149	.007	62.7	.116	6.27
P056	.972	5.76	.914	2.71
P101	.934	8.96	1.34	2.81
P199	.018	203.	1.43	4.41
P207	.957	45.0	1.48	3.43
P214	.896	22.1	.528	3.27
CDF1	.9994	1 <sup>(1)</sup>		
CDF2	.980	1 <sup>(1)</sup>		

<sup>(1)</sup>The noise variances of the CDFs were fixed

groundwater head data. In all five time series a temporal trend was observed. The location of the observation wells and the time series are shown in Figure 6.5. The form of the VTFN-DF model is similar to the VTFN-DF model of the first case study. The only difference is that the current model has two common dynamic factors. The total number of unknown parameters (deterministic and stochastic component) is 82. The calibrated parameters are given in Table 6.8. For convenience, only the parameters of the stochastic component are given. The smoothed estimates of the CDFs are presented in Figure 6.6. The upper figure shows the first CDF (CDF1 in

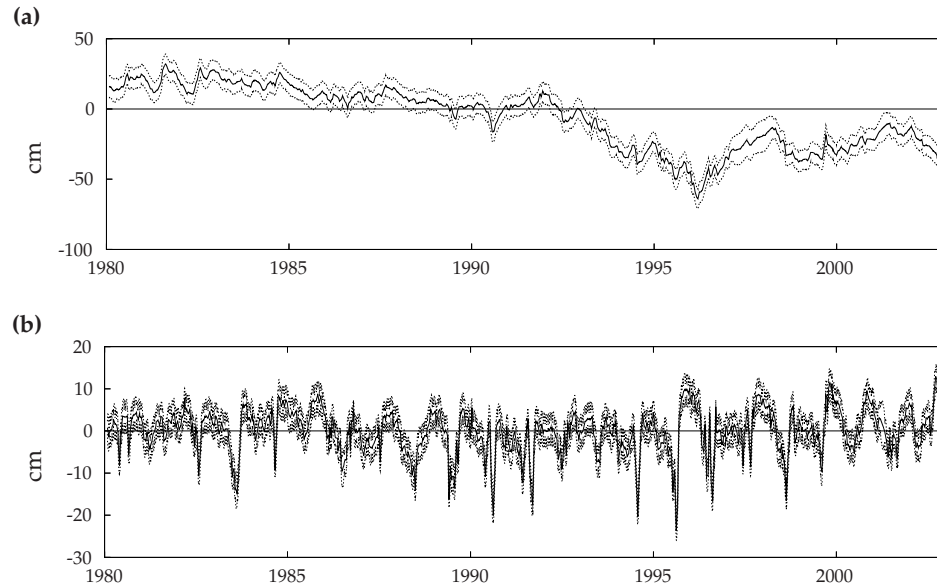


**Figure 6.6:** Smoothed estimates with 95% confidence interval of (a) CDF1 and (b) CDF2

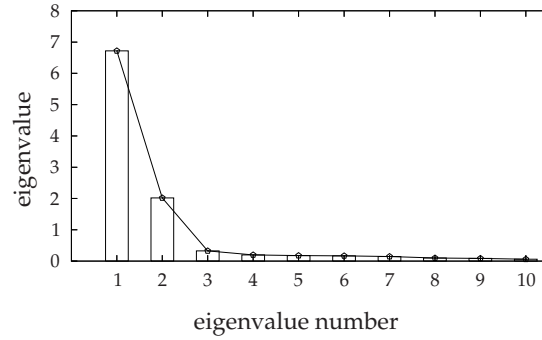


Figure 6.7: Eigenvalues of the prediction error correlation matrix  $\Xi$

Table 6.8), the lower figure shows the second CDF. The 95% confidence intervals were derived from the smoothed estimate of the state covariance matrix. The first CDF clearly shows the common trend in the time series. The low-frequency behavior of the CDF is reflected in the autoregressive parameter of CDF1, which is close to 1. The second CDF looks similar to that in Figure 6.3. The 95% confidence intervals of the CDFs are rather small (conditional on the calibrated parameters). For the first CDF, the average 95% confidence interval is 15 cm.

The number of CDFs were tested by evaluating the eigenvalues of the prediction error correlation matrix. For this test, the criteria discussed in Section 6.2.2 were used. Figure 6.7 shows the eigenvalues of the prediction error correlation matrix. Only the first and second eigenvalues are greater than one. Also, after the second eigenvalue, the graph flattens out. Since both tests suggest the use of two CDFs, the current number of CDFs is sufficient. An extra CDF will not improve the correlation structure much.

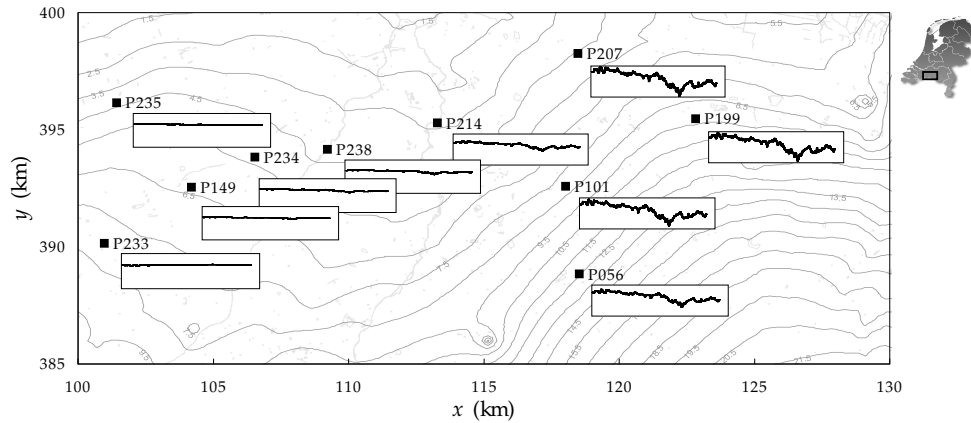


Figure 6.8: Spatial representation of smoothed estimates of the common trend (first CDF); the vertical scale of the charts has a range of 150 cm. In the background, main surface water and contours of the average groundwater head are given.

A spatial representation of the temporal trends in the groundwater time series is given in Figure 6.8. For each time series, the first CDF has been multiplied with the associated factor loading (i.e.,  $\Gamma_1$  from Table 6.8). The figure clearly shows the spatial pattern of the estimated temporal trend. In the western region, the trend is insignificant. Going from west to east, the lowering of the groundwater head increases. The maximum lowering is found in the north-east.

## 6.4 Summary and conclusions

This chapter proposed a vector transfer-function noise (VTFN) model for multiple time series of groundwater head. In this model, correlation among time series is modeled by the stochastic (noise) component. Since the number of parameters increases quadratically with the number of time series, the VTFN model is not suitable for handling large data sets. Therefore, the stochastic component of the VTFN model was written as a factor model. With this model, the number of parameters increases linearly with the number of time series. This opens the way to modeling a larger amount of time series simultaneously. Two different factor models were analyzed: a dynamic factor model, which can be seen as a reduced vector autoregressive (VAR) model, and an autoregressive model with factorized innovations (static factor model), which can be seen as a reduced contemporaneous autoregressive (CAR) model. The reduced models, referred to as the VTFN-DF model and VTFN-SF model respectively, were tested in two case studies.

The first case study consisted of five time series of groundwater head data. Since the number of time series was small, the calibration results of the reduced models could be compared with the results of a full model. From this, some important conclusions are drawn. First, it was not possible to calibrate the full VAR model. Although only five time series were used, the number of autoregressive parameters was too large. The full CAR model, on the other hand, was calibrated satisfactorily. Second, the VTFN-SF only needed one common factor to describe the same correlation structure as the full CAR model, implying a reduction of 5 parameters. The similarity between both models was further illustrated by performing an eigenvalue decomposition, showing that the CAR model indeed had only one dominant eigenvalue. Third, the VTFN-DF model (also with one common factor) produced the best representation of the correlation structure. The VTFN-SF model and CAR model slightly overfitted the deterministic component to compensate for lower correlations among the time series. Fourth, decomposition of the VTFN-DF showed that most of the stochastic component was described by the common factor. Only a small amount of the variance was specific. A plot of the specific factors provided useful information on local deviations from the regional pattern as well as observation errors. Finally, it was shown that knowledge of specific variances can be used for optimizing monitoring networks.

In the second case study 10 time series were analyzed to detect a common trend. For this purpose, the VTFN-DF model was calibrated. Only two common dynamic

factors were needed to describe most of the correlation among the time series. One of the common dynamic factors represented the trend in the time series. In addition to the trend itself, the associated confidence interval was estimated. Multiplication of the common trend with the factor loadings gave the trend at each location. Visualization of the trends in a map showed the spatial pattern of the temporal trends.

The case studies showed that the reduced VTFN model can be used in many applications. The model can be applied as a tool for characterizing hydrological systems. Once in possession of a calibrated model, one can use the Kalman filter to predict groundwater head online. In addition, the Kalman filter enables online detection of interventions and observation errors.



# 7

## Summary and conclusions

## State space modeling of groundwater fluctuations

**G**ROUNDWATER PLAYS AN IMPORTANT ROLE in both urban and rural areas. For instance, high groundwater levels may cause crop damage. On the other hand, low groundwater levels may be a threat to nature. It is therefore essential to monitor groundwater fluctuations. The measuring data can be used for characterizing the groundwater regime or for evaluating effects of interventions. However, to determine, for example, structural changes in groundwater regimes with a high level of certainty, one needs models that can accurately describe groundwater fluctuations.

The main objective of the research presented in this thesis, therefore, was to develop a generic and flexible framework for modeling groundwater time series based on the state space approach, in order to describe groundwater fluctuations more accurately. The modeling approach as presented here combines the state space model with Kalman filtering of the system state, and maximum-likelihood estimation of unknown model parameters. Following this approach, one can model a wide variety of groundwater time series.

A practical advantage of the state space approach is that the interval of input series may be smaller than the interval of output series. As a result, high-frequency input data – which are in general widely available – can be used to estimate groundwater fluctuations more accurately. This is discussed in Section 7.1. Nonlinear extensions of the state space model are discussed in Sections 7.2 and 7.3. Section 7.4 shows that spatial coherence between time series can be utilized to gain more insight into the dynamics of the system and to improve model predictions. This chapter concludes with a general discussion in Section 7.5, highlighting the most important contributions of this thesis to the practice of geohydrological time series modeling, and giving a glimpse of potential directions for future research.

### 7.1 Decoupling of modeling and measuring interval

The effects of reducing the modeling interval – and thus of using high-frequency input data – on the performance of time series models have been investigated using generated time series. The performance is measured by the ‘fit’ of the deterministic component and the accuracy of the estimated transfer function. Calculations on several samples (with varying measuring and modeling interval) of different time series show that the performance of groundwater time series models can be

improved simply by reducing the modeling interval. Conditions are that high-frequency input data is available and that the measuring interval remains a multiple of the modeling interval.

The degree of model improvement depends on several aspects. First, the modeling interval relative to the time of peak response of the system is important. If the modeling interval is large with respect to the time of peak response, a reduction of the interval will greatly improve the performance. In contrast, if the modeling interval is already small with respect to the time of peak response, a further reduction will not result in further improvement. Second, if the stochastic component of the system (part of the system dynamics that cannot be related to the input signal) is large, the relative effect of reducing the modeling interval will be less. A third aspect is the length of the time series: the effect of reducing the modeling interval increases with the length of the time series. This reduction effect is especially observed for the fit of the deterministic component.

In addition to reducing the modeling interval, one could extend a time series with easily obtainable high-frequency measurements (i.e. a reduction of the *measuring* interval). The effect of such an extra set of high-frequency measurements again strongly depends on the stochastic component: high-frequency measurements are much more effective if the stochastic component is large. Moreover, the first high-frequency measurements have the greatest influence on the model performance. It is therefore attractive to add a small time period of high-frequency measurements to an existing time series of low-frequency measurements.

A small modeling interval requires high-frequency observations of spatially distributed input data, i.e., of precipitation and evaporation. It must be noted, however, that input and output data are generally observed at different locations. Errors in input data resulting from spatial heterogeneity of precipitation and evaporation increase as the observation interval of input data decreases. Hence, as the modeling interval decreases, it becomes more and more important that input data is observed close to the location of the observation well.

The relevance of the presented results for hydrological practice is significant. In the Netherlands, for instance, daily observations on precipitation and evaporation are widely available. Time series models with daily modeling intervals can be constructed and hence, existing historical time series with bimonthly observations can be modeled more accurately. Combining the model with a Kalman filter gives a tool that can predict the groundwater level online on a daily basis without requiring daily observations of groundwater level. In addition, the prediction uncertainty calculated by the Kalman filter can be used to adjust the measuring interval. Water managers often allow for a certain level of uncertainty. When the prediction uncertainty exceeds this level, a new measurement need to be carried out.

## 7.2 Incorporation of a nonlinear root zone model

In time series modeling, groundwater fluctuations are commonly assumed to be linearly related to precipitation and evapotranspiration. However, physical knowledge shows that the response of the groundwater level to precipitation and evapotranspiration can be strongly nonlinear. An important source of nonlinearity is the root zone, where the degree of water saturation determines in a nonlinear way the hydraulic conductivity and the water uptake by roots (and thus the actual evapotranspiration). Therefore, we developed a nonlinear model that incorporates the degree of water saturation of the root zone (which may be unobserved) to model actual evapotranspiration and groundwater recharge for the purpose of predicting groundwater fluctuations.

The results of two case studies showed that the nonlinear time series model predicted groundwater level fluctuations better than a linear time series model. More specifically, extremes in the time series (very wet or dry periods) were handled much better by the nonlinear model. Since the variance of the system noise is reduced, structural changes in the groundwater regime can be estimated more accurately and in a shorter period of time.

Of practical interest is that the nonlinear model also predicts the degree of water saturation in the root zone fairly well. Although the degree of water saturation is only calculated as an average over depth, the model can be used to predict, for example, soil water deficits without actually needing soil water content measurements. Predictions of soil water content and groundwater level may be improved further by calibrating the model using measurements of soil water content.

The model also calculates actual evapotranspiration and percolation rates. It is shown that these quantities are close to water balance results obtained from field experiments. Estimates of groundwater recharge can be derived from the model as well.

In the developed state space model, noise is modeled as a separate state. One may improve the performance of the model even further by introducing additive noise entering the system in the root zone. In this way, system noise is processed through the nonlinear system. Several calculations have shown that this may lead to problems during parameter estimation. This is probably the result of using the (first-order) extended Kalman filter. More accurate filters such as an ensemble Kalman filter may produce better results.

A potential nonlinear extension of the developed model is to allow the transfer function in the percolation zone to depend on the actual groundwater level. This is prompted by the knowledge that the response of groundwater level to precipitation excess depends on the thickness of the percolation zone.

## 7.3 State space modeling in switching regimes

A class of nonlinearity that is often found in groundwater systems is threshold nonlinearity. Well-known examples are systems where the water table is controlled by

drains. Drains are only active when the water table is above drainage level. Consequently, the groundwater regime switches as the water table passes the drainage level.

We developed a state space threshold model for simulating and predicting the groundwater level in switching regimes. The model is based on physical concepts and is therefore suitable for intervention analysis. Drainage flux is modeled as a nonlinear function of water table depth in the sense that it switches from a constant (zero) flux when the water table is below drainage level to a flux that is linearly related to the water table depth when the water table is above drainage level. The system noise is also nonlinearly related to water table depth.

The model was tested on two time series of groundwater data. One of them showed a structural change in the groundwater regime. Calibration of the state space model showed that the drainage level (threshold) can be estimated accurately. Furthermore, verification and validation of the model showed that the model described the system well. Comparison with a linear model demonstrated that the performance of the nonlinear state space model is superior. In particular, validation results show that predictions of the linear model are biased and less accurate. In addition, the linear model can not describe the prediction errors well.

The development of this nonlinear state space model allows us to accurately model fluctuations of shallow water tables in, for example, wetlands and urban areas. Although the model used here has a single threshold, it is easy to extend the model with more thresholds. Model results can be used to characterize the groundwater system. The physical basis of the model makes it possible to quantify useful variables, such as groundwater recharge and seepage, or lateral flow.

In many lowland areas, water tables are influenced by surface water. If there are significant fluctuations in the surface water level – in particular artificially controlled fluctuations – the model performance can be improved by incorporating these fluctuations into the model. This can be done by modeling surface water levels as an exogenous input variable (driving force), or as an endogenous output variable. In the latter case, groundwater and surface water can be modeled as a coupled system influencing each other. Treating surface water level as an output variable also allows for the use of irregular observations of surface water levels.

## 7.4 Multiple time series modeling

Time series of groundwater level often show high spatial correlations. Utilizing these correlations improves the descriptive and predictive performance of time series models substantially. A common problem with multiple time series models, however, is that the dimension of the parameter space increases quadratically with the number of time series. Therefore, in this study a reduced vector transfer-function noise model has been developed. This model describes correlation among time series within the stochastic component using a factor model. Basically, factor models aim to describe correlation with only a few common factors. Part of the sto-

chastic component that is not described by the common factors is referred to as the specific factor. In this way, each time series is only indirectly related to other time series by means of one or more common factors. The result of using a factor model is that the number of parameters only increases linearly – instead of quadratically – with the number of time series. This opens the way to modeling a larger cluster of time series simultaneously.

The reduced model was tested in two case studies. The first case study consisted of five time series of groundwater level data. Results show that correlation among the time series could be described with only one common factor. Decomposition of the stochastic component shows that most of the noise is described by the common factor. Only a small amount of the noise is specific. A plot of the specific factors provides useful information on local deviations from the regional pattern (common factor) including observation errors.

The second case study modeled ten time series simultaneously in order to estimate a common trend. Only two common factors were needed to describe correlation among the time series. One of the common factors represented a trend. Multiplication of the common trend with estimated factor loadings gives the trend at each location. A spatial representation of the temporal trends is very useful in studies on structural changes in groundwater level.

The multiple time series model as developed here, describes correlation only within the stochastic component. This implies that the deterministic components of the time series are mutually uncorrelated. An advantage of this is that the nonlinearities described in the previous sections can be incorporated very easily. Hence, the multiple time series model is applicable in many different hydrological regimes.

Decomposition of the stochastic component into common factors and specific factors enables accurate detection of observation errors. This is a major advantage of the multiple time series model with respect to single time series models, where observation errors are often buried in noise.

In addition to reducing the modeling interval (Section 7.1), one can reduce the uncertainty in predicting groundwater fluctuations further by using a multiple time series model. Moreover, monitoring schemes may be adapted such that at some locations observations are carried out frequently (e.g. daily), while at others they are done less often. In this way, measurements of locations where observations are done frequently are used to increase the reliability of groundwater level predictions for the other locations.

## 7.5 Epilogue

The state space modeling approach as presented in this thesis provides scientists, engineers and water managers a comprehensive tool for carrying out systematic studies on groundwater fluctuations. The various models developed within this research make it possible to describe a broad range of groundwater time series. Moreover, models can easily be adapted to better describe specific (nonlinear) hy-

drological processes.

The state space models we developed for describing groundwater fluctuations has led to an increase in accuracy of the model results. The main practical consequence of this is that, given a requested level of accuracy, structural changes in groundwater regimes can be detected within a shorter space of time. This means that water managers can evaluate the effects of interventions sooner. Any adjustments or countermeasures can then be taken in an earlier stage.

The increase in model accuracy also helps in detecting outliers in groundwater data. In particular, the multiple time series model developed in this thesis filters out deviations from the regional pattern very well. Furthermore, the recursive operation of the Kalman filter provides a means to verify new data. This is done by testing a new observation against the model's prediction. The observation is considered to be an outlier if it falls outside a predefined confidence interval. The advantage of this "real-time" approach is that, when an outlier is detected, it can immediately be investigated whether this outlier is the result of an incorrect observation or of an identifiable event.

Considering future developments of state space modeling of groundwater fluctuations, two main topics are expected to predominate. Firstly, further research is needed on how time series models can be used in combination with numerical groundwater models. For instance, estimates of groundwater recharge produced by a time series model may be used as input for numerical models. Another way to combine time series models with numerical models is to apply time series models as "post-processors" of the numerical model results. Residual series of a calibrated numerical model can be further scrutinized with time series models to detect, for example, remaining natural fluctuations.

Secondly, so far, research on time series modeling of groundwater fluctuations has been mainly concerned with supporting decision making in long-term water policy. However, nowadays, groundwater systems must be operated efficiently in the short term as well. With the state space approach described in this thesis, the way is open for real-time control of groundwater levels. Knowledge of the response of groundwater to, for example, surface water fluctuations can be used for the design of operational control systems. In addition, current research on accurate forecasting of local precipitation and evaporation rates will eventually makes it possible to control groundwater fluctuations in an adaptive way. With the availability of automatic data loggers, a fully automatic control system may well become available for practical applications. Water management in agricultural and ecologically vulnerable areas may greatly improve with the application of such systems.





# Samenvatting en conclusies

## State space modelleren van grondwaterstandsfluctuaties

**G**RONDWATER SPEELT IN ZOWEL stedelijk als landelijke gebied een belangrijke rol. Zo kunnen gewassen veel schade oplopen door te hoge grondwaterstanden. Anderzijds kan een lage grondwaterstand schadelijk zijn voor bijvoorbeeld natuurgebieden. Het is daarom essentieel om grondwaterstandsfluctuaties te monitoren. Deze meetgegevens kunnen gebruikt worden voor het karakteriseren van het grondwaterregime of voor het evalueren van effecten van ingrepen. Om echter met een grote mate van zekerheid uitspraken te kunnen doen over bijvoorbeeld structurele veranderingen in het grondwaterregime, zijn er modellen nodig die in staat zijn de gemeten grondwaterstandsfluctuaties nauwkeurig te beschrijven.

De hoofddoelstelling van het in dit proefschrift gepresenteerde onderzoek was dan ook het ontwikkelen van een generiek en flexibel instrumentarium voor het modelleren van grondwatertijdreeksen gebaseerd op de state space benadering, ten einde grondwaterstandsfluctuaties nauwkeuriger te kunnen beschrijven. De in dit proefschrift beschreven modelaanpak combineert een state space model met een Kalman filter en een maximum-likelihood criterium voor het schatten van, respectievelijk, de systeemtoestand en onbekende modelparameters. Met behulp van deze aanpak is het mogelijk om een grote verscheidenheid aan grondwatertijdreeksen te modelleren.

Een praktisch voordeel van de state space benadering is dat het interval van de invoerreeks kleiner mag zijn dan het interval van de uitvoerreeks. Dit betekent dat hoogfrequente invoerdata – welke op veel plekken beschikbaar zijn – gebruikt kunnen worden voor het nauwkeuriger schatten van de grondwaterstandsfluctuaties. Dit wordt beschreven in de eerste paragraaf. Niet-lineaire uitbreidingen van het state space model worden beschreven in de twee daarop volgende paragrafen. De paragraaf daarna toont vervolgens aan dat ruimtelijke samenhang tussen tijdreeksen benut kan worden om inzicht in de systeemdynamiek te verhogen en om modelvoorspellingen te verbeteren. Dit hoofdstuk sluit af met een algemene discussie, waarin de belangrijkste bijdragen van dit proefschrift aan de praktijk van geohydrologische tijdreeksmodellering wordt beschreven. Tevens worden enkele potentiële richtingen voor toekomstig onderzoek aangestipt.

## Ontkoppelen van model- en meetinterval

Met behulp van gegenereerde tijdreeksen is onderzocht wat de effecten zijn van het reduceren van het modelinterval – en dus van het gebruik van hoogfrequente invoerdata – op de prestaties van tijdreeksmodellen. De prestatie is gemeten aan de hand van de ‘fit’ van de deterministische component en de nauwkeurigheid van de geschatte transferfunctie. Berekeningen aan de hand van verschillende tijdreeksen met variërend meet- en modelinterval tonen aan dat de prestatie van grondwater tijdreeksmodellen kunnen worden verbeterd door eenvoudigweg het modelinterval te reduceren. Randvoorwaarden hierbij zijn dat hoogfrequente invoerdata beschikbaar zijn en dat het meetinterval een veelvoud blijft van het modelinterval.

De mate waarin het model verbetert hangt af van verschillende aspecten. Allereerst is de grootte van het modelinterval ten opzichte van het moment van de piekrespons belangrijk. Als het modelinterval groot is ten opzichte van deze piekresponsstijd, dan zal een reductie van het modelinterval de modelprestaties aanzienlijk verbeteren. Is het modelinterval daarentegen al klein ten opzichte van de piekresponsstijd, dan zal een verdere reductie weinig verbetering opleveren. Ten tweede, als de stochastische component van het systeem (het deel van het systeem dat niet kan worden gerelateerd aan het invoersignaal) groot is, dan zal het relatieve effect van een reductie van het modelinterval geringer zijn. Een derde aspect is de lengte van de tijdreeks: het effect van een reductie van het modelinterval neemt toe met de lengte van de tijdreeks. Dit effect is het sterkst bij de fit van de deterministische component.

Naast een reductie van het modelinterval is het mogelijk om de waarnemingsfrequentie te verhogen (een reductie van het meetinterval). Het effect hiervan hangt wederom sterk af van de stochastische component: het verhogen van de waarnemingsfrequentie wordt effectiever naarmate de stochastische component groter wordt. Daarnaast blijken de eerste hoogfrequent waargenomen grondwaterstanden de grootste invloed te hebben op de modelprestaties. Het is dan ook de moeite waard om een bestaande reeks van laagfrequent waargenomen grondwaterstanden uit te breiden met een kleine periode met hoogfrequente waarnemingen.

Een klein modelinterval vereist hoogfrequent waarnemen van ruimtelijk verdeelde data zoals neerslag en verdamping. Hierbij dient echter te worden opgemerkt dat de invoer- en uitvoerdata meestal op verschillende locaties worden waargenomen. Fouten in de invoerdata ten gevolge van de ruimtelijke heterogeniteit van neerslag en verdamping worden groter naarmate het meetinterval van de invoerdata kleiner wordt. Indien het modelinterval dus verder wordt gereduceerd, wordt het belangrijker om over invoerdata te beschikken, die dichtbij de locatie van de peilbuis zijn waargenomen.

De relevantie van de gepresenteerde resultaten voor de hydrologische praktijk is significant. Zo zijn in Nederland dagelijkse waarnemingen van neerslag en verdamping in ruime mate beschikbaar. Tijdreeksen kunnen hiermee dus op dagbasis gemodelleerd worden, met als gevolg dat bestaande historische reeksen van 14-

daagse waarnemingen nauwkeuriger gemodelleerd kunnen worden. Indien het model in combinatie met een Kalman filter wordt gebruikt is het tevens mogelijk om grondwaterstanden *online* op dagbasis te voorspellen zonder dat er daadwerkelijk dagelijks gemeten wordt. Daarnaast kan het meetinterval aangepast worden aan de hand van de door het Kalman filter berekende voorspellingsonzekerheid. Waterbeheerders staan meestal een bepaald onzekerheidsniveau toe. Pas als de voorspellingsonzekerheid dit niveau overstijgt, hoeft er een nieuwe meting uitgevoerd te worden.

### **Inbouwen van een niet-lineair wortelzone model**

Bij het modelleren van grondwatertijdreeksen wordt over het algemeen aangenomen dat grondwaterstandsfluctuaties lineair afhangen van neerslag en verdamping. Vanuit de fysica is het echter bekend dat de respons van de grondwaterstand op neerslag en verdamping sterk niet-lineair kan zijn. Een belangrijke bron van niet-lineairiteit is de wortelzone, waar de verzadigingsgraad een niet-lineaire invloed heeft op de doorlatendheid en de wateropname van de wortels (en dus op de actuele verdamping). We hebben daarom een niet-lineair model ontwikkeld waarin de verzadigingsgraad in de wortelzone is meegenomen (deze hoeft overigens niet te zijn gemeten) om zodoende de actuele verdamping en de grondwateraanvulling te modelleren, met als uiteindelijk doel het voorspellen van grondwaterstandsfluctuaties.

Resultaten van twee case studies tonen aan dat het niet-lineaire tijdreeksmodel een betere voorspelling van de grondwaterstand geeft dan een lineair tijdreeksmodel. Vooral extremen in de tijdreeks (zeer natte of droge jaren) konden beter worden beschreven met het niet-lineaire model. Aangezien de variantie van de systeemruis is afgenomen, is het mogelijk om structurele veranderingen in het grondwaterregime sneller en nauwkeuriger vast te stellen.

Een ander voor de praktijk interessant resultaat is dat het niet-lineaire model een redelijk goede voorspelling geeft van de verzadigingsgraad in de wortelzone. Alhoewel de verzadigingsgraad slechts wordt berekend als een gemiddelde over de dikte van de wortelzone, kan het model gebruikt worden om bijvoorbeeld vochttekorten te voorspellen zonder daadwerkelijk het bodemvocht te meten. Overigens kunnen voorspellingen van het bodemvocht mogelijk nog verder verbeterd worden, door bodemvochtmetingen mee te nemen in de modelkalibratie.

Het model berekent ook de actuele verdamping en percolatie. Het blijkt dat de waarden zoals geschat door het model dichtbij de waarden liggen die zijn bepaald aan de hand van veldwaarnemingen. Tevens kan de grondwateraanvulling van de modelresultaten worden afgeleid.

In het ontwikkelde state space model is de ruis gemodelleerd als een aparte toestand. De modelresultaten zouden nog verder verbeterd kunnen worden door ruis aan te laten grijpen in de wortelzone. Op deze manier werkt de ruis door het gehele niet-lineaire systeem heen. Diverse berekeningen hebben echter aangetoond dat dit

leidt tot problemen tijdens de parameterschatting. Waarschijnlijk is dit het gevolg van het feit dat er gebruik wordt gemaakt van een (eerste orde) extended Kalman filter. Nauwkeurigere filters, zoals een ensemble Kalman filter, zullen waarschijnlijk betere resultaten geven.

Een mogelijke niet-lineaire uitbreiding van het ontwikkelde model is om de transferfunctie in de percolatie zone afhankelijk te maken van de grondwaterstand. Dit is gebaseerd op het feit dat de respons van het grondwater op neerslagoverschot afhangt van de dikte van de percolatie zone.

### State space modelleren in wisselende regimes

Een klasse niet-lineariteiten die vaak voorkomt in grondwatersystemen is drempel niet-lineariteit. Bekende voorbeelden zijn systemen waarin de grondwaterspiegel wordt gecontroleerd door drains. De drains zijn alleen actief als de grondwaterspiegel boven het drainageniveau uitkomt. Dit betekent dat het grondwaterregime verandert als de grondwaterspiegel het drainageniveau passeert.

Om de grondwaterstand in wisselende regimes te simuleren en te voorspellen hebben we een state space model met drempel niet-lineariteit ontwikkeld. Het model is gebaseerd op fysische concepten en is daardoor geschikt voor bijvoorbeeld interventie analyse. De drainage flux is gemodelleerd als een niet-lineaire functie van de grondwaterstand, in de zin dat de flux verandert van een constante (nul) flux als de grondwaterspiegel beneden het drainageniveau is, naar een flux die lineair afhangt van de grondwaterstand als de grondwaterspiegel boven het drainageniveau is. De systeemruis wordt ook niet-lineair gerelateerd aan de grondwaterstand.

Het model is getest op twee grondwatertijdreeksen. Een van deze reeksen vertoont een structurele verandering in het grondwaterregime. Uit de kalibratie van het state space model blijkt dat het drainageniveau (drempelniveau) nauwkeurig kan worden geschat. Verder tonen verificatie en validatie aan dat het model een goede beschrijving van het systeem geeft. In vergelijking met een lineair model blijkt het niet-lineaire model superieur. Vooral de validatie wijst uit dat het lineaire model *biased* en minder nauwkeurig is. Tevens is het lineaire model niet goed in staat om de voorspellingsfouten goed te beschrijven.

Met de ontwikkeling van dit niet-lineaire state space model is het mogelijk geworden om fluctuaties van ondiepe grondwaterspiegels in bijvoorbeeld *wetlands* en stedelijk gebied nauwkeurig te modelleren. De modelresultaten kunnen bijvoorbeeld worden gebruikt om het grondwaterregime te karakteriseren. De fysische basis van het model maakt het mogelijk om nuttige variabelen te kwantificeren, zoals grondwateraanvulling, kwel of laterale stroming. En hoewel het hier gepresenteerde model één drempelniveau bevatte, is het eenvoudig om het model uit te breiden met meerdere drempelniveaus.

In veel laaggelegen gebieden wordt de grondwaterstand direct beïnvloed door oppervlaktewater. Indien het oppervlaktewaterpeil significant fluctueert – en dan

hoofdzakelijk als gevolg van artificiële invloeden – kan het model aanmerkelijk verbeterd worden door deze fluctuaties mee te nemen. Dit kan worden gedaan door oppervlaktewater te modelleren als exogene invoervariabele (drijvende kracht), of als endogene uitvoervariabele. In het laatste geval worden grondwater en oppervlaktewater als een gekoppeld systeem gemodelleerd waarin ze elkaar onderling beïnvloeden. Door oppervlaktewater als uitvoervariabele mee te nemen is het ook mogelijk om onregelmatig waargenomen oppervlaktewaterpeilen mee te nemen.

### Meervoudige tijdreeksmodellering

Tijdreeksen van grondwaterstanden vertonen vaak een hoge ruimtelijke correlatie. Door gebruik te maken van deze correlatie neemt het beschrijvend en voorspellende vermogen van tijdreeksmodellen aanzienlijk toe. Een algemeen probleem bij meervoudige tijdreeksmodellen is echter dat de dimensie van de parameterruimte kwadratisch toeneemt met het aantal tijdreeksen. Daarom is in dit onderzoek een gereduceerd vector transferfunctie-ruis model ontwikkeld. Dit model beschrijft de correlatie tussen de tijdreeksen in de stochastische component met behulp van een factor model. Kort gezegd beschrijft een factor model de correlatie met slechts een paar gemeenschappelijke factoren. Het deel van de stochastische component dat niet kan worden beschreven door de gemeenschappelijke factor, wordt de specifieke factor genoemd. Op deze manier is elke tijdreeks dus alleen indirect gerelateerd aan andere tijdreeksen door middel van een of meerdere gemeenschappelijke factoren. Dit heeft tot gevolg dat bij een factor model het aantal parameters slechts lineair – in plaats van kwadratisch – toeneemt met het aantal tijdreeksen. Dit maakt het mogelijk om een groter cluster tijdreeksen simultaan te modelleren.

Het gereduceerde model is getest in twee case studies. De eerste studie bestaat uit vijf grondwatertijdreeksen. Het blijkt dat de correlatie tussen deze tijdreeksen beschreven kan worden met slecht één gemeenschappelijke factor. Decompositie van de stochastische component laat zien dat deze gemeenschappelijke factor tevens het grootste deel van de ruis beschrijft. Slechts een klein deel van de ruis is specifiek. Een grafiek van de specifieke factoren biedt nuttige informatie over de lokale afwijkingen – inclusief meetfouten – ten opzichte van het regionale patroon (gemeenschappelijke factor).

In een tweede studie werden tien tijdreeksen simultaan gemodelleerd, met als doel het detecteren van een gemeenschappelijk trend. Slechts twee gemeenschappelijke factoren waren nodig om de correlatie te beschrijven. Eén van deze factoren representeert een trend. Vermenigvuldiging van deze gemeenschappelijke trend met de geschatte factorgewichten geeft de trend op elke lokatie. Een ruimtelijke weergave van deze temporele trends is zeer nuttig in studies naar structurele veranderingen in het grondwaterniveau.

Het in deze studie ontwikkelde meervoudige tijdreeksmodel, beschrijft de correlatie alleen met de stochastische component. Dit impliceert dat de deterministische componenten van de tijdreeksen onderling onafhankelijk zijn. Dit heeft als

voordeel dat de niet-lineariteiten zoals beschreven in de vorige paragrafen, eenvoudig ingebouwd kunnen worden. Het meervoudige tijdreeksmodel is dus in veel verschillende hydrologische regimes toepasbaar.

Decompositie van de stochastische component in gemeenschappelijke factoren en specifieke factoren maakt het ook mogelijk om nauwkeurig meetfouten te detecteren. Dit is een groot voordeel ten opzichte van enkelvoudige modellen, waar meetfouten vaak nog verborgen zitten in de ruis.

Door, naast een reductie van het modelinterval, gebruik te maken van een meervoudig tijdreeksmodel, kan de onzekerheid in het voorspellen van grondwaterstandsfluctuaties verder worden verlaagd. Tevens is het mogelijk om meetfrequenties zodanig aan te passen, dat op enkele lokaties frequent wordt waargenomen (bijvoorbeeld dagelijks), terwijl op andere lokaties minder vaak wordt gemeten. Op deze manier wordt de informatie van hoogfrequent waargenomen lokaties gebruikt om de betrouwbaarheid van de voorspellingen op de overige lokaties te verhogen.

## Epiloog

De in dit proefschrift gepresenteerde state space modelbenadering biedt wetenschappers, modelleurs en waterbeheerders een uitgebreid instrumentarium voor het uitvoeren van systematische studies naar grondwaterstandsfluctuaties. De diverse modellen die binnen dit onderzoek zijn ontwikkeld bieden de mogelijkheid om een grote verscheidenheid aan grondwatertijdreeksen te modelleren. Bovendien kunnen de modellen eenvoudig aangepast worden om meer specifieke (bijvoorbeeld niet-lineaire) hydrologische processen te beschrijven.

De ontwikkeling van de state space modellen heeft geleid tot nauwkeurigere modelresultaten. De belangrijkste praktische consequentie hiervan is, dat structurele veranderingen in grondwaterregimes in een kortere periode waargenomen kunnen worden. Dit betekent dat waterbeheerders de effecten van ingrepen eerder kunnen vaststellen. Eventuele aanpassingen of tegenmaatregelen kunnen dan in vroeger stadium gedaan c.q. genomen worden.

De verhoging van de nauwkeurigheid maakt het ook eenvoudiger om uitschieters in grondwaterstandsdata te detecteren. Vooral het in dit proefschrift ontwikkelde meervoudige tijdreeksmodel is zeer geschikt voor het filteren van afwijkingen op het regionale patroon. Verder biedt de recursieve werking van het Kalman filter een middel om nieuwe data te verifiëren. Deze verificatie kan uitgevoerd worden door een nieuwe waarneming te vergelijken met de modelvoorspelling. Zodra de waarneming buiten een vooraf vastgesteld betrouwbaarheidsinterval valt, wordt het als een uitschieter beschouwd. Het voordeel van een dergelijke *real-time* aanpak is dat, wanneer er een uitschiet wordt gedetecteerd, er onmiddellijk kan worden nagegaan of deze uitschieter het gevolg is van een meetfout of van een identificeerbare gebeurtenis.

Wat betreft toekomstige ontwikkelingen in state space modelleren van grondwaterstandsfluctuaties, zullen naar verwachting twee belangrijke onderwerpen de

boventoon voeren. Allereerst is er meer onderzoek nodig naar de wijze waarop tijdreeksmodellen gecombineerd kunnen worden met numerieke grondwatermodellen. Zo zouden de met behulp van tijdreeksmodellen geschatte grondwateraanvullingen gebruikt kunnen worden als invoer voor numerieke modellen. Een andere mogelijkheid is om tijdreeksmodellen te gebruiken om resultaten van numerieke modellen na te bewerken. Residueksen van gekalibreerde numerieke modellen kunnen zo verder uitgeknepen worden om bijvoorbeeld overgebleven natuurlijke fluctuaties te detecteren.

Ten tweede is onderzoek op het gebied van tijdreeksmodellering van grondwaterstandsfluctuaties tot voorkort vooral gericht geweest op beslissingsondersteuning in het waterbeheer op lange termijn. Tegenwoordig dienen grondwatersysteem echter ook op korte termijn efficiënt beheerd te kunnen worden. Met behulp van de state space benadering zoals is beschreven in dit proefschrift, ontstaat de mogelijkheid tot *real-time* grondwaterpeilbeheer. Zo kan kennis van de respons van het grondwaterpeil op bijvoorbeeld oppervlaktewaterpeil gebruikt worden voor het ontwerpen van een operationeel beheerssysteem. Bovendien is het door huidig onderzoek naar het nauwkeurig voorspellen van lokale neerslag- en verdampingscijfers, misschien mogelijk om de grondwaterstandsfluctuaties adaptief te sturen. Door de beschikbaarheid van automatische data loggers zou dan uiteindelijk zelfs een volledig automatisch systeem geïmplementeerd kunnen worden.

Wilbert Berendrecht





# Bibliography

- Aboitiz, M., J. Labadie, and D. Heermann, Stochastic soil moisture estimation and forecasting for irrigated fields, *Water Resour. Res.*, 22, 180–190, 1986.
- Adamowski, K., and T. Hamory, A stochastic systems model of groundwater level fluctuations, *J. Hydrol.*, 62, 129–141, 1983.
- Alley, W. M., Water balance models in one-month-ahead streamflow forecasting, *Water Resour. Res.*, 21, 597–606, 1985.
- Anderson, B. D. O., and J. B. Moore, *Optimal filtering*, Prentice-Hall, New Jersey, 1979.
- Anselmo, V., and L. Ubertini, Transfer function-noise model applied to flow forecasting, *Hydrol. Sci. Bull.*, 24, 353–359, 1979.
- Ansley, C. F., and R. Kohn, A note on reparameterizing a vector autoregressive moving average model to enforce stationarity, *J. Statist. Comput. Simul.*, 24, 99–106, 1986.
- Aoki, M., *State space modeling of time series*, 2nd ed., Springer-Verlag, Berlin, 1990.
- Basilevsky, A., *Statistical factor analysis and related methods: theory and applications*, John Wiley, New York, 1994.
- Belmans, C., J. G. Wesseling, and R. A. Feddes, Simulation of the water balance of a cropped soil: SWATRE, *J. Hydrol.*, 63, 271–286, 1983.
- Bennett, A. F., B. S. Chua, and L. M. Leslie, Generalized inversion of a global numerical weather prediction model, *Meteorology and Atmospheric Physics*, 60, 165–178, 1996.
- Bidwell, V. J., P. F. Callander, and C. R. Moore, An application of time-series analysis to groundwater investigation and management in Central Canterbury, New Zealand, *J. Hydrol.*, 30, 16–36, 1985.
- Bierkens, M. F. P., Modeling water table fluctuations by means of a stochastic differential equation, *Water Resour. Res.*, 34, 2485–2499, 1998.
- Bierkens, M. F. P., M. Knotters, and F. C. Van Geer, Calibration of transfer function-noise models to sparsely or irregularly observed time series, *Water Resour. Res.*, 35, 1741–1750, 1999.
- Bierkens, M. F. P., M. Knotters, and T. Hoogland, Space-time modeling of water table depth using a regionalized time series model and the Kalman filter, *Water Resour. Res.*, 37, 1277–1290, 2001.
- Box, G. E. P., and G. M. Jenkins, *Time series analysis, forecasting and control*, Holden-Day, San Francisco, 1970.

- Bryson, A. E., and M. Frazier, Smoothing for linear and non-linear dynamic systems, *Tech. Rep. TDR-63-119*, Wright-Patterson Air Force Base, Ohio, Aer. Systems Division, 1962.
- Bryson, A. E., and Y. C. Ho, *Applied optimal control: optimization, estimation, and control*, Hemisphere Publishing Corp., New York, 1975.
- Bucy, R. S., and P. D. Joseph, *Filtering for stochastic processes with applications to guidance*, Interscience, New York, 1968.
- Camacho, F., A. I. McLeod, and K. W. Hipel, Contemporaneous autoregressive-moving average (CARMA) modelling in hydrology, *Water Resour. Bull.*, 21, 709–720, 1985.
- Camacho, F., A. I. McLeod, and K. W. Hipel, Multivariate contemporaneous ARMA models with hydrological applications, *Stochastic Hydrol. and Hydraulics*, 1, 141–154, 1987.
- Chow, K. C. A., W. A. Watt, and D. G. Watts, A stochastic-dynamic model for real time flood forecasting, *Water Resour. Res.*, 19, 746–752, 1983.
- De Jong, P., The likelihood for a state space model, *Biometrika*, 75, 165–169, 1988.
- Debrand, T., and N. Patrat, Dynamic factor demands model: continuous time vs. discrete time, *Economic Modelling*, 18, 133–157, 2001.
- Dempster, A. P., N. M. Laird, and D. B. Rubin, Maximum-likelihood from incomplete data via the EM-algorithm, *J. Roy. Statist. Soc. Ser. B*, 39, 1–38, 1977.
- Deutsch, S. J., and P. E. Pfeifer, Space-time ARMA modeling with contemporaneously correlated innovations, *Technometrics*, 23, 401–409, 1981.
- Engle, R. F., and M. W. Watson, A one-factor multivariate time series model of metropolitan wage rates, *J. Amer. Statist. Assoc.*, 76, 774–781, 1981.
- Feddes, R. A., Crop factors in relation to Makkink reference-crop evapotranspiration, in *Commissie Hydrologisch Onderzoek TNO, Versl. Meded.*, vol. 39, pp. 33–45, CHO-TNO, The Hague, 1987.
- Feddes, R. A., P. J. Kowalik, and H. Zaradny, *Simulation of field water use and crop yield*, PUDOC, Wageningen, 1978.
- Feddes, R. A., P. Kabat, P. J. T. Van Bakel, J. J. B. Bronswijk, and J. Halbertsma, Modelling soil water dynamics in the unsaturated zone - State of the art, *J. Hydrol.*, 100, 69–111, 1988.
- Forni, M., M. Hallin, M. Lippi, and L. Reichlin, The generalized dynamic-factor model: identification and estimation, *Rev. Econom. and Statist.*, 82, 540–554, 2000.
- Fraser, D. C., and J. E. Potter, The optimum linear smoother as a combination of two optimum linear filters, *IEEE Trans. Automat. Control*, 7, 387–390, 1969.
- Gardner, G., A. C. Harvey, and G. D. A. Phillips, An algorithm for exact maximum likelihood estimation of autoregressive-moving average models by means of Kalman filtering, *Appl. Statist.*, 29, 311–322, 1980.
- Gehrels, J. C., Groundwater level fluctuations; separation of natural from anthropogenic influences and determination of groundwater recharge in the Veluwe area, the Netherlands, Ph.D. thesis, Vrije Universiteit, Amsterdam, 1999.

- Gehrels, J. C., F. C. Van Geer, and J. J. De Vries, Decomposition of groundwater level fluctuations using transfer modelling in an area with shallow to deep unsaturated zones, *J. Hydrol.*, 157, 105–138, 1994.
- Gelb, A., *Applied optimal estimation*, MIT Press, Cambridge, Massachusetts, 1974.
- Geweke, J., The dynamic factor analysis of economic time-series models, in *Latent variables in socio-economic models*, edited by D. J. Aigner and A. S. Goldberger, pp. 365–383, North-Holland, Amsterdam, 1977.
- Gill, P., W. Murray, and M. H. Wright, *Practical optimization*, 6th ed., Ac. Press, New York, 1981.
- Granger, C. W. J., and P. Newbold, *Forecasting economic time series*, Ac. Press, New York, 1977.
- Hannan, E. J., *Multiple time series*, John Wiley, New York, 1970.
- Harvey, A. C., *Forecasting, structural time series models and the Kalman filter*, Cambridge University Press, Cambridge, 1989.
- Heij, C., W. Scherrer, and M. Deistler, System identification by dynamic factor models, *Environmetrics*, 14, 665–685, 1997.
- Hipel, K. W., and A. I. McLeod, *Time series modelling of water resources and environmental systems*, Dev. Water Sci. Ser., vol. 45, Elsevier, New York, 1994.
- Hipel, K. W., A. I. McLeod, and E. A. McBean, Stochastic modelling of the effects of reservoir operation, *J. Hydrol.*, 32, 97–113, 1977.
- Hoeben, R., and P. A. Troch, Assimilation of active microwave observation data for soil moisture profile estimation, *Water Resour. Res.*, 36, 2805–2819, 2000.
- Huisman, L., *Groundwater Recovery*, MacMillan, London, 1972.
- Isaaks, E. H., and R. M. Srivastava, *An introduction to applied geostatistics*, Oxford Univ. Press, New York, 1989.
- Janacek, G., and L. Swift, *Time series forecasting, simulation, applications*, Ellis Horwood, London, 1993.
- Jazwinsky, A. H., *Stochastic processes and filtering theory*, Ac. Press, New York, 1970.
- Jobson, J. D., *Applied multivariate data analysis*, vol. 2: Categorical and multivariate methods, Springer-Verlag, New York, 1992.
- Kalman, R. E., A new approach to linear filtering and prediction problems, *ASME Trans. J. Basic Eng.*, 82, 35–45, 1960.
- Kalman, R. E., and R. S. Bucy, New results in linear filtering and prediction theory, *ASME Trans. J. Basic Eng.*, 83, 95–108, 1961.
- Kendall, M. K., and A. S. Stuart, *The theory of advanced statistics*, vol. 2: Inference and relationship, 4th ed., Charles Griffin & Company Ltd., 1979.
- Knotters, M., Regionalised time series models for water table depths, Ph.D. thesis, University of Wageningen, Wageningen, 2001.
- Knotters, M., and M. F. P. Bierkens, Physical basis of time series models for water table depths, *Water Resour. Res.*, 36, 181–188, 2000.
- Knotters, M., and M. F. P. Bierkens, Predicting water table depths in space and time using a regionalised time series model, *Geoderma*, 103, 51–77, 2001.

- Knotters, M., and J. G. De Gooijer, TARSO modeling of water table depths, *Water Resour. Res.*, 35, 695–705, 1999.
- Koopman, S. J., and J. Durbin, Fast filtering and smooting of multivariate state space models, *J. Time. Ser. Anal.*, 21, 281–296, 2000.
- Koopman, S. J., and J. Durbin, *Time series analysis by state space methods*, Oxford University Press, 2001.
- Krishnamurthy, V., and L. A. Johnston, On the equivalence of the extended Kalman smoother and the expectation maximisation algorithm for polynomial signal models, in *Proceedings of Information Decision and Control 99*, edited by R. Evans, L. White, D. McMichael, and L. Sciacca, pp. 303–308, Institute of Electrical and Electronic Engineers, Inc., Adelaide, Australia, 1999.
- Lütkepohl, H., *Introduction to multiple time series analysis*, Springer-Verlag, Berlin, 1991.
- Maas, C., On convolutional processes and dispersive groundwater flow, Ph.D. thesis, Delft University of Technology, Delft, 1994.
- Maidment, D. R., S. P. Miaou, and M. M. Crawford, Transfer function models of daily urban water use, *Water Resour. Res.*, 21, 425–432, 1985.
- Maybeck, P. S., *Stochastic models, estimation and control*, vol. 1, 141-1 in Math. in science and engineering, Ac. Press, New York, 1979.
- Maybeck, P. S., *Stochastic models, estimation and control*, vol. 2, 141-2 in Math. in science and engineering, Ac. Press, New York, 1982.
- McDonald, D. C., and A. W. Harbaugh, *A modular three-dimensional finite-difference groundwater flow model*, Manual 83-875, U.S. Geological Survey, USA, 1988.
- Ministry of VROM, *Nationaal Milieubeleids Plan – kiezen of delen*, Ministerie van Volkshuisvesting, Ruimtelijke Ordening en Milieuhygiëne, SDU, The Hague, 1989.
- Molenaar, P. C. M., A dynamic factor model for the analysis of multivariate time series, *Psychometrika*, 50, 181–202, 1985.
- Molenaar, P. C. M., and J. R. Nesselroade, Rotation in the dynamic factor modeling of multivariate stationary time series, *Psychometrika*, 66, 99–107, 2001.
- Moss, M. E., and M. C. Bryson, Autocorrelation structure of monthly streamflows, *Water Resour. Res.*, 10, 737–744, 1974.
- Neuman, S. P., R. A. Feddes, and E. Bresler, Finite element simulation of flow in saturated-unsaturated soils considering water uptake by plants: Development of methods, tools and solutions for unsaturated flow, *Tech. Rep. 3rd annual report, part 1*, Israel Inst. of Technol., Haifa, 1974.
- Olsder, G. J., *Mathematical systems theory*, Delft University Press, 1994.
- Or, D., and R. J. Hanks, Spatial and temporal soil water estimation considering soil variability and evapotranspiration uncertainty, *Water Resour. Res.*, 28, 803–814, 1992.
- Pandit, S. M., and S. M. Wu, *Time series and system analysis with applications*, John Wiley, New York, 1983.
- Parlange, M. B., G. G. Katul, R. H. Cuenca, M. L. Kavvas, and D. R. Nielsen, Physical

- basis for a time series model of soil water content, *Water Resour. Res.*, 28, 2437–2446, 1992.
- Parlange, M. B., G. G. Katul, M. V. Folegatti, and D. R. Nielsen, Evaporation and the field scale soil water diffusivity function, *Water Resour. Res.*, 28, 2437–2446, 1993.
- Pfeifer, P. E., and S. J. Deutsch, Identification and interpretation of first order space-time ARMA models, *Technometrics*, 22, 397–408, 1980.
- Rolf, H. L. M., *Verlaging van de grondwaterstanden in Nederland, analyseperiode 1950-1986*, Rijkswaterstaat, Dienst Binnenwateren / RIZA, SDU, The Hague, 1989.
- Salas, J. D., and J. T. B. Obeysekera, ARMA model identification of hydrologic time series, *Water Resour. Res.*, 18, 1011–1021, 1982.
- Salas, J. D., and R. A. Smith, Physical basis of stochastic models of annual flows, *Water Resour. Res.*, 17, 428–430, 1981.
- Schweppe, F. C., *Uncertain dynamic systems*, Prentice-Hall, New Jersey, 1973.
- Shea, B. L., Estimation of multivariate time series, *J. Time Ser. Anal.*, 8, 95–109, 1987.
- Shumway, R. H., and D. S. Stoffer, An approach to time series smoothing and forecasting using the EM algorithm, *J. Time Ser. Anal.*, 3, 253–264, 1982.
- Shumway, R. H., and D. S. Stoffer, *Time series analysis and its applications*, Springer-Verlag, New York, 2000.
- Šimuněk, M. Sejna, and M. Th. Van Genuchten, *The HYDRUS-1D software package for simulating the one-dimensional movement of water, heat, and multiple solutes in variably-saturated media, version 2.0*, IGWMC-TPS-70, Golden, Colorado, 1998.
- Skaggs, T. H., and B. P. Mohanty, Water table dynamics in tile-drained fields, *Soil Sci. Soc. Am. J.*, 62, 1191–1196, 1998.
- Snyder, D. L., *The state variable approach to continuous estimation with applications to analog communication theory*, MIT Press, Cambridge, Massachusetts, 1969.
- Spolia, S. K., and S. Chander, Modeling of surface runoff systems by an ARMA model, *J. Hydrol.*, 22, 317–332, 1974.
- Szollósi-Nagy, A., E. Todini, and E. F. Wood, A state-space model for real-time forecasting of hydrological time series, *J. Hydrol. Sci.*, 4, 61–76, 1977.
- Tankersley, C. D., and W. D. Graham, Development of an optimal control system for maintaining minimum groundwater levels, *Water Resour. Res.*, 30, 3171–3181, 1994.
- Tankersley, C. D., W. D. Graham, and K. Hatfield, Comparison of univariate and transfer function models of groundwater fluctuations, *Water Resour. Res.*, 29, 3517–3533, 1993.
- Tarantola, A., *Inverse problem theory*, 2nd ed., Elsevier, 1987.
- Todini, E., and J. R. Wallis, A real-time rainfall-runoff model for an on-line flood warning system, in *AGU conference on applications of Kalman filter to hydrology, hydraulics and water resources*, edited by Chao-lin Chiu, pp. 355–368, Dept. of Civil Engineering, Pittsburgh, USA, 1978.
- Tong, H., *Non-linear time series: a dynamical system approach*, Oxford Univ. Press, New York, 1990.

- Van Dam, J. C., Field-scale water flow and solute transport. SWAP model concepts, parameter estimation and case studies, Ph.D. thesis, University of Wageningen, Wageningen, 2000.
- Van Geer, F. C., Transfer/noise modelling in groundwater management: an example, in *Proc. KNGMG Symp. coastal lowlands, geology and geotechnology*, pp. 255–260, Kluwer Ac. Publ., Dordrecht, 1989.
- Van Geer, F. C., and P. R. Defize, Detection of natural and artificial causes of groundwater fluctuations, in *The influence of climate change and climatic variability on the hydrologic regime and water resources*, pp. 597–606, IAHS Publ., No. 168, 1987.
- Van Geer, F. C., and A. F. Zuur, An extension of Box-Jenkins transfer/noise models for spatial interpolation of groundwater head series, *J. Hydrol.*, 192, 65–80, 1997.
- Van Genuchten, M. Th., A closed form equation for predicting the hydraulic conductivity of unsaturated soils, *Soil Sci. Soc. Am. J.*, 44, 892–898, 1980.
- Van Genuchten, M. Th., A comparison of numerical solutions of the one-dimensional unsaturated-saturated flow and mass transport equations, *Adv. Wat. Resour.*, 5, 47–55, 1982.
- Verlaan, M., and A. W. Heemink, Nonlinearity in data assimilation applications: a practical method for analysis, *Mon. Weather Rev.*, 129, 1578–1589, 2001.
- Vermeulen, P. T. M., A. W. Heemink, and C. B. M. te Stroet, Reduced models for linear groundwater flow models using empirical orthogonal functions, *Adv. Water Resour.*, 27, 57–69, 2004.
- Watson, M. W., and R. F. Engle, Alternative algorithms for the estimation of dynamic factor, MIMIC and varying coefficient regression models, *J. Econometrics*, 23, 385–400, 1983.
- Wiener, N., *Extrapolation, interpolation and smoothing of stationary time series*, John Wiley, New York, 1949.
- Winter, T. C., D. O. Rosenberry, and A. M. Sturrock, Evaluation of 11 equations for determining evaporation for a small lake in the north central United States, *Water Resour. Res.*, 31, 983–994, 1995.
- Winters, P. R., Forecasting sales by exponentially weighted moving averages, *Management Sci.*, 6, 324–342, 1960.
- Wu, L., W. A. Jury, and A. Chang, Time-series analysis of field-measured soil water content of a sandy soil, *Soil Sci. Soc. Am. J.*, 61, 736–742, 1997.
- Wu, L., T. H. Skaggs, P. J. Shouse, and J. E. Ayars, State space analysis of soil water and salinity regimes in a loam soil underlain by shallow groundwater, *Soil Sci. Soc. Am. J.*, 65, 1065–1074, 2001.
- Wu, L. S.-Y., J. S. Pay, and J. R. M. Hosking, An algorithm for estimating parameters of state-space models, *Statist. Probab. Lett.*, 28, 99–106, 1996.
- Young, P. C., Data-based mechanistic modelling and validation of rainfall-flow processes, in *Model validation: perspectives in hydrological science*, edited by M. G. Anderson, pp. 117–161, John Wiley, Chichester, 2001.
- Young, P. C., and K. J. Beven, Data-based mechanistic (DBM) modelling and the

- rainfall-flow nonlinearity, *Environmetrics*, 5, 335–363, 1994.
- Young, P. C., and P. E. H. Minchin, Environmentric time-series analysis: modelling natural systems from experimental time-series data, *Int. J. Biol. Macromol.*, 13, 190–201, 1991.
- Young, P. C., and S. G. Wallis, Solute transport and dispersion in channels, in *Channel networks*, edited by K. J. Beven and M. J. Kirkby, pp. 129–173, John Wiley, Chichester, 1994.
- Young, P. C., A. J. Jakeman, and D. A. Post, Recent advances in the data-based modelling and analysis of hydrological systems, *Wat. Sci. Tech.*, 36, 99–116, 1997.
- Zuur, A. F., R. J. Fryer, I. T. Jolliffe, R. Dekker, and J. J. Beukema, Estimating common trends in multivariate time series using dynamic factor analysis, *Environmetrics*, 14, 665–685, 2003.





# Index

## A

- abstraction well, 114, 116
- adjoint method, 40
- agricultural area, 127
- Akaike Information Criterion, 53
- anthropogenic activity, 16
- aquifer, 73, 107
  - semi-confined, 17, 87
- autocorrelation, 50, 95, 106
- automatic data loggers, 18, 58, 127

## B

- Bayes Information Criterion, 53
- bias correction, 39
- boundary conditions, 88

## C

- calibration, 49, 52, 60, 75, 88, 91, 93, 109
- characteristic equation, 27
- civil engineering works, 17
- climatic conditions, 18
- clusters, 16, 17
- coefficient of determination, 63
- common dynamic factors, 105–107, 109, 112, 117
  - frequency of, 106, 116
  - interpretation of, 112
  - number of, 118
- common factor, 111
- common noise factor, 108, 111
- common trend, 103, 116
- communality, 112
- control, 20, 25, 127
- convection-dispersion equation, 72
  - discretization of, 74
- convolution integral, 72
- correlation, 102
  - spatial pattern in, 114

- structure, 109, 112, 119
  - validation of, 115
- coupled system, 125
- Cramer-Rao lower bound, 42
- crop factor, 70, 76, 87, 91, 93, 104, 109
- cross validation, *see* validation

## D

- Darcy's law, 71
- delay time, 29
- density function, 38
- deterministic component, 28, 32, 51, 54, 64, 78, 104, 109, 112
- dewatering
  - effect of, 18
  - systems, 17
- diagnostic checking, 24
- discretization, 54, 74
- ditch, 91, 93
- drainage, 72
  - artificial, 15
  - base level, 87
  - flux, 72, 90
  - level, 86, 94
  - level, local, 88
  - resistance, 72, 87, 88, 94
  - system
    - main, 87
    - local, 87, 88, 92, 94
- drawdown, 11, 17, 72, 73, 75–77, 114, 116
- driving force, 111, 125

## E

- eigenvalue-1-criterion, 111
- eigenvalues, 110–112, 118
  - pattern of, 111
- eigenvectors, 110
- EM algorithm, 42

error  
 estimation, 35  
 mean, 98, 99, 115  
 mean absolute, 54, 98, 115  
 measurement, *see* measurement  
 root mean square, 98, 115  
 standard, *see* standard deviation  
 evaporation, 18, 48, 60  
 evapotranspiration, 104, 111  
   actual, 68, 70, 79, 82  
   potential, 70  
   reference, 51, 76, 87, 91  
 exfiltration areas, 17  
 extrapolation, 18

## F

factor loadings  
   dynamic, 106, 117, 119, 120  
   noise, 106  
 factorized matrix, 107, 108  
 filter  
   backward, 43  
   Kalman, *see* Kalman filter  
   second-order, 39  
   truncated first-order, 38, 86, 91  
 filter performance, 39, 75, 90  
 filtering, 24, 34  
 forecasting, 20, 25–27, 102  
 frequency  
   domain, 24  
 frequency of exceedance, 92, 96, 98  
 frequency of observation, 75  
   reduction of, 115

## G

groundwater  
   abstraction, 114  
   data, 60  
   decline, 15, 78, 80, 95  
   dynamics, 18  
   fluctuations, 15, 48, 63, 68, 74, 80, 86, 127  
     control of, 127  
     local, 114  
     regional, 112, 114  
   head, 14, 17, 18, 108  
   level, 15, 25  
     cumulative probability of, 96  
     lowering of, 112

    structural change in, 16  
 recharge, 69, 82  
 regime, 15, 18, 86  
 studies, 14, 24  
 system, 14, 48, 68, 86, 93, 127  
   characterization of, 86, 95  
   management of, 15  
   schematization of, 69, 86  
 withdrawal, 16, 72, 78

## H

hydraulic conductivity, 68, 71  
 hydraulic head gradient, 71  
 hydrological system, 120

## I

identification, 60, 105, 109  
 identity matrix, 31, 106  
 impulse response function, 28, 30, 62, 63, 92  
 infiltration, 95  
 initial conditions, 33, 34, 37, 40, 43  
 innovation, 36, 37, 40, 49, 50, 97  
   covariance matrix, 36, 37  
   percentiles of, 95  
   standardized, 50  
   variance, 53, 63  
   whiteness of, 95  
 input, 73, 76  
   errors in, 111, 112  
   spatial heterogeneity of, 123  
   vector, 73, 89, 103  
 interaction analysis, 102  
 interception factor, 11, 70, 76, 77, 87, 91, 93  
 interpolation, 20, 26, 43, 102  
 interval  
   measuring, 48, 54–56, 64, 82  
     adjustment of, 123  
     modeling, 19, 48, 53–56, 63, 64  
 intervention, 15, 25, 68, 89  
   analysis, 102, 125  
   detection of, 102, 120  
   effect of, 86, 91–93, 99, 127  
 inverse covariance form, 43  
 irrigation, 17, 114

## K

Kalman filter, 25, 34, 35, 37, 50, 107, 115, 123, 127  
 ensemble, 124

- extended, 38, 69, 75
- linear, 34, 49
- nonlinear, 37, 88
- Kalman gain, 35–37
- Kronecker
  - delta, 33
  - product, 105

## L

- Lagrange multipliers, 45
- likelihood function, 40, 50, 111
- logarithmic integral, 73
- lowland areas, 86, 125

## M

- Markov process, 27
- maximum likelihood estimate, 75, 91, 107
- measurement
  - error, 14, 75, 77, 89, 109, 114
    - detection of, 120
  - noise, 33, 34, 49, 91, 93, 104
  - update, 35, 43
- measurements
  - high-frequency, 18, 19, 58, 63, 64
  - irregularly, 26, 34
  - number of, 57, 59
  - of soil moisture, 75
- meteorological
  - input, 51, 60
  - station, 76, 91, 93, 107
- model
  - autoregressive, 26, 51, 105
  - autoregressive moving-average, 28
  - autoregressive moving-average exogenous variables, 31
  - black-box, 14, 25
  - Box-Jenkins, 18, 24, 26
  - construction, 24
  - contemporaneous autoregressive, 103, 105
  - contemporaneous autoregressive moving-average, 102
  - data-based mechanistic, 25
  - dynamic factor, 103, 105, 114, 119
  - empirical, 14
  - exponential, 71, 77
  - factor, 103
  - linear, 26, 31, 77
  - Markov, 25

- moving-average, 27
- nonlinear, 37, 45, 68
- numerical, 19, 127
- performance of, 48, 86, 124
- physical-mechanistic, 19, 68
- reduction, 103, 105
- regionalized autoregressive exogenous variable, 102
- reservoir, 29, 69, 104
- space-time autoregressive moving-average, 102
- state space, *see* state space model
- static factor, 103
- stochastic, 68
- structure of, 25
- TARSO, 86
- threshold, 86
- time series, 14, 24
- transfer function-noise, 25, 28, 30, 68, 97, 102
- vector autoregressive, 102, 103, 105
- vector transfer-function noise, 103
- modeling interval, 60
- monitoring, 15, 18, 59, 107
  - network, optimization of, 102, 114
  - scheme, 126

## N

- natural component, 15, 18
- Netherlands
  - center of the, 75
  - southern part of the, 17, 91, 107
- noise
  - colored, 102
  - covariance matrix, 33, 104, 106, 108
    - factorized, 110
  - local, 107, 112
  - measurement, *see* measurement
  - regional, 107, 112
  - specific, 106
  - system, 33, 49, 63, 77, 81, 89, 104, 124
    - influence of, 90, 94
    - weighting of, 92
  - variance, 69
  - white, *see* white noise
- non-natural component, 15, 18
- nonlinear
  - function, 74
  - system, 19, 68

**O**

observation matrix, 34, 105  
 observation well, 73, 87, 107, 114  
 off-line filter, 42  
 online  
   filter, 42  
   prediction, 102, 120, 123  
   processing, 99  
 operator  
   autoregressive, 27, 29  
   backward shift, 27  
   moving-average, 27, 29  
 optimality, 35, 36, 43  
 optimization, 24, 39–42, 50, 109  
   procedure, 41  
 outliers, 102, 127

**P**

parallel computing, 40  
 parameter  
   accuracy, 42, 57  
   autoregressive, 29, 49, 74, 97, 104, 118  
   moving-average, 29, 49, 97  
   vector, 39, 75, 91  
     Jacobian of, 50  
 parsimony, 21, 68, 69, 109  
 pasture, 91, 93  
 peak response, 60  
   time of, 52, 54, 64  
 percolation, 68  
   flux, 79, 80, 82  
   zone, 69, 72, 74, 81  
   thickness of, 124  
 physical  
   concepts, 14  
   interpretation, 111  
   knowledge, 26, 65, 68, 86  
 piezometer, 15  
 poles, 29  
 precipitation, 18, 48, 60, 87, 91, 104, 111  
   excess, 18, 25, 51, 94  
 prediction, 20, 27, 34, 69, 81  
   accuracy, 115  
   error, 78, 98, 115  
   bias of, 115  
   correlation matrix, 109, 118  
   covariance matrix, 109, 110  
   decomposition, 39  
   variance, 112

interval, 62, 93, 94, 99  
 space-time, 102  
 uncertainty, 78  
 predictive performance, 96  
 probability density function, 36, 51  
 propagation of, 37

**Q**

quasi-Newton algorithm, 40

**R**

rainfall-runoff modeling, 25  
 real time, 18, 20, 26, 127  
 recharge, 25  
   estimation, 82  
 redundancy, 109  
 reference level, 73, 75, 97  
   lowering of, 92  
 regional  
   flow, 88  
   noise pattern, 114  
 reservoir  
   function, 72  
   modeling, 25  
 resistance, 73, 87, 107  
 response, 18, 80, 81  
 risk analysis, 96  
 root zone, 68, 69  
   thickness of, 70

**S**

saturated zone, 69, 72, 74  
 scaling variance, 49  
 scenario analysis, 20  
 scree test, 111  
 seasonal pattern, 94  
 second-order filter, *see* filter  
 seepage, 87  
 simulation, 27, 93, 96  
 smooth function, 90  
 smoothed estimate, 42, 107, 112, 114  
 smoothing, 34, 42  
   fixed-interval, 42, 43, 107  
   fixed-lag, 42  
   fixed-point, 42  
 soil moisture pressure head, 70  
 soil water  
   content, 25, 70

- estimation of, 81
- dynamics, 26
- measurements, 82
- solute transport modeling, 25
- spatial
  - coherence, 19
  - pattern, 17
- specific
  - dynamic factor, 106, 112, 114
  - factor, 111
  - yield, 73
- stability, 29
- standard deviation, 57, 60, 77, 81, 95
- state
  - covariance matrix, 33–35
    - smoothed estimate of, 118
  - definition of, 32
  - equation, 31, 60, 74, 88
  - propagation of, 37–39
  - unobserved, 65
  - update of, 37
  - variable, 26
  - vector, 31, 32, 34, 40
    - common part of, 106
    - specific part of, 106
- state space model, 14, 25, 31, 48, 73, 86, 90, 103
- static factor model, 119
- stationarity, 27, 109
- steady-state gain, 29, 54, 57, 63
- stochastic component, 28, 30, 33, 48, 51, 57, 59, 63,  
64, 74, 103–105, 112, 116
  - correlation in, 103, 108
  - decomposition of, 107
- stochastic process, 27
- storage coefficient, 72, 87
- streamflow modeling, 25
- structural change, 17, 18, 127
- surface water, 125
- switching regime, 86, 90, 99
- system matrix, 31, 34, 39, 104, 108

## T

threshold, 86, 88, 125

## time

- characteristic response, 56, 81
- domain, 24
- response, 92
- update, 37
- time series, 14, 27
  - decomposition of, 112, 113
  - extrapolation of, 114
  - length of, 56, 64
  - multiple, 102
- trace, 111
- tracer methods, 82
- transfer function, 28, 31, 51, 54, 72, 105, 109
  - errors in, 112
- transition matrix, 31, 104, 105
  - factorized, 109, 110
- trench, 88, 91
- trend, 68
  - analysis, 102
  - common, *see* common trend
  - detection of, 116
  - spatial correlation in, 116
- truncated first-order filter, *see* filter

## U

- univariate statistics, 95, 97
- unsaturated zone, 71, 83
- urban water-use, 25

## V

- validation, 60, 62, 75, 91
  - cross, 114, 115
- vegetation, 17, 70, 76
- verification, 75, 93, 98

## W

- water
  - balance, 86, 88
  - management, 15, 86, 99, 127
  - saturation, 68, 69, 74, 79, 82
- white noise, 27, 37, 75, 93, 97, 103, 106



# Curriculum vitae

**W**ILBERT BERENDRECHT werd geboren op 30 oktober 1976 in Den Haag. In 1994 behaalde hij het eindexamen VWO aan het St. Jans College (tegenwoordig Hofstad College) te Den Haag. Hij ging civiele techniek studeren aan de faculteit Civiele Techniek van de Technische Universiteit Delft. De propedeuse behaalde hij in juni 1995. Het afstudeerwerk getiteld *Generieke aspecten van gemanipuleerde smart pump-and-treat sanering* werd mede onder leiding van Prof.dr.ir. C. van den Akker en dr.ir. C.B.M. te Stroet verricht bij het Nederlands Instituut voor Toegepaste Geowetenschappen TNO (TNO-NITG). Dit werk werd in 2000 door de Vereniging van Waterbouwers in Bagger-, Kust- en Oeverwerken bekroond met een eervolle vermelding. In februari 2000 ontving hij zijn diploma met lof. Vervolgens is hij in dienst getreden als promovendus aan de faculteit Electrotechniek, Wiskunde en Informatica van de Technische Universiteit Delft. Gedurende deze periode is hij bij TNO-NITG gestationeerd geweest. In januari 2003 ontving hij de Publicatieprijs 2003 van TNO-NITG voor het artikel *Decoupling of modeling and measuring interval in groundwater time series analysis based on response characteristics* gepubliceerd in *Journal of Hydrology*. Sinds maart 2004 is hij werkzaam als wetenschappelijk onderzoeker bij TNO-NITG.

